AD-A266 599

AFIT/GAE/ENY/93J-01

EXPERIMENTAL INVESTIGATION OF THE EFFECTS OF BLOWING RATIO PARAMETER ON HEAT TRANSFER TO A FILM-COOLED FLAT PLATE

THESIS

Marco R. Valencia, B.S.

AFIT/GAE/ENY/93J-01

DTIC
ELECTE
JUL 0 6 1993
S E D

93-15242

AFIT/GAE/ENY/93J-01

EXPERIMENTAL INVESTIGATION OF THE EFFECTS

OF BLOWING RATIO PARAMETER ON HEAT TRANSFER

TO A FILM-COOLED FLAT PLATE

THESIS

Presented to the Faculty of the School of Engineering

of the Air Force Institute of Technology

Air University

In Partial Fulfillment of the

DTIC QUALITY INSPECTED 5

Requirements for the Degree of

Master of Science in Aeronautical Engineering

Accesion For		
NTIS CRA&I		☒
DTIC TAB		☒
Unannounced		☐
Justification		
By		
Distribution /		
Availability Codes		
Dist	Avail and / or Special	
A-1		

Marco R. Valencia, B.S.

June 1993

Approved for public release; distribution unlimited

Preface

This study continues the film cooling research done in the AFIT Low Speed Shock Tube by previous researchers. Most of this research focused on having reliable information about the effects of film cooling on the rate of heat transfer to the test plates. For this reason each test, with similar flow conditions, was repeated at least three times and the results then averaged. A more capable data acquisition system is in place with associated data reduction programs written in Fortran 77. Much effort was dedicated to analyze and compare reduced data.

Many people were involved in the accomplishment of this research. My greatest gratitude goes to my advisor Dr. William C. Elrod, who at all times was available to give me directions and answer my questions. I thank Mr. Andrew Pitts and Capt. Tomas Eads for their support during the execution of this thesis. Also, I thank Mr. John Brohas of the AFIT Model Fabrication Shop for his extremely prompt and precise machining work. Finally, my special thanks go to my wife María and my daughter Andrea, for enduring my time at AFIT with love, patience, and understanding.

Marco Valencia

ii

Table of Contents

List of Figures

List of Tables

x

List of Symbols

Symbol	Description	Units
a	Sonic velocity	m/sec
A	Cross Sectional Area	m^2
B	Mass flux (blowing ratio) parameter $(\rho_c U_c / \rho_\infty U_\infty)$	
c	Capacitance per unit length	μFarad/m
c_p	Specific heat at constant pressure	J/kg-K
D	Diameter of cooling holes	mm or m
d	Diameter of flat plate leading edge	mm or m
DR	Density ratio (ρ_c / ρ_∞)	
G	Electrical analog amplifier gain	
h	Convective heat transfer coefficient	W/m^2-K
HFC	Heat flux calibration constant	W/m^2/Volt
i	Current flow into analog circuit	Amperes
I	Momentum flux ratio $(\rho_c U_c^2 / \rho_\infty U_\infty^2)$	
k	Thermal Conductivity	W/m-K
L	Hole length	mm
M	Mach number (U/a)	
MW	Molecular weight	kg/kmol

Nu	Nusselt number (hx/k)	
p	Pitch or lateral hole-to-hole spacing	mm
P	Pressure	psi or in. Hg
Pr	Prandtl number ($\mu C_p/k$)	
q	Heat flux	W/m^2
r	Resistance per unit length	Ohm/m
r_c	Recovery factor	
R	Gas constant ($\bar{R}/MW$)	J/kg-K
R	Resistance	Ohm
$\bar{R}$	Universal gas constant (8314.34)	J/kmol-K
Re_x	Local Reynolds number ($\rho Ux/\mu$)	
S	Sutherland constant	
St	Stanton number ($h/\rho UC_p$)	
t	Time	sec
T	Temperature	K
Tu	Turbulence intensity (longitudinal)	percent
U	Velocity	m/sec
V	Electrical voltage or potential	Volt
VR	Velocity ratio (U_c/U_∞)	
V'	Voltage across resistor R_1 in analog circuit	Volt
x	Distance from stagnation point at plate leading edge	mm
X	Distance from center of cooling holes	m

Greek Letters

α	Thin film gage temperature coefficient	K^{-1} ($^\circ R^{-1}$)
γ	Ratio of specific heats (C_p/C_v)	
Δ	Change in	
η_c	Adiabatic film-cooling efficiency	
ρ	Density	kg/m^3
μ	Dynamic viscosity	Pa-sec
μ	Constant	
π	Arithmetic constant (3.14159265359)	
Φ	Semi-empirical parameter for mixture viscosity or conductivity	
χ	Mole fraction	
ω	Frequency	rad/sec, Hz
$(\rho C_p k)^{1/2}$	Bulk thermal diffusivity	J/m^2-K-sec$^{1/2}$

Subscripts

air	Air
atm	Atmospheric
c	Coolant
avg	Average
gly	Glycerin USP, 95%
He	Helium
mix	Mixture of gases

o	Without film cooling, or output (for voltage)
oc	Coolant stagnation condition
out	Output
pyrex	Corning Pyrex$^\bullet$ 7740
s	Shock
subs	Substrate of thin-film gauge
v	Variable (potentiometer)
w	Wall
x	Local, or based on distance
1	Shock tube driven section (before shock)
2	Driven section (after shock), test mainstream condition
4	Driver section
∞	Free-stream or test mainstream condition

AFIT/GAE/ENY/93J-01

Abstract

Experimental investigation of the effects of film cooling parameters, such as density and blowing ratios, on the heat transfer to a flat plate in a shock tube was carried out. Two round-nosed test plates were used. One plate was made of aluminum and the second of corian. The corian plate simulated an adiabatic surface because of its very low thermal conductivity. The plates have a single row of injection holes at 35 degrees in the downstream direction, with a two-hole-diameter lateral spacing. Helium was mixed with air inside the shock tube driven section to produce a density ratio of 1.6 and 2.0, while the blowing ratio was varied from 0.3 to 2.2. Surface temperature was measured by thin film resistance gages located up to a nondimensional downstream distance X/D of 30, and their output was then converted to heat flux using an electrical analog.

Two injection regimes, weak and strong, were found. In the weak injection regime, film cooling reduced gage heat flux at all thin film gage locations, however, film cooling was more effective for X/D < 10. In the strong injection regime, the effectiveness of film cooling for X/D < 10 was greatly reduced. Maximum film cooling effectiveness occured between the weak and strong regime at a blowing ratio of 1.0. Changing the density ratio from 1.6 to 2.0 varied the measured gage heat flux less than 5 percent.

Film cooling heat transfer is correlated by the velocity ratio scaling parameter $(X/D)VR^{-4/3}$ either in the weak or in the strong injection regime. Measured gage heat flux with no film cooling, assuming a turbulence level of 10 percent, deviated less than 10 percent from theoretical results.

xv

EXPERIMENTAL INVESTIGATION OF THE EFFECTS OF

BLOWING RATIO PARAMETER ON HEAT TRANSFER

TO A FILM-COOLED FLAT PLATE

I. Introduction

1.1 Background

Aeroengine designers aim toward the attainment of high-performance propulsion

gas turbine engines. The thermal efficiency of gas turbine engines can be improved by

increasing the temperature at the inlet to the turbine section. This increase in temperature

reduces the lifetime of the turbine blades and combustor components due to an increase

in the thermal-stress fields.

The reduction in turbine performance makes necessary the use of sophisticated

cooling schemes to protect the exposed components. Three different cooling methods are

being used, internal convection, impingement, and film cooling. For the modern gas

turbine engines with very high gas temperatures, protection given by internal convection

and impingement cooling alone are not enough. Film cooling is employed to provide the

extra protection required for the hot section components.

In film cooling, relatively cool air is injected through discrete holes located on

the surface of the component in such a way that establishes a protective film on the

component. For the case of blade film cooling in a gas turbine, compressor bleed air is

introduced into the hollow core of each blade and then injected through rows of holes located on high thermally loaded zones. Figure 1.1 illustrates a typical arrangement for blade film cooling.

The use of compressor bleed air for purposes other than combustion reduces the engine efficiency; however, according to Hill and Peterson (1992:394) the gains obtained for operating the engine at a much higher turbine inlet temperature are greater than the losses.

1.2 Problem

In order to minimize the amount of coolant airflow needed to protect gas turbine blades from the hot gas stream, an estimate of the heat transfer must be known. " To be effective, film cooling must result in acceptable blade surface temperature and thermal stress distributions in the presence of potentially blade-melting high-enthalpy combustion gases to prolong life of the blade. " (Pietrzyk et al., 1990:437)

Studies of film cooling vary in their approach to analyze the heat exchange phenomena because of the difficulty in matching complex experimental conditions. These complexities make analytical modeling of blade turbine heat transfer very complicated. Therefore, experimental research is needed to correlate heat transfer variables to film cooling parameters. "The utilization of numerical codes for the prediction of the heat transfer in separated flow is dependent on reliable experimental data with well-known boundary conditions. " (Wittig and Scherer, 1987:572)

1.3 Summary of Current Knowledge

For more than twenty years, researchers have been working on film cooling experimentation in order to provide reliable information to aeroengine designers. To study film cooling phenomena, investigators have been using simple geometries to reduce the complexity of the flow affecting the heat exchange between the test model and the gas flow. One geometry preferred by researchers is that of a flat plate.

Film cooling effectiveness is dependent upon a large number of parameters. According to Sinha and others (1991:442), there are two types of parameters, geometrical and fluid mechanical. Injection hole shape, angle, spacing, and pattern are considered geometrical parameters. Fluid mechanical parameters are the coolant-to-crossflow ratios of density, DR, Velocity, VR, mass flux or blowing, B, and momentum flux, I. These ratios are defined as

$$DR = \frac{\rho_c}{\rho_\infty} \qquad\qquad (1.1a)$$

$$VR = \frac{U_c}{U_\infty} \qquad\qquad (1.1b)$$

$$B = \frac{\rho_c U_c}{\rho_\infty U_\infty} \qquad\qquad (1.1c)$$

$$I = \frac{\rho_c U_c^2}{\rho_\infty U_\infty^2}$$ (1.1d)

where ρ_c and ρ_∞ represent the coolant and mainstream density, and U_c and U_∞ the coolant and mainstream velocities respectively.

Results in film cooling are generally presented nondimensionally in terms of film cooling effectiveness, defined as

$$\eta_c = \frac{T_{aw} - T_\infty}{T_c - T_\infty}$$ (1.2)

where T_{aw} is the adiabatic wall temperature, T_∞ is the mainstream temperature, and T_c is the coolant fluid temperature. Up through the late 1960s most of the literature reported effectiveness distribution associated with slot injection, porous injection, and from a single hole, mostly carried out at a density ratio near unity.

The first in a series of research reports began with Goldstein and others (1968:384) reporting the effectiveness results from a circular hole. This was followed by a study of Goldstein and others (1971:321-379) that contrasted the single hole results with that from a row of holes. This study reported a blowing ratio, B, of 0.5 for maximum effectiveness at density ratios around 1.0. However, test flow conditions did not resemble those found in gas turbine engines (density ratio greater than 1.0).

According to Ammari and others (1990:444), turbine inlet temperatures of up to 1700 K and coolant air temperature in the range of 700 to 1000 K are common in modern jet engines, resulting in coolant-to-mainstream density ratios well in excess of unity.

Pedersen and others (1977:620-627) presented the first study of the effects of density ratio on film cooling. Their experimentation was made using a plexiglass test section placed inside of a low-turbulence subsonic wind tunnel with a turbulence intensity between 0.3 and 0.4 percent. The injection geometry consisted of 15 holes, 11.7 millimeters in diameter, spaced three diameters apart, and with their axis inclined at an angle of 35 degrees toward the plate surface in the main flow direction. The results are presented in Figure 1.2 showing the centerline effectiveness versus velocity ratio, U_2 / U_∞, for a dimensionless downstream distance, X/D, of 10.29. Film cooling effectiveness, η_c, has a maximum value for a velocity ratio between 0.4 and 0.6 for a density ratio varying from 0.75 to 4.17.

According to Pietrzyk and others (1990:437), the density ratio parameter can be matched in three ways, using a hot free-stream flow, a cryogenically cooled injectant flow, or foreign gas injection such as carbon dioxide, helium, etc.. The use of foreign gases other than air to simulate flow conditions existing around a gas turbine blade is a practical approach. According to Teakaram and others (1989:60), " there is a close agreement between film-cooling heat transfer results obtained where the injection-to-mainstream density ratio is achieved either by changing the injection-to-mainstream temperature ratio or by using a foreign injection gas."

1.5

Studies have been recently carried out at Oxford University to study the effect of density and blowing ratio on film cooling. Forth and Jones (1986:1271-1276) determined scaling parameters for the effects of density ratio on heat transfer. Their research showed the presence of two injection regimes, a weak injection regime where no total separation of the injection flow occurs from the surface, and a strong injection regime where the injection jets penetrate into the freestream and lift off the surface. Jet lift off was found to occur at a blowing ratio of 0.4 for $X/D=2$.

For the weak injection regime, the momentum flux ratio is the correct scaling parameter. This parameter is defined as $(X/D)I^{-2/3}$. Where X is the downstream distance relative to the injection holes and D is the injection hole diameter. For the strong injection regime the velocity ratio is the correct scaling parameter, defined as $(X/D)VR^{-4/3}$.

Another important parameter is the mainstream turbulence. Hancock and Bradshaw (1983:288,289) determined the effects of mainstream turbulence on heat transfer. They showed that for every 1 percent increase in turbulence intensity, the heat transfer coefficient increases about 5 percent. In a typical gas turbine engine, the turbulence levels are of the order of 10 to 20 percent (Rivir, 1987). Increasing the turbulence level reduces the effective film cooling length and increases the optimum blowing ratios in contrast with the low turbulence data bases (Jumper et al., 1990).

Clearly the use of low turbulence data bases is inadequate for high turbulence applications. Furthermore, evolution of experimental procedures in film cooling has also increased the cost of such investigations. Economic budget uncertainties usually affect

research and development programs with unexpected reductions. Thus, low cost experimentations are being increasingly required these days.

At AFIT, film cooling studies have been carried out using a low speed shock tube. One of the advantages of the shock tube is its low operational cost. Jurgelewicz (1989) developed a numerical technique to obtain heat flux from temperature history of highly-responsive heat flux gages for a flat plate with normal injection. According to Forth and Jones, transition from weak to strong injection regime occurred at a blowing ratio of 0.4. Jurgelewicz's research was basically related to the strong injection regime with blowing ratios between 1 and 5. Rockwell (1989) simultaneously developed an analog electrical circuit based on prior work by Oldfield and others (1978) to convert the gage output voltage directly into heat flux potential.

Gul (1991) expanded the data obtained by Jurgelewicz to lower blowing ratios (weak injection regime) for the same injection geometry. Background turbulence intensity was of the order of 9.5 percent according to Gul's and Rockwell's measurements. Eads (1992) used a mixture of air and helium inside the shock tube to vary the density ratio from 1.2 to 2.1. For this case the injection geometry was changed to a single row of holes inclined 35 degrees downstream, and a blowing ratio range from 0.4 to 3.0. The heat flux results obtained by Eads were well correlated using the velocity ratio parameter, $(X/D)VR^{-4/3}$ for the case of strong injection regime.

1.7

1.4 Objective and Scope

This research is based upon the work done by Eads (1992). It addresses the determination of film cooling effectiveness in a round-nosed flat plate with a single-row inclined-injection holes using a low speed shock tube. A shock wave is generated inside the shock tube once the diaphragm separating the pressurized section from the lower pressure section is ruptured. As the shock wave moves downstream and over the test model, a hot turbulent flow is induced behind the wave. This increase in temperature initiates heat transfer from the hot gas stream to the cool flat plate. The main objectives of this research were:

1. To determine the rates of heat transfer to a round-nosed flat plate behind the shock wave in a shock tube.

2. To determine the effects of film cooling parameters, geometrical and fluid mechanical, on the rates of heat transfer to a flat plate.

3. To determine optimum blowing ratio for maximum film cooling effectiveness.

4. To compare the differences in heat transfer behavior for two types of test model materials, aluminum and corian[*].

The limits of this research included a Mach number range from 0.31 to 0.45 for the flow over the flat plate, density ratios of 1.6 and 2.0, and blowing ratios ranging from 0.24 to 2.21. In order to obtain a desired density ratio, a mixture of air and helium was used inside the shock tube. A film cooling injection hole angle of 35 degrees relative to the plate was used to be consistent with previous experimentations, and the freestream turbulence level in the shock tube was found to be 9.5 percent in previous work by

1.8

Rockwell and Gul.

The test time available at conditions established behind the incident shock wave over the test model is just a few milliseconds. Thus, highly responsive instrumentation is required for data acquisition. Thin-film heat-flux gages and piezoresistive pressure transducers were used to meet these requirements.

II. Theory

2.1 The Shock Tube

A shock tube is a device for generating gas flows of very short duration. It provides an inexpensive mean of producing a hot turbulent flow required for this study. A simple shock tube consists of a tube of constant cross section in which a diaphragm initially separates two bodies of gas at different pressures but at the same temperature, i.e., room temperature. The high pressure section is called the driver section while the low pressure section is called the driven section. Figure 2.1(a) shows a simple shock tube. Initial conditions inside the shock tube are typically labeled "4" for the driver section and "1" for the driven section.

Rapid rupture of the diaphragm produces compression and expansion waves. Compression waves travel into the low pressure gas and coalesce to form a normal shock wave while expansion waves move into the high pressure gas and form a rarefaction wave.

According to Glass (1958:1), the flow regions behind the compression and expansion waves are separated by a contact surface moving into the driven section, across which, pressure and velocity are equal but temperature and density are different. The region between the shock wave and the contact surface is labeled "2" while the region between the rarefaction wave and the contact surface is labeled "3".

Flow parameters such as pressure and temperature behind the shock wave, region

2, are critical because they establish the conditions in the test section for this study. Figure 2.1(b) depicts the events occurring in the shock tube immediately after the diaphragm is ruptured. The shock wave moves at velocity corresponding to its Mach number, the rarefaction wave propagates at local sonic velocity, while the contact surface propagates with the same velocity imparted to the flow behind the passing shock.

Upon reaching the respective ends of the shock tube, both waves, normal shock and rarefaction, reflect back and change flow conditions behind them. These new conditions are labeled "5" and "6" corresponding to the normal shock and rarefaction waves respectively as depicted in Figure 2.1(c).

The test time for data acquisition begins after the shock wave passes the test section and ends before the next disturbance passes over the test point, changing flow properties in region 2. Several factors influence the arrival of the next disturbance. This disturbance could be either the shock wave reflected back from the driven end, the rarefaction wave reflected back from the driver end, or the contact surface, whichever arrives first at the test section. Figure 2.1(d) provides a scheme to determine the test time considering the various disturbances.

The flow properties of region 2 can be determined from the known properties of region 1 once the shock speed is known. Shock strength depends on the initial conditions of the gases confined in the driver and driven sections. Using normal shock theory for ideal gases, Gaydon and Hurle (1963:20) and Glass (1958:78) derived an implicit relationship to determine shock Mach number from the static pressure ratio, P_4/P_1, across the diaphragm

<center>2.2</center>

$$\frac{P_4}{P_1} = \frac{2\gamma_1 M_s^2 - \gamma_1 + 1}{\gamma_1 + 1} \left[1 - \frac{\gamma_4 - 1}{\gamma_1 + 1} \frac{a_1}{a_4} \left(M_s - \frac{1}{M_s} \right) \right]^{\frac{-2\gamma_4}{\gamma_4 - 1}} \tag{2.1}$$

where M_S is the shock wave Mach number defined as U_S / a_1, U_S is the velocity of the shock wave, a_1 is the sonic velocity defined as $(\gamma_1 R_1 T_1)^{1/2}$, γ is the ratio of specific heats, R is the gas constant, and T is the absolute static temperature. Flow properties in region 2 are determined by the following equations:

For pressure, from Gaydon and Hurle (1963:72).

$$\frac{P_2}{P_1} = \frac{2\gamma_1 M_s^2 - (\gamma_1 - 1)}{\gamma_1 + 1} \tag{2.2}$$

For temperature, from Gaydon and Hurle (1963:17).

$$\frac{T_2}{T_1} = \frac{\left(\gamma_1 M_s^2 - \frac{\gamma_1 - 1}{2} \right)\left(\frac{\gamma_1 - 1}{2} M_s^2 + 1 \right)}{\left(\frac{\gamma_1 + 1}{2} M_s \right)^2} \tag{2.3}$$

2.3

For velocity, from Gaydon and Hurle (1963:25).

$$U_2 = \frac{2a_1}{\gamma_1 + 1}\left(M_S - \frac{1}{M_S}\right)$$
(2.4)

Density is determined using the ideal gas law.

$$\rho_2 = \frac{P_2}{R_1 T_1}$$
(2.5)

2.2 Mixture of Gases

To obtain density ratios greater than one a mixture of helium and air was used in the driven section of the shock tube. Accurate determination of flow properties behind the shock wave requires exact knowledge of the ratio of specific heats and the gas constant for the mixture. Two assumptions were made:

1. The mixture is composed by perfect gases that do not interact chemically.

2. The constituent gases are in thermal equilibrium with each other at the mixture temperature T_1.

The two above conditions satisfy the requirements for Dalton's law, that is, the static pressure of the mixture is equal to the sum of the partial pressures of each constituent. Mathematically

2.4

$$P = \sum_{i=1}^{n} P_i \qquad (2.6)$$

According to Zucrow and Hoffman (1976:49), the mole fraction of the ith species, χ_i , and the molecular weight of the mixture, MW_{mix}, are defined as

$$\chi_i = \frac{P_i}{P} \qquad (2.7)$$

$$MW_{mix} = \sum_{i=1}^{n} \chi_i MW_i \qquad (2.8)$$

where MW_i is the molecular weight of the ith constituent. The mixture gas constant, R_{mix}, the mixture specific heat, $c_{p,mix}$, and the mixture ratio of specific heats, γ_{mix}, are computed from

$$R_{mix} = \frac{\bar{R}}{MW_{mix}} \qquad (2.9)$$

2.5

$$c_{P_{mix}} = \sum_{i=1}^{n} \chi_i c_{P_i} \frac{MW_i}{MW_{mix}} \tag{2.10}$$

$$\gamma_{mix} = \frac{c_{P_{mix}}}{c_{P_{mix}} - R_{mix}} \tag{2.11}$$

where $\bar{R}$ is the universal gas constant. Other mixture properties such as viscosity and thermal conductivity are calculated by a semi-empirical formula proposed by C.R. Wilke and quoted by White (1991:35)

$$\mu_{mix} = \sum_{i=1}^{n} \frac{\chi_i \mu_i}{\sum_{j=1}^{n} \chi_j \Phi_{ij}} \tag{2.12}$$

where

$$\Phi_{ij} = \frac{\left[1 + \left(\frac{\mu_i}{\mu_j} \right)^{1/2} \left(\frac{MW_j}{MW_i} \right)^{1/4} \right]^2}{\left[8 \left(1 + \frac{MW_i}{MW_j} \right) \right]^{1/2}} \tag{2.13}$$

For mixture thermal conductivity, k_{mix}, equations (2.12) and (2.13) are used, but μ is replaced by k (White,1991:36).

2.6

2.3 Flat Plate Boundary Layer

As the shock wave and the induced flow behind it traverse the test section, transient and steady-state boundary layers develop on the test plate and shock tube walls because of the friction between the fluid particles and the solid surfaces. The point of initiation of the transient boundary layer moves with the shock wave, growing upstream. Schlichting (1968:441) stated that the transient nature of this unsteady boundary layer is similar to an impulsively started flat wall, but slightly thicker.

Similarly, after the shock wave passes the plate leading edge, the steady-state boundary layer is formed. It begins with a laminar layer which is detached near the plate stagnation point. Reattachment of the boundary layer occurs immediately, following transition to a fully developed turbulent layer. At some point on the surface of the plate a transition occurs from the flow conditions that characterize the transient boundary layer, to those of a steady-state layer that develops from the leading edge as depicted in Figure 2.2. Finally, after the shock wave has completely traversed the test plate, the steady-state layer overcomes the transient boundary layer imposing a turbulent boundary layer all over the plate and establishing the test conditions.

Besides a velocity boundary layer, a thermal boundary layer is developed whose effects influence the heat transfer mechanism between the fluid and the solid surface. Inside the velocity boundary layer, velocity decreases from the mainstream value to zero at the wall, while for the thermal boundary layer temperature changes from the freestream value to the wall temperature. For gases, the thickness ratio of momentum boundary layer to thermal boundary layer is slightly less than unity, so both thicknesses

can be assumed equal (Arpaci and Larsen, 1984:101). Figure 2.2 also depicts typical velocity and temperature profiles.

2.4 Heat Transfer through the Boundary Layer

To provide an effective cooling protection, heat flux between the hot gas stream and test plate must be estimated. According to Arpaci and Larsen (1984:3), there are two basic modes for the occurrence of heat transfer, diffusion and radiation. At a microscopic level, diffusion represents the exchange of energy between adjacent particles, whereas radiation is the transportation of energy through electromagnetic waves between separate particles. Diffusion with bulk motion is the predominant heat transfer mechanism for moving media, and for customary reasons this phenomenon is known as convection.

The convective heat transfer at the solid-fluid interfaces can be described using Newton's law of cooling

$$q = h(T_{aw} - T_w) \qquad (2.14)$$

where q is the convective heat flux, h is the local heat transfer coefficient, T_{aw} the adiabatic wall temperature, and T_w the local wall temperature.

The adiabatic wall temperature is the temperature that would be attained by the surface of an adiabatic or insulating wall. According to Hill and Peterson (1992:546), "the temperature rise accompanying stagnation is large enough that the viscous slowing

down process is not exactly adiabatic. That is, there is significant heat transfer from the low speed (high T_∞) fluid near the wall to the higher speed (lower T_∞) fluid farther from the wall." Therefore, fluid stagnation temperature at the wall is less than that of the freestream. Figure 2.3 shows a scheme of the nature of these parameters.

In the absence of film cooling, the magnitude of T_{aw} is determined by the recovery factor, r_c, which is defined by

$$r_c = \frac{T_{aw} - T_\infty}{T_{o_\infty} - T_\infty} \qquad (2.15)$$

where

$$T_{o_\infty} - T_\infty = \frac{U_\infty^2}{2c_{p_\infty}} \qquad (2.16)$$

or equally

$$T_{aw} = T_\infty \left[1 + r_c \frac{\gamma_1 - 1}{2} M_\infty^2 \right] \qquad (2.17)$$

2.9

To apply equations (2.15) through (2.17) in this study, parameters such as U_∞, $c_{p\infty}$, T_∞, and M_∞, have to be replaced by U_2, $c_{p,mix}$, T_2, and M_2 respectively. Where M_2 is the induced flow Mach number defined as U_2/a_1. According to Hill and Peterson (1992:395), the adiabatic wall temperature for the film cooling case can be quite different from that with no injection of coolant air. The recovery factor for turbulent boundary layers is given by (Eckert, 1972:422)

$$r_c = \sqrt[3]{Pr} \qquad (2.18)$$

where Pr is the Prandtl number defined as $c_p\mu/k$, k being the thermal conductivity of the fluid.

The heat transfer through a turbulent steady-state boundary layer for the case of a flat plate with constant wall temperature and flow properties, no film cooling, and no freestream turbulence is given by (Kays and Crawford, 1980:213)

$$St\,Pr^{0.4} = 0.0287\,Re_x^{-0.2} \qquad (2.19)$$

where St and Re_x are the Stanton and Reynolds number respectively, defined as

$$St = \frac{h_o}{\rho_2 U_2 c_{p_{mix}}} \qquad (2.20)$$

2.10

$$Re_x = \frac{(U_2 \rho_2 x)}{\mu_{mix}} \qquad (2.21)$$

where h_o is the heat transfer coefficient with no film cooling, ρ_2 is the induced flow density, and x is the downstream distance from the plate stagnation point at the leading edge.

For the case of high speed flows, fluid properties such as density, specific heat, Prandtl number, and viscosity vary within the boundary layer due to compressibility effects and temperature gradients. Eckert (1955:585,586) found that heat transfer parameters within the turbulent layer are well predicted using constant-property relationships, but with the above properties evaluated at a reference temperature, T^*, defined as

$$T^* = 0.5(T_2 + T_w) + 0.22 r_c \frac{\gamma_1 - 1}{2} M_2^2 T_2 \qquad (2.22)$$

Although the recovery factor is a function of T^* (Prandtl number evaluated at T^*), the convergence of equation (2.22) is rapid. According to White (1991:31), Prandtl number is a function of the ratio of specific heats

$$Pr = \frac{4\gamma_1}{7.08\gamma_1 - 1.8} \qquad (2.23)$$

As the mainstream turbulence increases, mixing inside the boundary layer also increases supporting a strong energy diffusion, thus increasing heat transfer. Hancock and Bradshaw (1983:289) determined that for every 1 percent increase in turbulence, heat transfer is increased 5 percent, that is

$$\frac{St}{St_{(Tu=0)}} = 1 + 0.05\,Tu \qquad (2.24)$$

where Tu is the turbulence intensity in percentage.

2.5 Shock Dynamics

Analysis of plane waves in uniform media can be easily understood using linear theory. However, in more dimensions or in nonuniform media even linear theory becomes complicated. Nonuniform media such as changes in cross section modify the flow conditions behind the wave. This occurs inside the shock tube when the tube cross section is reduced by the presence of the test model.

One approach to solve this problem is by using small perturbation theory. The objective then is to obtain a relationship determining how the Mach number of the transmitted shock depends on the local cross section area. Although the flow is not one dimensional, taking averaged flow properties across the tube provides a good approximation. For small area changes, $(A-A_o)/A_o \ll 1$, Whitham (1974:263-270)

2.12

determined the following relationships

$$\frac{A-A_o}{A_o} = -g(M_o)(M-M_o)$$
(2.25)

$$g(M) = \frac{M}{M^2-1}\left(1+\frac{2}{\gamma+1}\frac{1-\mu^2}{\mu}\right)\left(1+2\mu+\frac{1}{M^2}\right)$$
(2.26)

$$\mu^2 = \frac{(\gamma-1)M^2+2}{2\gamma M^2-(\gamma-1)}$$
(2.27)

where A_o is the shock tube cross-sectional area, A is the given tube cross-sectional area, M is the transmitted shock wave Mach number, and M_o is the undisturbed shock wave Mach number. In order to apply equations (2.25) through (2.27) M_o must be replaced by M_s, and γ by γ_1.

2.6 Electrical Analog for Heat Transfer

Calculation of wall heat flux requires the processing of surface temperature history. The flow of heat into a semi-infinite material is similar to the current flow into a medium with distributed capacity and resistance. The one-dimensional heat transfer partial differential equation can be written as

2.13

$$\frac{\partial T}{\partial t} = \frac{k}{\rho c_p} \frac{\partial^2 T}{\partial x^2}$$

(2.28)

while the one-dimensional current transmission partial differential equation can be written as

$$\frac{\partial V}{\partial t} = \frac{1}{rc} \frac{\partial^2 V}{\partial x^2}$$

(2.29)

The development of the analogy between these two equations to the electrical analog for transient heat transfer can be referenced to Schultz and Jones (1973:37,38,111). The parallelism between heat and current flow results in an equation relating the wall heat flux, q, and the output voltage from the electrical analog, V_{out}.

$$q = \left(\rho \, c_p k\right)^{1/2}_{subs} \left(\frac{r}{c}\right) \frac{1}{V_o \alpha} \frac{V_{out}}{GR_1}$$

(2.30)

where ρ, c_p, and k are properties of the thin-film gage substrate; r and c are analog block resistor and capacitor values; V_o is the applied d.c. voltage to the thin film of temperature coefficient α; and V_{out} is G times the voltage V'_{out} of the current flowing through the resistor R_1. Figure 2.4 presents a scheme of the electrical analog.

2.14

III. Experimental Apparatus

As stated above, this study is an extension of the research performed by Eads (1992). Consequently, most of the facilities and equipment are similar. Changes were made to improve film cooling and heat transfer analysis. These were (1) use of a pressure tank to maintain a suitable coolant air supply free of instabilities, (2) use of a second plate made of corian to simulate an adiabatic wall, and (3) use of a pressure transducer located on the upper surface of the corian plate to measure the pressure behind the shock wave.

3.1 Shock Tube

The AFIT low-pressure shock tube, located in room 146 Building 640, was used in this research. This shock tube consists of two sections, a driver section with a length of 1.22 m, and a driven section with a length of 6.10 m separated by a mylar diaphragm. Only 127.0 μm thick mylar was used for all the test runs to be consistent with previous studies. Selection of mylar thickness is based on the required wave strength. A scheme of the shock tube is depicted in Figure 3.1.

The driver section is movable to permit the removal of the ruptured diaphragm and shattered pieces, and to place a new sheet of mylar. Driver section, driven section, and the sheet of mylar are securely locked together by means of hand pump-driven hydraulic actuators.

3.1

The pressure of the driver section (P_4) is measured by a calibrated bourdon tube pressure gage in inches of mercury. The pressure of the driven section (P_1) was measured by a MKT Baratron Portable Vacuum Standard Type PVS-2 in psia. To pressurize the driver section, dry-filtered compressed air from the 100 psig-maximum facility air compressor is used. Following the pressurization of the driver section, the diaphragm is ruptured using a pneumatically actuated plunger to start the shock.

The cross section of the shock tube is 0.1016 m wide by 0.2032 m high. The test plate is located horizontally at the vertical mid-plane of the shock tube (0.1016 m), and longitudinally at 3.73 m from the diaphragm interface.

3.2 Instrumented Flat Plate

Three test models were used, one aluminum plate and two corian plates. Corian is a registered mark of Dupont, and its properties are similar to those of ceramic materials. The aluminum plate was previously used in the research done by Eads (1992). This plate has one laterally-centered row of 41 one-millimeter-diameter coolant injection holes. The holes are laterally spaced at two diameters, and have a length-to-diameter ratio of 3.05 with an injection angle of 35 degrees with respect to the downstream direction.

The round-nosed aluminum plate is 0.0192 m thick, 0.1016 m wide, and 0.648 m long. On the upper surface, an o-ring-sealed plate insert is instrumented with seven platinum thin-film heat flux gages downstream from the injection holes (see Figure 3.2). The heat flux gages were surface mounted, and placed symmetrically with respect to the

3.2

longitudinal axis of the plate.

Two corian plates were investigated. One was designed with 15 two-millimeter-diameter injection holes (a 46 percent increase in total cross-sectional injection area with respect to the aluminum plate), and the second with no injection holes. The holes are laterally spaced at two diameters, and have a length-to-diameter ratio of 3.5. The injection angle was 35 degrees with respect to the downstream direction to be consistent with previous studies.

Coolant injection holes and heat flux gages have a fixed positional configuration. Heat flux gage layouts are depicted in Figure 3.2 and 3.3. An additional pressure transducer was placed flush with the upper surface, next to the heat flux gages, with the purpose of measuring the pressure increase behind the shock wave. The use of bigger injection holes allowed positioning the first heat flux gage relatively closer (based on ratio X/D) to the injection holes as compared to the respective heat flux gage for the aluminum plate.

Both corian plates have a semi-cylindrical leading edge, and are 0.0192 m thick, 0.1016 m wide, and 0.1524 m long. The corian plates are shorter because they are fastened to an aluminum afterbody to complete the required length of 0.648 m. Since the aluminum afterbody is located downstream of the heat flux gages, it has minimal influence on the measured heat transfer mechanism.

The aluminum and corian plates used in film cooling studies have two internal chambers, the film-cooling chamber, and the instrumentation chamber. The film cooling chamber was instrumented with a pressure transducer to register coolant-air stagnation

3.3

pressure. The instrumentation chamber served to conduct the instrument leads out of the test plate through two 0.013-meter-O.D. tubes. Coolant air was supplied to the film cooling chamber through two 0.0095-meter-O.D. x 0.0079-meter-I.D. tubes.

The corian plate with no coolant injection holes has only one internal chamber for instrumentation, similar to the previously described instrumentation chamber. This plate was used to obtain wall heat flux with no film cooling. The measured heat flux served as a reference to determine film cooling effectiveness. For the case of the aluminum plate, wall heat flux with no film cooling was obtained sealing the injection holes with epoxy.

3.3 Film Cooling System

The film-cooling supply and control system is depicted in Figure 3.4. Dry filtered air is supplied to a pressure tank from the 100 psig compressor facility. Pressure level inside the tank was controlled by a Grove Instruments dome valve with reference pressure set by a high-pressure helium cylinder. Two reasons demanded the use of a pressure tank, (1) to reduce flow instabilities due to a sudden increase of back pressure as the shock wave passes by the injection holes, and (2) to eliminate the dynamic response of the dome valve.

Film cooling was manually activated before the rupture of the diaphragm by energizing a solenoid valve. In order to minimize response time of the coolant flow to changing conditions in the shock tube, the solenoid valve was located very close to the test plate. A pressure transducer located in the plate coolant cavity insured accurate

3.4

determination of coolant hole pressure ratio for injection velocity determination.

3.4 Shock Tube Gas Control System

The gas fill and control system for the driven section is depicted in Figure 3.5. Vacuum was created inside the driven section by a W.C. Heraeus type E-70 vacuum pump, which is driven by a 3-phase motor. A push on/push off control switch starts the motor-pump system when required. The vacuum pump is connected to the shock tube through a 0.051-meter-I.D. line, containing a 1/4-turn valve. The 1/4-turn valve closed the pump off from the shock tube and sealed the pump from leaking back into the evacuated driven section.

Two high-pressure bottles supplied helium to the driven section. Pressure supply was set to 50 psi by means of a pressure regulator. Upon evacuation of the driven section to a given pressure (6 to 7 psia), a 0.0254-meter orifice solenoid valve was activated allowing helium to flow through the lines into the shock tube at three locations to enhance mixing with air in the driven section. Once the required amount of helium was supplied, the solenoid valve was closed and a hand-operated valve opened. Opening this valve allowed air flow into the driven section through the same three locations bringing the driven section up to atmospheric pressure, thus further promoting mixing of the helium and air.

3.5 Data Acquisition System

The following description of the Data Acquisition System was taken from Eads (1992). The Nicolet System 500 Data Acquisition System is a high-speed analog/digital recorder. This system registers the output voltages from the instruments, heat flux gages and pressure transducers, through the use of 20 input channels.

The Data Acquisition Unit Pedestal has a Nicolet model 540 CPU and five model 514 digitizer boards with four channels each. Lack of a digitizer board battery reduced the amount of available channels from 20 to 16. Figure 3.6 presents a diagram of the data acquisition set-up. The data is acquired, stored, and analyzed with Nicolet System 500 Software version 6.1 running on a DTK model KEEN-2000 80386 computer with Windows* 3.0.

Data can be acquired by triggering automatically, continuously, by individual board trigger levels, or by all boards triggering off of a bus trigger set by one or a combination of other channels. In this study the last option was used, that is, all boards were triggered off of a bus trigger set by the input voltage to the channel corresponding to the forward pressure transducer. As soon as the shock wave passes over the forward pressure transducer, output voltage from this instrument is increased, thus giving a valid trigger to begin the data acquisition sweep for all the boards.

Each channel can be labeled with units, and multiplied by a scalar and added to an offset, giving output in actual calibrated engineering units. For this study 5,000 data points were sampled per channel at a rate of 500,000 samples per second.

3.6 Instrumentation

3.6.1 Pressure Transducers.

A total of four Endevco pressure transducers were used, two absolute pressure transducers Model 8530A-100 and two differential pressure transducers Model 8510B-50. The two absolute transducers plus one differential transducer were used for measuring shock-tube driven section pressure, while the remaining differential pressure transducer was used for measuring film-cooling supply pressure. The transducers were connected to Endevco Model 4423 Signal Conditioner and power supply modules with four-wire shielded cables. Location of transducers in the shock tube can be seen in Figure 3.1.

3.6.2 Thin-Film Resistance Gages.

The Medtherm thin-film resistance heat flux gages are made of a platinum film 0.4 mm wide and 0.1 μm thick deposited on a Corning Pyrex 7740 substrate. Figure 3.7 shows a scheme of a typical thin-film gage. Location of the thin-film gages for the aluminum and corian test plates can be visualized in Figures 3.2 and 3.3. The gages were flush-mounted, fastened to the test models by small 1-72 UNF-3A nuts, and connected to a constant voltage Wheatstone bridge.

3.6.3 Bridge/Amplifier/Analog.

In a Wheatstone bridge circuit one thin-film gage replaces one leg of the bridge. The remaining circuit is completed with a Transamerica Model PSC 8115 bridge supply module with 2.5 V dc voltage applied to the bridge.

Temperature changes are sensed by a variation in the resistance of the thin-film gage, thus unbalancing the bridge. The output voltage change of the unbalanced bridge

is very low and must be amplified and filtered. PSC 8015-1 high gain differential DC amplifier modules were used for this function. The amplified output was converted into voltage proportional to heat flux using the heat transfer analog circuits designed by Rockwell (1989). For further information about bridge/amplifier/analog connections and analog circuits the reader could refer to Eads (1992) and Rockwell (1989). Only seven analog circuits were built, this imposed a restriction on the number of thin-film gages that can be mounted on the test models.

IV. Experimental Procedure

Confidence on experimental works is based on the accuracy of collected data. In order to have reliable data, sensing element properties and its dynamic behavior must be well known. Determination of such parameters is called calibration, which is a very tedious and time consuming routine. Since the time schedule for this research was very tight, thin-film gage and pressure transducer calibration constants were directly taken from Eads' research (1992), thus giving enough time for data processing. Previous studies (Gul, 1991:45; Rockwell, 1989:5.11) have shown that errors as high as 20 percent can be introduced by using theoretical values for the bulk thermal diffusivity, $(\rho c_p k)^{1/2}$, of the thin-film gages.

4.1 Instrument Calibration

The reader could refer to Eads (1992:4.1-4.8) for detailed information on instrument calibration procedures. The following sections just present calibration constant results and the relationships used to obtain them.

4.1.1 Calibration for Thin-Film Gage Temperature Coefficient. Temperature coefficients are summarized in Table 4.1 for the seven heat flux gages.

Table 4.1

Temperature Coefficients of the Heat Flux Gages[a]

Gage Number	Gage Serial Number	Temp. Coef. $(V_o\alpha)$ Volt/K
1	702	0.04017
2	705	0.03162
3	706	0.03176
4	710	0.03387
5	768	0.04701
6	703	0.02919
7	824	0.05566

[a] Table taken from Eads (1992:4.2)

4.1.2 Calibration of Heat Flux Gages for Bulk Thermal Diffusivity. Bulk thermal diffusivity for the Coring Pyrex 7740 substrate, defined as $(\rho c_p k)^{1/2}$, is obtained using the calibration technique given by Schultz and Jones (1973:23-25). They developed a relationship to determine the substrate property based on its ohmic heating behavior with the aid of a fluid of known thermal properties such as glycerine.

$$(\rho\, c_p k)^{1/2}_{subs} = \frac{(\rho\, c_p k)^{1/2}_{gly}}{\dfrac{(\Delta V / t^{1/2})_{air}}{(\Delta V / t^{1/2})_{gly}} - 1}$$

(4.1)

where the thermal diffusivity of glycerine is equal to 930 $J/m^2 K\ sec^{1/2}$.

Table 4.2 contains the results of the above calibration procedure for the seven thin-film gages.

Table 4.2

Bulk Thermal Diffusivity of the Heat Flux Gages[a]

Gage Number	Serial Number	$\Delta V_{air}/t^{1/2}$ Volt/sec$^{1/2}$	$\Delta V_{gly}/t^{1/2}$ Volt/sec$^{1/2}$	$(\rho C_p k)^{1/2}$ J/m^{2}Ksec$^{1/2}$
1	702	12.802	8.027	1563
2	705	8.678	5.402	1534
3	706	11.689	7.258	1525
4	710	12.780	8.028	1571
5	768	11.390	7.118	1551
6	703	11.906	8.309	2151
7	824	23.387	14.229	1447

[a] Table taken from Eads (1992:4.5)

All values are within a ± 5 percent deviation from the theoretical bulk diffusivity for Pyrex which is 1520 J/m^{2}Ksec$^{1/2}$, except for gage number 6. However, previous heat transfer measurements for gage 6 were in accordance with this result.

4.1.3 Calibration of Heat Flux Analog. Equation (2.30) shows that the output of the electrical analog is proportional to the heat flux through the thin-film gage. In this equation there is one value left to be calibrated, $(r/c)^{1/2}/(R_1 G)$ from the analog circuits. Figure 2.4 presents a scheme of the analog circuits. Table 4.3 contains the calibration

constant of the analog circuits.

Table 4.3

Calibration Constant of Analog Circuits[a]

Circuit Number	Serial Number	$(r/c)^{1/2}/(R_1G)$ $(rad/sec)^{-1/2}$	Correlation
1	31-280	0.2890	0.9994
2	32-200	0.2776	0.9991
3	31-850	0.2917	0.9992
4	31-150	0.2953	0.9994
5	31-790	0.3138	0.9993
6	31-870	0.3204	0.9991
7	32-100	0.2920	0.9991

[a] Table taken from Eads (1992:4.7)

4.1.4 Calibration of Pressure Measuring Instruments. Appendix A contains calibration plots showing instrument output voltage versus input pressure. The transducers and bourdon tube gage were calibrated in positive gage pressure.

4.2 Preparing the Shock Tube

Preparing the driven section to insure an accurately known air-helium mixture was done as follows. The driven section was evacuated with a vacuum pump to check for leaks. This procedure revealed the existence of numerous points of leakage. All of the spots where leakage was found were sealed with modeling clay, and all the screws and

bolts were well tightened. The leakage rate of the driven section was determined through recording the pressure history from the pressure transducers located inside the shock tube.

This leakage was taken into account when the driven section was charged with air and helium as described in Section 3.4. Figures 4.1 and 4.2 present plots of the pressure history for the forward pressure transducer performed on two different occasions. The pressure variation rate was determined using a least square linear fit for the pressure range shown in each plot.

4.3 Shock Generation

To compare collected data, the flow conditions affecting the phenomena being studied must be approximately the same. Investigating film cooling processes for a given set of flow conditions requires repeatability of the Mach number for the generated shock wave. Several factors can influence the attainable shock strength, such as driver-to-driven pressure ratio, diaphragm expansion, and ambient temperature.

The driver section pressure was measured using a bourdon type pressure gage in inches of mercury. The pressurization of this section was done slowly to avoid pressure fluctuations and to have an even stretching of the mylar diaphragm. Enough time (approx. 2 minutes) to stabilize the required driver pressure was taken into account for each run.

The driven section pressure was measured with the MKS Baratron Portable Vacuum Standard Type PVS-2 in psia once the driver pressure was attained. Ambient

4.5

temperature was measured with a mercury bulb-type thermometer with a resolution of 0.1°C. Usually for a given set of conditions the ambient temperature and the atmospheric pressure changed within a 0.5 percent range. For test runs with film cooling, coolant air supply was activated just before rupturing the diaphragm.

4.4 Data Collection and Reduction

All the thin-film gage output voltages were amplified and filtered by the programmable Transamerica PSC 8015-1 amplifier modules, converted into heat flux potential by the electrical analog circuits, and recorded by the Nicolet System 500 Data Acquisition System. At least four channels in the Nicolet Data Acquisition System were available to directly record the amplified output voltage from the thin-film gages, which is proportional to the wall temperature. The PSC amplifier modules were set to the following signal conditioning settings, operational mode in AMPD, filter at 10 KHz, and gain at 250.

Pressure transducer output voltages were amplified and conditioned by the Endevco Model 4423 Signal Conditioners, and recorded by the Nicolet Data Acquisition System. The settings were, for the forward pressure transducer a gain of 50, for the rear pressure transducer a gain of 20, for the film cooling pressure transducer a gain of 50, and for the plate pressure transducer a gain of 50. Data acquisition was initiated by an output voltage signal from the forward pressure transducer, with a 1 msec pre-trigger. The time interval between data was 2 μsec, and 5000 data samples were acquired simultaneously for each channel.

Data were reduced and averaged by the fortran computer programs SHOCK.FOR and AVERAGE.FOR, respectively on the AFIT VAX/VMS mainframe. The above two computer programs could not be run on the Nicolet computer because of the lack of a fortran compiler. SHOCK.FOR was developed to automate the data analysis and reduction process, based on STFCRT.FOR written by Eads, while AVERAGE.FOR was developed to average the output of the rear and film cooling pressure transducers. The two computer programs were run independently to ease calculation procedures.

4.5 Film Cooling

The flow through injection holes may be considered adiabatic, but it is never isentropic because of the internal friction, wall friction, and eddies accompanying the flow. Checking the coolant flow conditions using the relationships for Fanno flow showed that the entropy increase was very small for all test conditions. Therefore, this flow could be well approximated as an isentropic expansion for ease of calculation.

With the film-cooling chamber pressure, P_{oc}, and the measured pressure behind the shock wave, P_2, the velocity of the coolant flow, U_c, is determined by the isentropic relationship

$$U_c = \left[\frac{2\gamma_{air} R_{air} T_{oc}}{\gamma_{air}-1} \left[1 - \left(\frac{P_2}{P_{oc}} \right)^{\frac{\gamma_{air}-1}{\gamma_{air}}} \right] \right]^{1/2} \qquad (4.2)$$

4.7

where T_{oc} is assumed to be equal to the ambient temperature T_1 since air at ambient temperature was supplied to the film-cooling chamber. The density and the temperature of the expanded coolant flow are determined by

$$\rho_c = \frac{P_{oc}}{R_{air} T_{oc}} \left(\frac{P_{oc}}{P_2} \right)^{\frac{-1}{\gamma_{air}}}$$

(4.3)

$$T_c = T_{oc} \left(\frac{P_2}{P_{oc}} \right)^{\frac{\gamma_{air}-1}{\gamma_{air}}}$$

(4.4)

V. Data

5.1 Test Identification

More than 170 tests, including repetition tests, were performed for this research. Each test was unique depending on the conditions involved during its execution. Therefore, test results such as flow conditions, film cooling parameters, and heat fluxes were also unique, being dependent on a group of shock tube and test plate conditions. To identify each test, an alphanumerical code was used. Each test code was formed by three characters, the first character was an alphabetical prefix and the remainder formed a numerical affix, i.e., A12.

To be accurate, each test was repeated at least three times and its results then averaged. Those repetition tests were codified with the same numerical affix but with a different alphabetical prefix, i.e., A12, B12, C12. The averaged test results were codified with five characters, the three first characters corresponded to an alphabetical prefix made up by each alphabetical prefix test code; while the other two characters formed the same numerical affix test code, i.e., ABC12.

Results for the aluminum and corian plates, with film cooling or no film cooling, can be easily recognized by the different alphabetical prefixes used. The results for both plates are presented in Appendices D, E, and F. Appendix D contains test conditions, Appendix E presents film cooling parameters and flow conditions, and Appendix F presents heat transfer parameters for all the tests performed.

5.2 Test Conditions

Helium partial pressure was calculated by the pressure difference registered by the MKS Vacuum Standard, when helium was injected. The resultant pressure was then adjusted by an amount equal to the product of the shock-tube leaking rate and the time required to add the helium to the shock tube. Helium injection was started when the vacuum pressure inside the shock-tube driven section was in the range of 6 to 7 psia, requiring between 13 to 30 seconds to perform this operation. All the other variables were directly measured by their corresponding gages. Results are presented in Appendix D.

5.3 Film Cooling Parameters and Flow Conditions

Appendix E contains film cooling parameters and flow conditions calculated using Equations (2.1) through (2.13) and (4.2) through (4.4). A description of the procedure used to determine these variables is detailed below.

- The ratio of specific heats, γ_1, was calculated from Equation (2.11); while the sonic velocity, a_1, was calculated from $(\gamma_1 R_1 T_1)^{1/2}$.

- The shock Mach number, M_s, was calculated using the measured time required for the shock to travel between the forward and rear pressure transducer, $M_s = U_s/a_1$.

- The theoretical shock Mach number, $M_{s,theo}$, was determined using Equation (2.1).

- The pressure of the induced flow behind the shock wave, P_2, was experimentally determined. In this case, the output signal from the rear pressure transducer for the aluminum plate,and from the plate pressure transducer for the corian plate was

averaged once the shock wave established the test conditions over the entire test section. The resultant average pressure P_2 for the aluminum plate had to be reduced by 6 percent as a consequence of the offset position of the rear pressure transducer compared to the location of the test model. This correction factor was determined based on information for the corian plate which showed that P_2 measured by the rear pressure transducer was higher than P_2 measured by the plate pressure transducer .

- The temperature of the induced flow, T_2, was determined using Equation (2.3) and the measured shock Mach number.

- The density of the induced flow, ρ_2, was determined by Equation (2.5).

- The velocity of the induced flow, U_2, was determined by Equation (2.4).

- The induced flow Mach number, M_2, was determined by $M_2 = U_2/(\gamma_1 R_1 T_2)^{1/2}$.

- The coolant stagnation pressure for both plates, P_{oc}, was experimentally determined by averaging the output signal from the film cooling pressure transducer.

- The density of the coolant flow, ρ_c, required to compute the density ratio, DR, was determined using Equation (4.3), where $T_{oc} = T_1$, $R_{air} = 287$ J/KgK, and $\gamma_{air} = 1.4$.

- The exit velocity of the coolant flow, U_c, required to compute the velocity ratio, VR, was calculated using Equation (4.2).

- The blowing ratio, B, was determined by the product of the density ratio and the velocity ratio.

- The momentum ratio, I, was determined by the product of the blowing ratio and the velocity ratio.

5.4 Heat Flux Parameters

Appendix F is divided into three sections. The first section, contains the thermodynamic properties of the induced flow behind the shock wave. Details of the procedure used to determine these properties are indicated below.

- For all the tests, the wall temperature, T_w, was assumed to be equal to the mixture temperature T_1.

- The helium-air mixture Prandtl number, Pr, was determined using Equation (2.23).

- The recovery factor was determined using Equation (2.18).

- The mixture specific heat, c_p, was determined using Equation (2.10).

- The reference temperature, T^*, was determined using Equation (2.22).

- The mixture viscosity, μ, was determined using Equation (2.12) with the helium and air viscosities evaluated at the reference temperature.

- The mixture thermal conductivity, k, was determined using the equivalent form of Equation (2.12) with the helium and air thermal conductivities evaluated at the reference temperature.

- The adiabatic wall temperature, T_{aw}, was determined using Equation (2.17).

The second section contains heat transfer parameters for the no film cooling case. These heat transfer parameters were required to compute the theoretical heat flux for both plates with no coolant injection. Details of the methods used to determine these parameters are indicated below.

- The local Reynolds number, Re_x, was determined using Equation (2.21), where the mixture viscosity was evaluated at the reference temperature T^*.

- The theoretical Stanton number with no turbulence, St_{th}, was evaluated using Equation (2.19). This result was then adjusted to a 9.5 percent turbulence level according to Equation (2.24).

- The theoretical heat transfer coefficient with no film cooling, $h_{o,th}$, was determined using Equation (2.20), where the flow density, ρ_2, was evaluated at the reference temperature.

- The theoretical heat flux with no film cooling, $q_{o,th}$, was determined using Equation (2.14).

- The measured gage heat flux with no film cooling, q_o, was obtained by averaging the output response from each thin-film gage.

- The heat transfer coefficient, h_o, was determined using Equation (2.14).

- The Stanton number, St_o, was determined using Equation (2.20).

The third section of Appendix F contains the average heat flux for each thin-film gage in both plates, with film cooling and no film cooling. When averaging the output signal from a gage or a transducer was required, a time interval was defined. The definition of this time interval was made based on the stability of the signal within the specified range. Three factors were basically required, a constant coolant supply pressure, a constant mainstream pressure, and a stable heat flux through the turbulent boundary layer. The averaging process was executed by the computer programs AVERAGE.FOR and SHOCK.FOR. With zero reference for the time scale taken as the instant when the shock passed by the forward pressure transducer, the time intervals defined, as presented by Tables 5.1, 5.2, and 5.3, were the following:

5.5

Table 5.1

Time Intervals for Averaging the Output from the Film Cooling
Pressure Transducer and Heat Flux Gages in the Aluminum Plate

Test	Time Interval (msec)	
	From	To
H03,H04,H05,H06,H07,J02,J03,J04,J05,J06 J07,K02,K03,K04,K05,K06,K07,T02,U02,V02	3.792	5.012
H11,H12,H13,H14,H15,H16,J11,J12,J13,J14 J15,J16,K11,K12,K13,K14,K15,K16	3.662	4.792
H21,H22,H23,H24,H25,H26,J21,J22,J23,J24,J25 J26,K21,K22,K23,K24,K25,K26,T21,U21,V21	3.702	4.852
H31,H32,H33,H34,H35,H36,J31,J32,J33,J34 J35,J36,K31,K32,K33,K34,K35,K36	3.612	4.742
T11,U11,V11	3.400	4.800
T31,U31,V31	3.500	4.600

Table 5.2

Time Intervals for Averaging the Output from the
Rear Pressure Transducer in the Aluminum Plate

Tests	Time Interval (msec)	
	From	To
H03,H04,H05,H06,H07,J02,J03,J04,J05,J06 J07,K02,K03,K04,K05,K06,K07,T02,U02,V02	5.100	6.100
H11,H12,H13,H14,H15,H16,J11,J12,J13,J14,J15 J16,K11,K12,K13,K14,K15,K16,T11,U11,V11	4.600	5.600
H21,H22,H23,H24,H25,H26,J21,J22,J23,J24,J25 J26,K21,K22,K23,K24,K25,K26,T21,U21,V21	5.200	6.200
H31,H32,H33,H34,H35,H36,J31,J32,J33,J34,J35 J36,K31,K32,K33,K34,K35,K36,T31,U31,V31	4.800	5.800

Table 5.3

Time Intervals for Averaging the Output from the Plate and Film Cooling
Pressure Transducers and the Heat Flux Gages in the Corian Plate

Tests	Time Interval (msec)	
	From	To
A02,A03,A04,A05,A06,A07,B02,B03,B04,B05,B06 B07,C02,C03,C04,C05,C06,C07,Q01,Q02,Q03,Q04	3.752	5.462
A11,A12,A13,A14,A15,A16,B11,B12,B13,B14,B15 B16,C11,C12,C13,C14,C15,C16,R01,R02,R03,R04	3.872	5.422

Figures 5.1 and 5.2 depict typical responses from a heat flux gage and a pressure

transducer, and how their corresponding time interval was determined.

VI. Results and Discussion

Heat transfer results for the aluminum and corian plates, with and without film cooling, are presented for two flow conditions based on the driver to driven pressure ratio in the shock tube. For tests with film cooling, two density ratios of 1.6 and 2.0 were studied. Keeping the density ratio and the flow conditions constant, the blowing ratio was varied within a range from 0.2 to 2.2, insuring heat transfer measurements in the weak and strong injection regimes.

To determine the shock speed, the output of the forward and rear pressure transducers was used. As the normal shock propagated inside the shock tube, a jump in pressure occurred across the wave which was registered by the transducers as depicted in Figure 6.1. The time interval between the two pressure increases combined with the known distance between the transducers and the initial acoustic velocity of the gas mixture in the driven section determined the shock Mach number. This parameter had good repeatability, its deviation being not greater than 0.8 percent.

After the shock passes the test model, a laminar flow develops on the round leading edge followed by a separation boundary layer (Mehendale and others, 1991:847). They also found that reattachment of the boundary layer occurs where the leading edge semi-cylinder merges with the flat plate, at $x = 0.79d$, where x is the downstream distance relative to the leading edge and d is the semi-cylinder edge diameter. Following reattachment, the flow becomes turbulent and very unstable. Relaxation of the turbulent

6.1

flow to predictable values occurs at a distance x = 1.4d. Thus, placing the injection holes at a distance of 5.08 cm (2.7d) ensures the existence of a fully developed turbulent flow and avoids leading edge effects over the instrumentation.

Likewise, the boundary layer over the test plate changed its nature as the flow settled down. Figure 6.2 depicts a typical heat flux gage response. In this figure, three types of boundary layers can be observed. The first two types, the unsteady laminar and transition boundary layers, are very unstable and exist only for a few tenths of a millisecond. The third type, the steady turbulent layer, is stable and exists for two to three milliseconds before becoming unsteady. Gage heat-flux averaging for all the tests was performed within the steady-turbulent boundary layer range.

Simultaneously, as the normal shock wave traverses the test plate a cylindrical wave is reflected off from the plate leading edge. This wave grows radially propagating upstream and downstream of the plate leading edge. As the cylindrical wave grows, further reflections with the shock tube walls and the upper and lower plate surfaces occur, decreasing in strength at each reflection due to stretching and viscous dissipation. These reflections are able to affect the flow conditions over the entire test plate. Figure 6.3 shows a typical output of the plate pressure transducer. This figure clearly presents the existence of several pressure peaks, thus verifying the presence of these shock reflections. It took approximately one millisecond before the pressure registered by the plate pressure transducer became stable, additional pressure signal oscillations within the first millisecond were due to the dynamic response of the transducer as it is shown by the periodic decaying signal in Figure 6.3.

6.2

Experimentally, the above shock reflections increased the pressure of the induced flow behind the normal shock wave by 2 psi. This pressure increase can be clearly observed in Figure 6.1 from the output of the rear pressure transducer between 4 and 7 milliseconds. The measured static flow pressure, P_2, over the test section was within a range from 23.5 to 30 psi. The additional cylindrical shock reflections increased the flow pressure at the instrumented test section between 8.7 and 9.8 percent above to the pressure increase obtained from normal shock theory alone. Further, checking of the variation of other flow properties such as temperature (T_2), density (ρ_2), and velocity (U_2), using normal shock relationships and the measured pressure variation, revealed that the changes in these parameters were less than 3 percent. Therefore, in this research it was assumed that the only property that changed due to the cylindrical shock reflections was the static pressure, P_2, keeping the other properties constant as they were determined by the normal shock wave strength.

For the aluminum plate where there was not a pressure transducer next to the heat flux gages, P_2 was determined from the output of the rear pressure transducer. This measured pressure was then adjusted due to the location of the rear transducer. Data obtained with the corian plate indicated that P_2 measured at the shock tube rear pressure transducer was 6 percent higher than the pressure at the test section. Therefore, for the aluminum plate, a correction factor of 0.94 was applied to the rear transducer data to correct its value to a proper value at the test section.

The presence of the test plate inside the shock tube produced a change in the tube cross-sectional area, from a full area of 0.0206 m^2 down to 0.0187 m^2. This change

6.3

could affect the shock wave strength, and consequently also the flow properties. To investigate the magnitude of this phenomenon, relationships provided by Whitham, Equations (2.25) through (2.27), were used. This approach determined that the changes in Mach number were less than 0.8 percent, and therefore they were neglected.

6.1 Heat Transfer Results without Film Cooling

Tests were grouped in different series as explained in Section 5.1 and presented as a function of the downstream distance x with respect to the plate leading edge. Initially, gage heat flux measurements for the aluminum plate without film cooling were obtained by covering the injection holes with tape. This gave erroneous results for the gage closest to the injection holes and sealing tape. It was decided to seal the injection holes with epoxy, thus attaining a smooth surface next to the first heat flux gage. Figure 6.4 shows the effects of the injection hole sealing with tape based on the gage heat flux. The use of tape influenced only the first gage, increasing the measured heat flux by more than 40 percent, while the remaining heat flux gages registered a variation less than 10 percent. This increase in heat flux for the first gage was due to a detachment of the boundary layer, followed by a rapid reattachment, thus not appreciably influencing the other heat flux gages.

Heat flux results for the aluminum plate with smooth surface are presented in Figure 6.5. The difference in gage heat flux between each pair of curves, test TUV02 with TUV11 and test TUV21 with TUV31, was due to the shock strength. When the shock wave is stronger (higher P_4) the flow temperature (T_2) behind the shock wave is

6.4

higher, therefore heat flux is increased. Heat flux gage 4 consistently registered a lower heat flux compared to the other heat flux gages. This possibly could be caused by an inaccuracy of the bulk thermal diffusivity calibration for this gage or the occurrence of a change in boundary layer characteristics. Disparities in gage heat flux between tests TUV02 and TUV11, and between tests TUV21 and TUV31, were caused by differences in helium concentration.

Typical gage temperature increase histories for the aluminum and corian plates are presented in Figures 6.6.1 and 6.6.2. Temperature increases rather than actual total temperatures are presented in order to have the same reference level (zero) before the shock wave passes over the thin film gages. In both plates as the downstream distance with respect to the plate leading edge, x, was increased, the gage temperature rise was reduced for x less than 71 mm. For x greater than 71 mm the gage temperature began to increase, being even higher that at some upstream locations. The same phenomenon can be observed in Figure 6.6.3 where the gage temperature increase was plotted at a given time at several gage locations. This pattern suggests that a change in boundary layer nature occurred at $x \approx 71$ mm. The circumstances for this change are not clear. Inaccuracies in gage calibration constants for temperature measurements, as being the cause of this phenomenon, were discarded because the gage temperature increase for the farthest gage location ($x \approx 80$ mm) was measured by two different heat flux gages. Further study of this event is required.

For the no film cooling case, heat transfer, and therefore temperature change, strongly depended on the gage location and flow temperature. In Figure 6.6.3 a

6.5

comparison of the gage temperature increase between the aluminum and corian plates is presented. For x less than 71 mm, the reduction in gage temperature increase for the aluminum plate was faster than for the corian plate. This pattern can be explained by the difference in thermal conductivity between the aluminum and corian plates.

Heat is transferred from the turbulent boundary layer to the test plate and thin film gages. The test plate made of aluminum has a higher thermal conductivity than the test plate made of corian. Therefore, heat flows easier from the boundary layer to the aluminum plate removing more energy from the fluid, and so cooling it. That is, the use of a surface with low thermal conductivity (nearly adiabatic) decreases the heat flux from the boundary layer to the surface, keeping the boundary layer temperature more stable.

Heat flux results for the corian plate are presented in Figures 6.7 and 6.8. In these figures, gage heat-flux measurements were compared with those from the aluminum plate. The results showed that the heat flux registered by the gages in the corian plate were always less than in the aluminum plate. Heat transfer is proportional to the difference of the flow temperature and wall temperature. If the flow temperature is higher or the wall temperature is lower then heat transfer is increased. For the tests with the aluminum plate, the flow temperature was higher, so gage heat flux was also higher compared with the corian plate.

Comparison of experimental results with theoretical results is presented in Figure 6.9. This figure presents a plot of the Stanton number versus the Reynolds number for a turbulence level of 9.5 percent. The measured Stanton number for the tests with the

aluminum plate presented a good correlation, exhibiting an even spread of data points. The data spread could be attributed to the assumption of a thermal boundary layer for an adiabatic heat flux gage substrate (Corning Pyrex 7740), a variable turbulence level, and gage calibration inaccuracies. The measured Stanton number for the tests with the corian plate presented a better correlation than the aluminum, with the exception of gages 4 and 5. The behavior of gages 4 and 5 could be attributed to a gage calibration inaccuracy, variable turbulence level, and changes in boundary layer nature.

6.2 Heat Transfer with Film Cooling

Heat transfer measurements with film cooling were very difficult, many parameters had to be taken into account or previously checked in order to be sure of the actual flow conditions over the test plate. Several improvements were made and new ideas were proposed to improve reliability of the results on film cooling using transient facilities. For the film cooling case, gage heat flux results were presented as a function of the nondimensional downstream distance X/D with respect to the injection hole axis.

Heat transfer results were classified by shock strength and density ratio, the variable being the blowing ratio. Figures 6.10.1 through 6.11.2 present gage heat flux versus nondimensional downstream distance X/D for several tests. Figures 6.10.1 and 6.10.2 present the gage heat flux for tests HJK21, HJK22, HJK23, HJK24, HJK25, and HJK26 in the weak and strong injection regimes. The above tests were performed with the aluminum plate for a density ratio of 1.6 and a blowing ratio varying from 0.27 to 1.33. One test, HJK24, was repeated in Figures 6.10.1 and 6.10.2 as reference to

compare the characteristics of the two injection regimes. Similarly, Figures 6.11.1 and 6.11.2 present the results for tests ABC11 through ABC16 with the corian plate for a density ratio of 1.95 and a blowing ratio varying from 0.33 to 1.56. Test ABC13 was used as reference to compare the characteristics of the two injection regimes.

For the aluminum and corian plates as the blowing ratio was increased, the measured heat flux was reduced in all the gages, even for $X/D > 10$. This pattern was observed until the blowing ratio equaled 1.0. For blowing ratios greater than 1.0 the heat flux for the first four gages ($X/D < 10$) began to increase, being almost constant for the other three gages ($X/D > 10$). The same pattern was observed in all of the other tests with film cooling for both plates, indicating that the optimum blowing ratio for minimum heat transfer to the gages was approximately equal to 1.0.

Additional information deduced from Figures 6.10.1 to 6.11.2 indicated that film cooling was more effective for X/D less than 10, and that the heat flux distribution over the plate surface was quite different between the aluminum and corian plates. For the aluminum plate with a blowing ratio of 1.0 (test HJK24), the heat flux of the first gage ($X/D = 3.9$) was 72 kW/m^2 and for the sixth gage ($X/D = 20.3$) was 76 kW/m^2. For the corian plate with a blowing ratio of 1.01 (test ABC13), the heat flux of the second gage ($X/D = 4.0$) was 56 kW/m^2 and for the sixth gage ($X/D = 20$) was 82 kW/m^2. Even though the density ratios were different, the same pattern was observed when tests with similar density ratios were compared. For a quick check, the reader is referred to Appendix E, pages E.18 to E.20.

These differences in gage heat flux between the corian and aluminum plates could

6.8

be explained by two reasons. The first reason could be the change in injection geometry (bigger injection holes) made for the corian plate compared to the aluminum plate, which produced bigger jets (four times greater in sectional area), altering flow conditions and boundary layer nature over the corian plate and so gage heat flux. The second reason could be the lower thermal conductivity of the corian plate, which allowed the coolant flow to maintain its low temperature much longer, protecting more effectively the plate surface from the hot mainstream.

The optimum blowing ratio served as a reference to differentiate between the weak and strong injection regimes. In the weak injection regime, blowing ratio less than 1.0, the jet is turned quickly into the direction of mainstream flow reattaching to the plate surface and forming a cool protective film. In the strong injection regime, blowing ratio greater than 1.0, the jet is caused to lift off , penetrating further into the mainstream reattaching at some point depending on the magnitude of the blowing ratio. The strong injection regime greatly influences the heat flux for gages located at $X/D < 10$, indicating less effective cooling at these locations.

Tables 6.1 and 6.2 present the results for the heat flux ratio with film cooling at two density ratios for the aluminum and corian plates respectively.

From Table 6.2 the gage heat flux ratios for test ABC02 were greater than 1.0. This incongruence was due to the low blowing ratio, which produced a very unstable coolant injection, resulting at some time in boundary layer suction, thus increasing gage heat flux. This idea of having a very low blowing ratio to match no coolant injection was tried for tests without film cooling, unfortunately the situation became highly unstable

Table 6.1

Gage Heat Flux Ratio for the Aluminum Plate with Film Cooling

Test Code	DR	VR	B	Gage Location						
				3.9	5.9	7.8	9.8	15.6	20.5	30.3
HJK03	1.53	0.27	0.41	0.93	0.92	0.97	0.99	1.01	0.98	1.02
HJK04	1.54	0.48	0.74	0.72	0.75	0.81	0.84	0.89	0.94	0.93
HJK05	1.55	0.68	1.05	0.71	0.73	0.76	0.78	0.80	0.86	0.90
HJK06	1.56	0.81	1.27	0.83	0.83	0.81	0.81	0.77	0.86	0.85
HJK07	1.58	0.96	1.51	0.92	0.94	0.89	0.85	0.83	0.87	0.87
HJK11	1.94	0.35	0.68	0.79	0.84	0.87	0.89	0.93	0.92	0.98
HJK12	1.96	0.57	1.11	0.76	0.79	0.86	0.85	0.89	0.93	0.94
HJK13	1.97	0.69	1.37	0.80	0.82	0.83	0.82	0.85	0.88	0.88
HJK14	1.99	0.83	1.66	0.90	0.94	0.92	0.84	0.79	0.85	0.88
HJK15	1.99	0.98	1.96	1.05	1.05	1.00	0.88	0.86	0.82	0.87
HJK16	2.02	1.10	2.21	1.15	1.12	1.02	0.93	0.86	0.84	0.84
HJK21	1.60	0.17	0.27	0.81	0.82	0.84	0.89	0.91	0.91	0.93
HJK22	1.61	0.35	0.56	0.69	0.74	0.77	0.79	0.83	0.84	0.90
HJK23	1.63	0.50	0.81	0.65	0.69	0.72	0.76	0.80	0.84	0.87
HJK24	1.63	0.61	1.00	0.69	0.72	0.72	0.72	0.75	0.79	0.84
HJK25	1.64	0.72	1.18	0.73	0.77	0.75	0.71	0.72	0.76	0.80
HJK26	1.65	0.81	1.33	0.80	0.83	0.80	0.76	---	0.76	0.82
HJK31	1.91	0.28	0.54	0.72	0.75	0.82	0.81	0.87	0.89	0.92
HJK32	1.92	0.41	0.79	0.66	0.72	0.75	0.77	0.84	0.85	0.89
HJK33	1.94	0.51	0.98	0.68	0.70	0.74	0.74	0.80	0.83	0.86
HJK34	1.94	0.62	1.21	0.71	0.77	0.77	0.73	0.78	0.81	0.86
HJK35	1.97	0.71	1.40	0.83	0.85	0.81	0.79	0.78	0.81	0.82
HJK36	1.99	0.80	1.59	0.91	0.93	0.85	0.80	0.78	0.79	0.81

Table 6.2

Gage Heat Flux Ratio for the Corian Plate with Film Cooling

Test Code	DR	VR	B	Gage Location				
				2.5	4.0	6.0	10.0	15.0
ABC02	1.58	0.15	0.24	0.97	1.11	1.01	1.08	1.05
ABC03	1.59	0.40	0.64	0.45	0.63	0.66	0.83	0.86
ABC04	1.60	0.49	0.78	0.42	0.55	0.58	0.79	0.80
ABC05	1.61	0.59	0.95	0.51	0.62	0.62	0.80	0.80
ABC06	1.61	0.71	1.14	0.59	0.74	0.64	0.69	0.72
ABC07	1.64	0.77	1.27	0.73	0.81	0.74	0.78	0.78
ABC11	1.91	0.17	0.33	0.74	0.92	0.90	1.03	0.99
ABC12	1.92	0.39	0.75	0.43	0.58	0.66	0.87	0.87
ABC13	1.93	0.52	1.01	0.47	0.61	0.58	0.74	0.76
ABC14	1.95	0.65	1.21	0.61	0.71	0.63	0.76	0.75
ABC15	1.96	0.73	1.44	0.73	0.78	0.72	0.81	0.77
ABC16	1.97	0.79	1.56	0.80	0.87	0.77	0.82	0.79

when the blowing ratio was too low. The test data presented herein for the corian plate without film cooling were obtained with a plate without cooling holes.

On the other hand, Table 6.1, tests HJK15 and HJK16 shows that the three first gages also presented heat flux ratios greater than 1.0. In this case, the very high coolant jet velocity, blowing ratio greater than 2.0, produced the detachment of the coolant jets and also the turbulent boundary layer. Stronger jets increased turbulence in the region next to them, so the heat flux was also increased. Figures 6.12.1 to 6.17.2 graphically present the data of Tables 6.1 and 6.2.

Density ratio did not play an important role in heat transfer measurements for this research, possibly because of the proximity between the two density ratios used. Gage heat flux changed less than 5 percent as the density ratio increased from 1.6 to 2.0, when comparing tests with approximately the same shock strength and blowing ratio for $X/D < 10$. For example, test HJK22 with HJK31, HJK23 with HJK32, and HJK24 with HJK33.

Forth and Jones proposed two scaling parameters for the heat flux with coolant injection through inclined holes. For the weak injection regime the parameter $(X/D)I^{-2/3}$ must be used, while for the strong injection regime the parameter $(X/D)VR^{-4/3}$ gave a good correlation. The present research found that for the weak injection regime, the parameter $(X/D)VR^{-4/3}$ was also a good scaling parameter to correlate gage heat flux for both plates. This velocity ratio scaling parameter is plotted against the heat flux ratio. Even though Forth and Jones used a ratio of Nusselt numbers with and without film cooling, the way they defined this ratio is similar to the heat flux ratio used in this research. Figure 6.18 presents the velocity ratio scaling parameter versus the heat flux ratio for the aluminum plate for all the tests performed, while Figure 6.19 presents the same parameters but for the corian plate.

From Figure 6.18 the minimum heat flux ratio, 0.65, was attained for a scaling parameter ranging from 9 to 14. Meanwhile, from Figure 6.19 the minimum heat flux ratio ranges from 0.40 to 0.60 corresponding to a scaling parameter ranging from 6 to 15. For Figure 6.19 it was difficult to specify a narrower range because of the small amount of data plotted.

VII. Conclusions and Recommendations

7.1 Conclusions

Accurate determination of the bulk thermal diffusivity for the thin-film heat flux gages is extremely important. Eads estimated that the range of error for the heat flux gage calibration was 10 percent. The turbulence level of 9.5 percent applied in establishing the theoretical heat transfer curve for this research agreed with the experimental results without film cooling .

Shock reflections must be taken into account. They caused a significant pressure increase in the mainstream static pressure, which greatly affected the film cooling parameters such as DR, VR, B, and I. Changes in pressure generally lasted 1 msec before becoming stable.

The location of a pressure transducer next to the heat flux gages was very helpful. Also the use of a pressure tank helped to decrease pressure losses by friction and eliminated the dynamic response of the pressure regulator, resulting in a more stable coolant supply pressure.

The experimental determination of time intervals for averaging pressure transducer and heat flux gage outputs was a good approach to insure reliable flow conditions.

For tests without film cooling the use of tape for sealing the injection holes affected the measured heat flux for the first gage because of boundary layer lift-off. Heat

flux increase for the first gage was as high as 50 percent, while the remaining heat flux gages were unaffected.

For tests with no film cooling an increase in gage temperature rise began to develop for downstream distances greater than 71 mm relative to the plate leading edge. This phenomenon could be attributed to a change in boundary layer nature, but the origins of this change are not still clear. Further study is required.

Trying to match no film cooling conditions by decreasing cooling source pressure to bring the blowing ratio to zero was not a good approach. Boundary layer instabilities due to boundary layer suction and further blowing made heat transfer measurements very erratic.

The use of corian to simulate an adiabatic surface gave good results. Gage temperature increase with no film cooling in the downstream direction was more stable for x less than 71 mm. Heat transfer results correlated better with theoretical results as was shown in Figure 6.8.

Two injection regimes were found, the limit of each region was imposed by the optimum blowing ratio. An optimum blowing ratio of 1.0 was found for both plates.

Further increase of the blowing ratio beyond the optimum value did not improve film cooling. On the contrary, for blowing ratios greater than 1.0 the first three gages were affected by a jet and turbulent boundary layer lift-off, increasing the measured heat flux.

Film cooling was highly effective for downstream distances X/D less than 10. However in the weak injection regime, film cooling was effective for all the heat flux

7.2

gages, the last gage being located at a distance X/D of 30.

Density ratio did not affect heat transfer measurements. However, the difference between the two density ratios use in this research, 1.6 and 2.0, is relatively small. Therefore this conclusion can not be generalized for a broader range of density ratios.

The scaling parameter $(X/D)VR^{-4/3}$ presented a good correlation for both injection regimes and both plates. The minimum heat flux ratio attained was 0.68 for the aluminum plate, and 0.40 to 0.60 for the corian plate.

7.2 Recommendations

The execution of this research lead to the following recommendations:

- Further study of heat transfer with and without film cooling for the corian plate.

- Use of a different surface temperature measurement technique such as thin-film ribbon to avoid damage of gages by handling them.

- Further study to determine an experimental procedure to calculate the adiabatic wall temperature.

- Use of more plate pressure transducers along with more heat flux gages to better correlate heat transfer measurements.

- Use of high speed photography to better understand boundary layer development and reflected shock interactions.

- Study of new injection geometries, such as varying the injection angle and hole spacing.

- Use of plates with no injection holes for heat transfer measurements with no film

cooling.

- Seal the shock tube better to have a good control of gas mixture inside the driven section.

- Automate coolant injection and helium fill for better control of the test and to insure repeatability.

7.4

VIII. References

Ammari, H. D., and others. "The Effect of Density Ratio on the Heat Transfer Coefficient From a Film-Cooled Flat Plate," ASME Journal of Turbomachinery. 112: 444-450 (July 1990).

Arpaci, V. S., and P. S. Larsen. Convection Heat Transfer. Englewood Cliffs: Prentice Hall Inc., 1984.

Eads, Capt. Thomas. Shock Tube Study of the Effects of Large Density Differences and Blowing Ratio on Heat Transfer to a Film-Cooled Flat Plate. MS Thesis, AFIT/GAE/ENY/92D-25. School of Engineering, Air Force Institute of Technology (AU), Wright-Patterson AFB OH, December 1992.

Eckert, E. R. G. "Engineering Relations for Friction and Heat Transfer to Surfaces in High Velocity Flow," Journal of the Aeronautical Sciences, 585-587 (August 1955).

Eckert, E. R. G., and R. M. Drake. Analysis of Heat and Mass Transfer. New York: McGraw-Hill Book Company, 1972.

Forth, C. J. P., and T. V. Jones. "Scaling Parameters in Film-Cooling," Proceedings of the Eighth International Heat Transfer Conference. 1271-1276. San Francisco: Hemisphere Publishing Corporation, 1986.

Gaydon, A. G., and I. R. Hurle. The Shock Tube in High-Temperature Chemical Physics. New York: Reinhold Publishing Corporation, 1963.

Glass, I. I. Shock Tubes, Part I: Theory and Performance of Simple Shock Tubes. UTIA Review No. 12. Toronto: University of Toronto Institute of Aerophysics, 1958.

Goldstein, R. J., and others. "Film Cooling with Injection through Holes: Adiabatic Wall Temperature Downstream of a Circular Hole," ASME Journal of Engineering for Power. 90: 384-395, 1968.

Goldstein, R. J., and others. "Film Cooling," <u>Advances in Heat Transfer, 7</u>. New York: Academic Press, 1971.

Gul, Flt Lt Rakhman. <u>Transient Heat Transfer Measurements on a Film Cooled Flat Plate in a Shock Tube</u>. MS Thesis, AFIT/GAE/ENY/91M-4. School of Engineering, Air Force Institute of Technology (AU), Wright-Patterson AFB OH, March 1991 (AD-A319472).

Hill, Philip G. and Carl R. Peterson. <u>Mechanics and Thermodynamics of Propulsion</u> (Second Edition). New York: Addison-Wesley Publishing Company, 1992.

Jurgelewicz, Capt Scott A. <u>Investigation of Heat Transfer With Film Cooling to a Flat Plate in a Shock Tube</u>. MS Thesis, AFIT/GAE/ENY/89D-17. School of Engineering, Air Force Institute of Technology (AU), Wright-Patterson AFB OH, December 1989 (AD-A216379).

Kays, William M. and Michael E. Crawford. <u>Convective Heat and Mass Transfer</u> (Second Edition). New York: McGraw-Hill Book Company, Inc., 1980.

Mehendale, A. B., and others. "Influence of High Mainstream Turbulence on Leading Edge Heat Transfer," <u>ASME Journal of Heat Transfer</u>, 113: 843-850 (November 1991).

Oldfield, M. L. G. and others. "On Line Computer for Transient Turbine Cascade Instrumentation," <u>IEEE Transactions on Aerospace and Electronic System</u>, Vol. AES-14 N°5 (September 1968).

Pedersen, D. R., and others. "Film Cooling With Large Density Differences Between the Mainstream and the Secondary Fluid Measured by the Heat-Mass Transfer Analogy," <u>ASME Journal of Heat Transfer</u>, 99: 620-627 (November 1977).

Pietrzyk, J. R., and others. "Effects of Density Ratio on the Hydrodynamics of Film Cooling," <u>ASME Journal of Turbomachinery</u>, 112: 437-443 (July 1990).

Rivir, R. B., and others. "Visualization of Film Cooling Flows Using Laser Sheet Light," Paper No. AIAA-87-1914. New York: American Institute of Aeronautics and Astronautics, 1987.

Rockwell, Capt Richard K. Transient Heat Transfer Measurements on a Flat Plate in Turbulent Flow Using an Electrical Analog. MS Thesis, AFIT/GAE/ENY/89D-31. School of Engineering, Air Force Institute of Technology (AU), Wright Patterson AFB OH, December 1989 (AD-A216286).

Schlichting, Hermann, Boundary-Layer Theory (Sixth Edition). New York: McGraw-Hill Book Company, Inc., 1968.

Schultz, D.L. and Jones, T.V. Heat Transfer Measurements in Short Duration Hypersonic Facilities. AGARDograph AG-165, February, 1973.

Sinha, A. K. and others. "Film Cooling Effectiveness Downstream of a Single Row of Holes with Variable Density Ratio," ASME Journal of Turbomachinery. 103: 442-449 (July 1991)

Teakaram, A. J. H. and others. The Use of Foreign Gas to Simulate the Effects of Density Ratios in Film Cooling," ASME Journal of Turbomachinery. 111: 57-6. (January 1989)

Whitham, G. B. Linear and Nonlinear Waves. New York: John Wiley & Sons, 1974.

White, Frank M. Viscous Fluid Flow (Second Edition). New York: McGraw-Hill Inc., 1991.

Wittig, S. and V. Scherer. "Heat Transfer Measurements Downstream of a Two Dimensional Jet Entering a Crossflow," ASME Journal of Turbomachinery. 109: 572-578 (October 1987)

Zucrow M. J. and J. D. Hoffman. Gas Dynamics Volume I. New York: John Wiley & Sons, 1976.

8.3
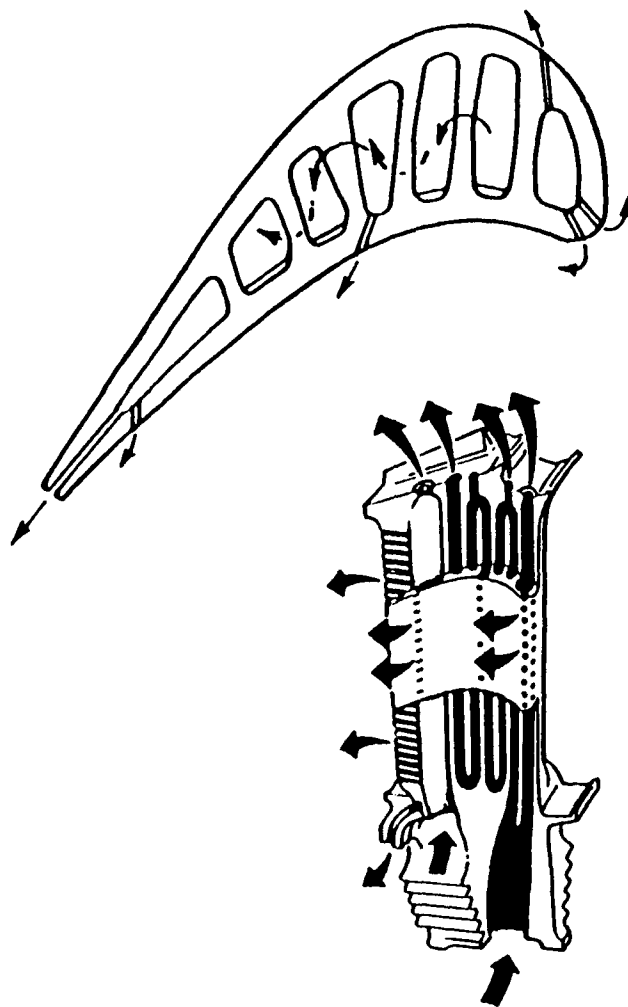
Figure 1.1 Film Cooling in a Turbine Rotor Blade (Hill and Peterson, 1992:396)
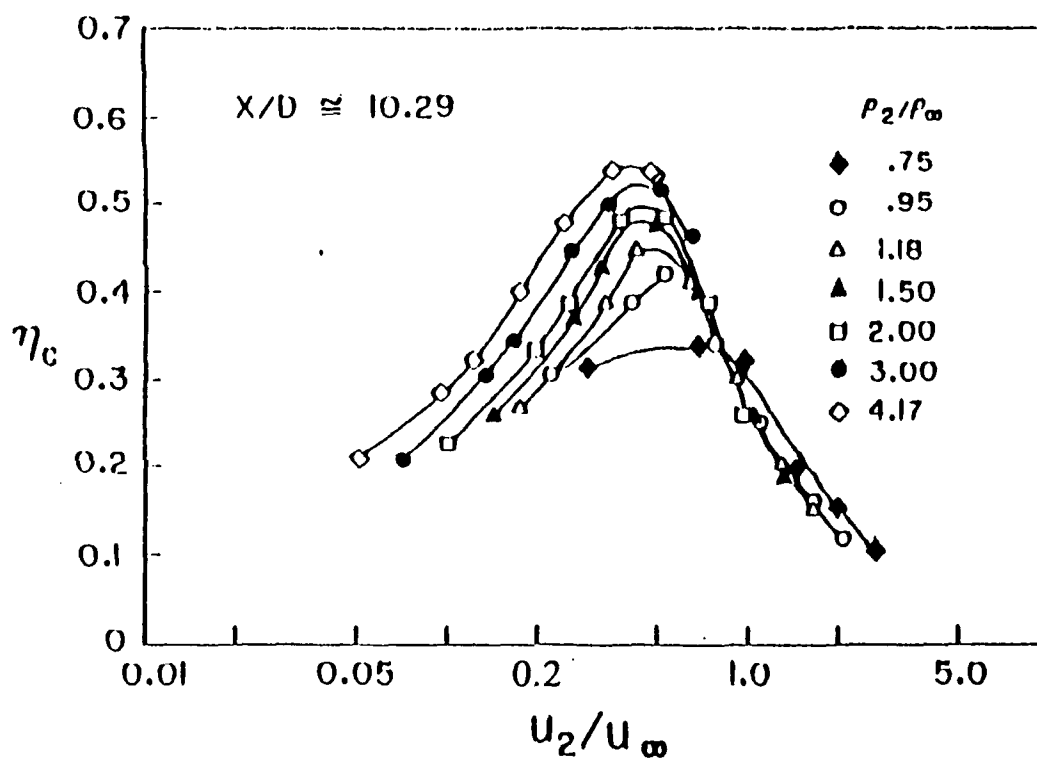
Figure 1.2 Effect of Injection Velocity on Film Cooling Effectiveness
(Pedersen and others, 1977:620)

A.2
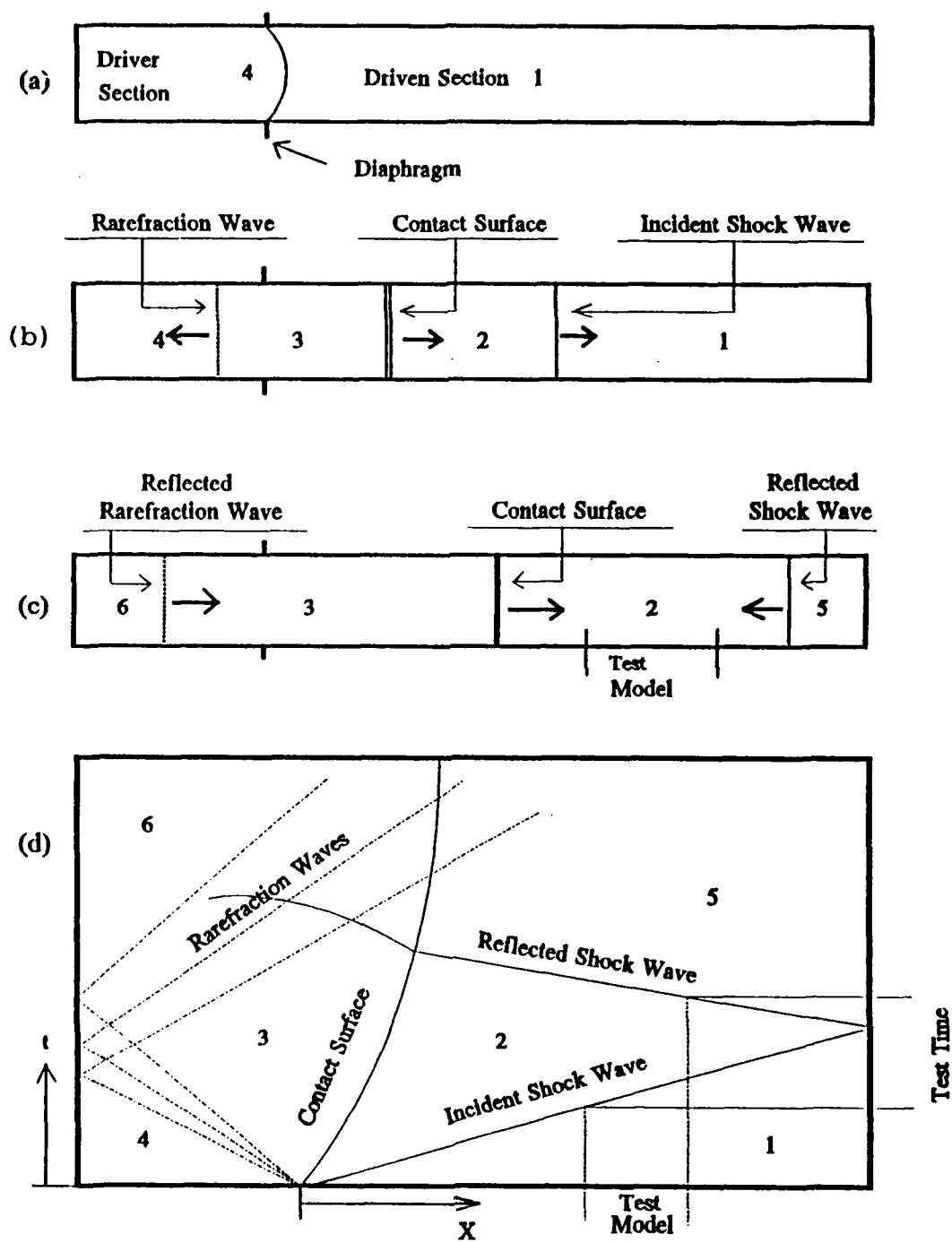
Figure 2.1 Shock Tube Behavior (Shapiro, 1987:1007)

A.3
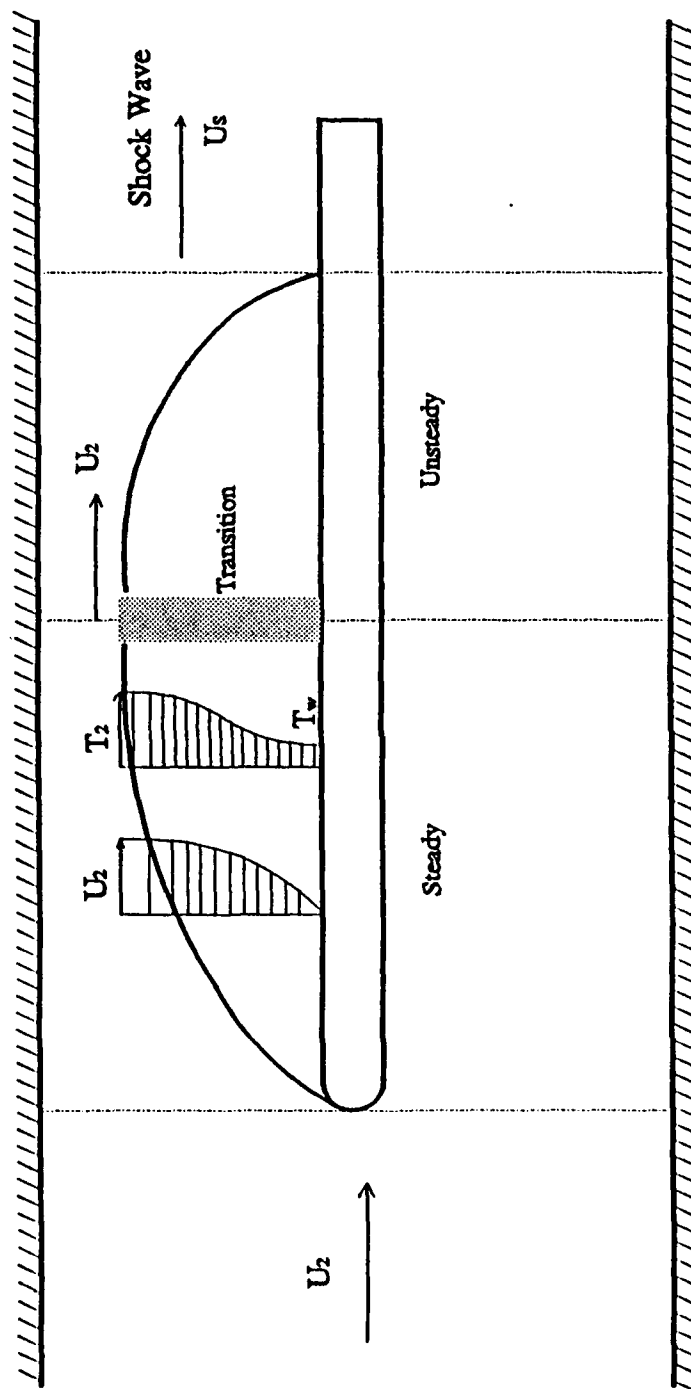
Figure 2.2 Nature of the Boundary Layer.

A.4

ADIABATIC WALL

T_{o2}

T_{aw}

T_2
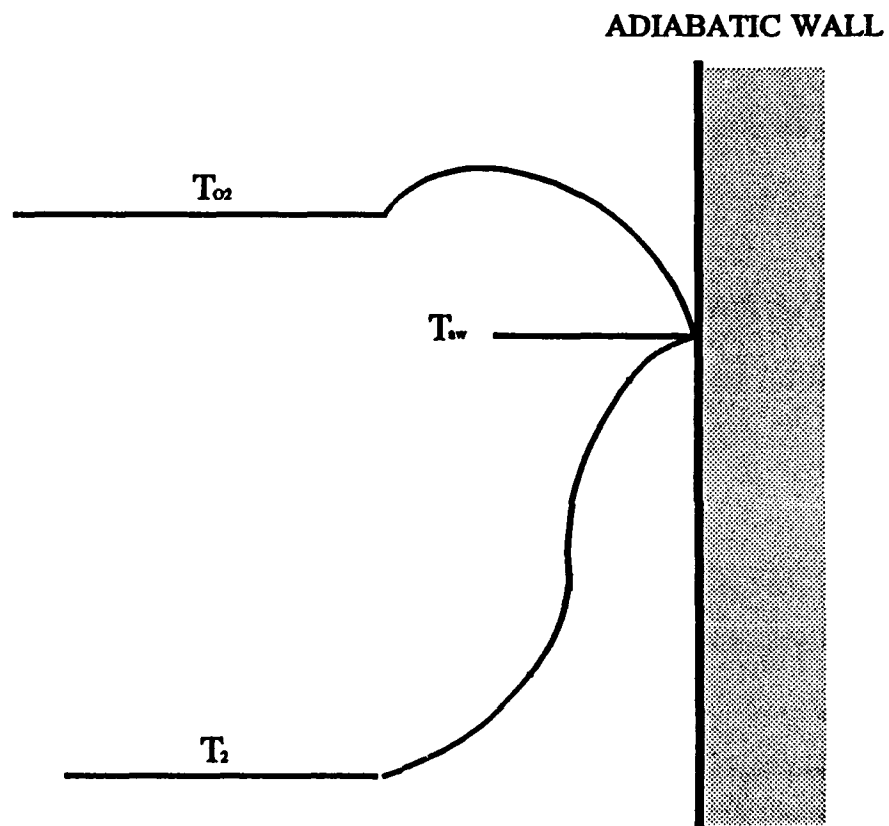
Figure 2.3 The Adiabatic Wall Temperature (Hill and Peterson,1992:546)

A.5
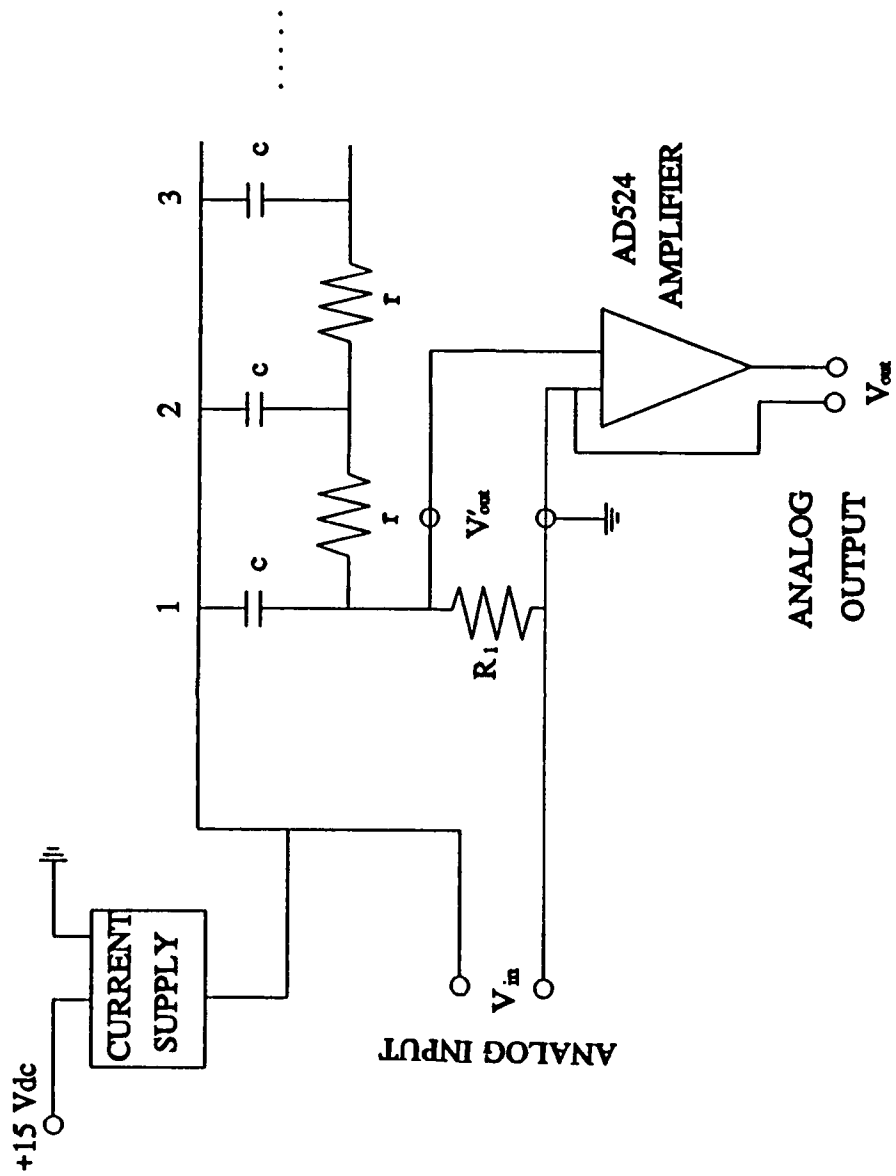
Figure 2.4 Schematic of Analog Circuit

A.6

TEST PLATE

1220

REAR PX

472.7

711.2

3730

FORWARD PX

DRIVEN SECTION

3658

DIAPHRAGM

DRIVER SECTION

1220

101.6

101.6

25.4

101.6
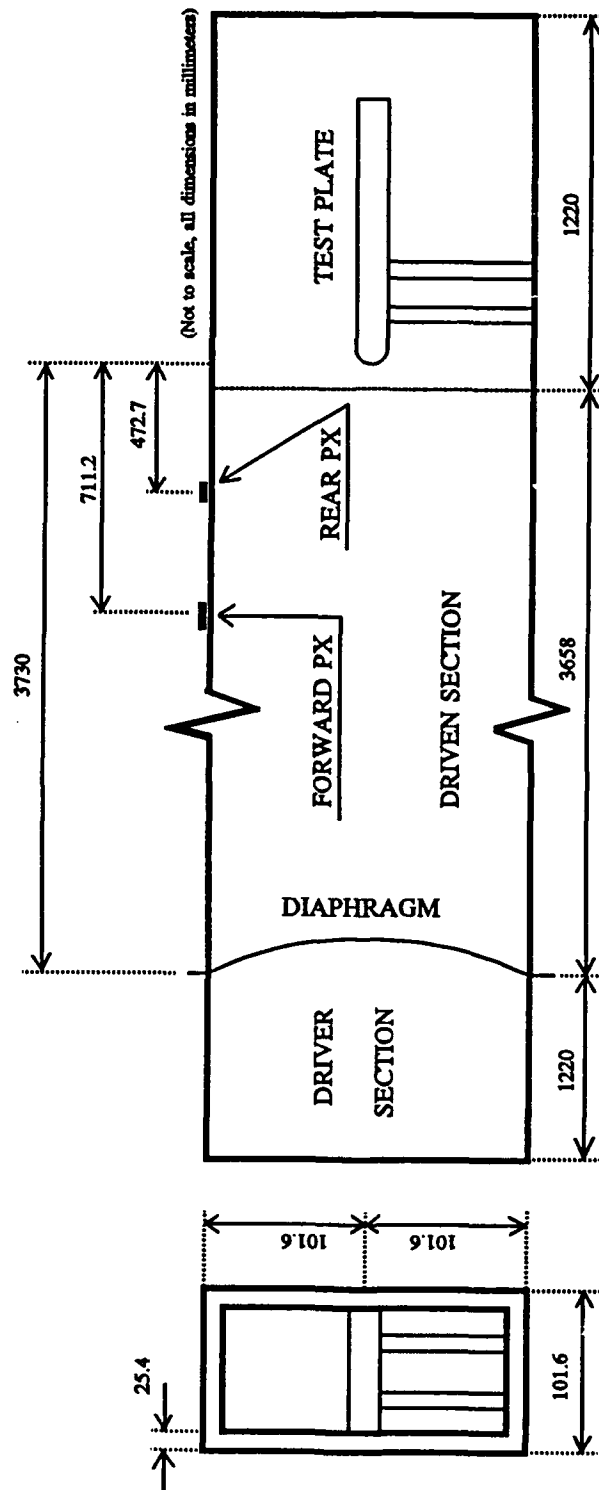
Figure 3.1 Low Pressure Shock Tube

A.7
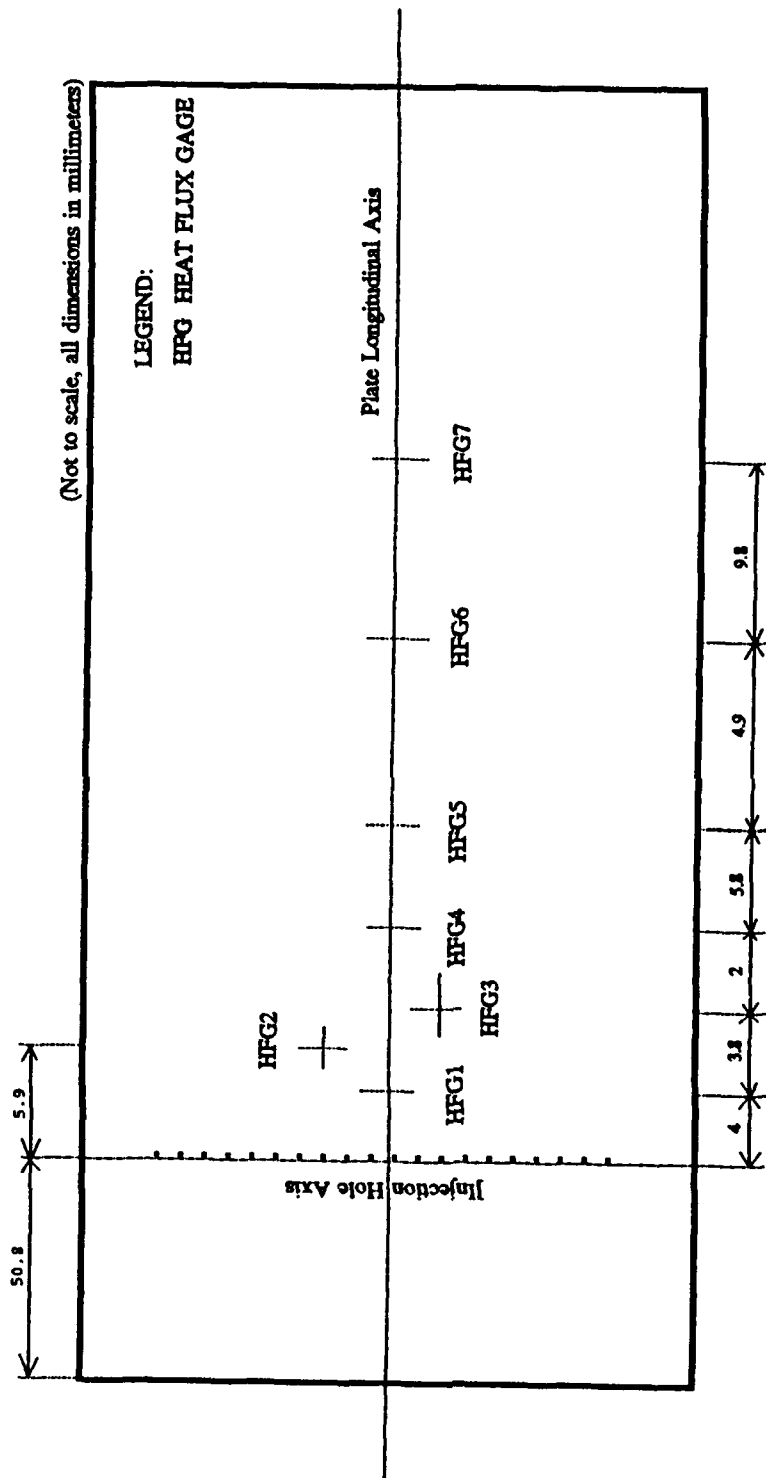
Figure 3.2 Thin-Film Gage Locations on the Aluminum Plate

A.8
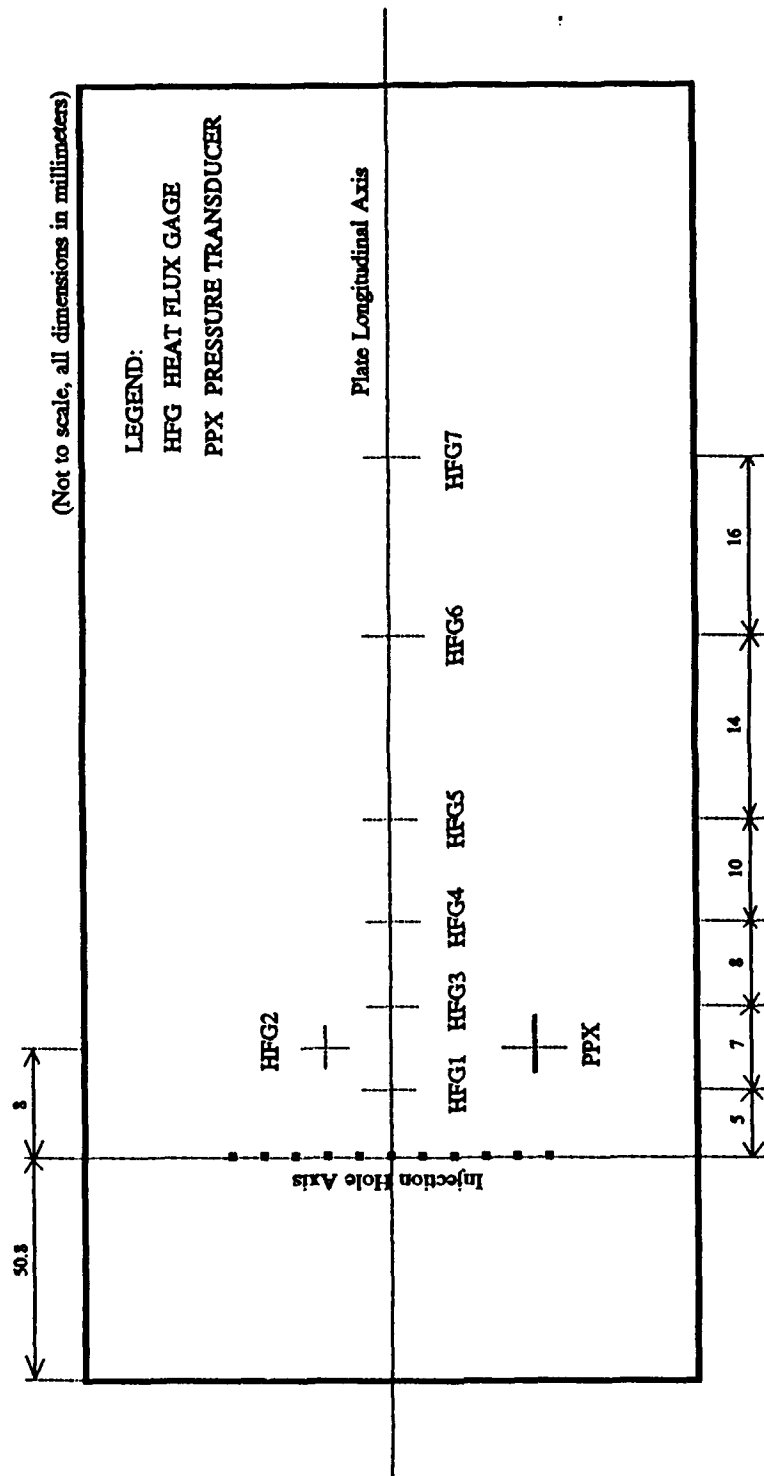
Figure 3.3 Thin-Film Gage Locations on the Corian Plate
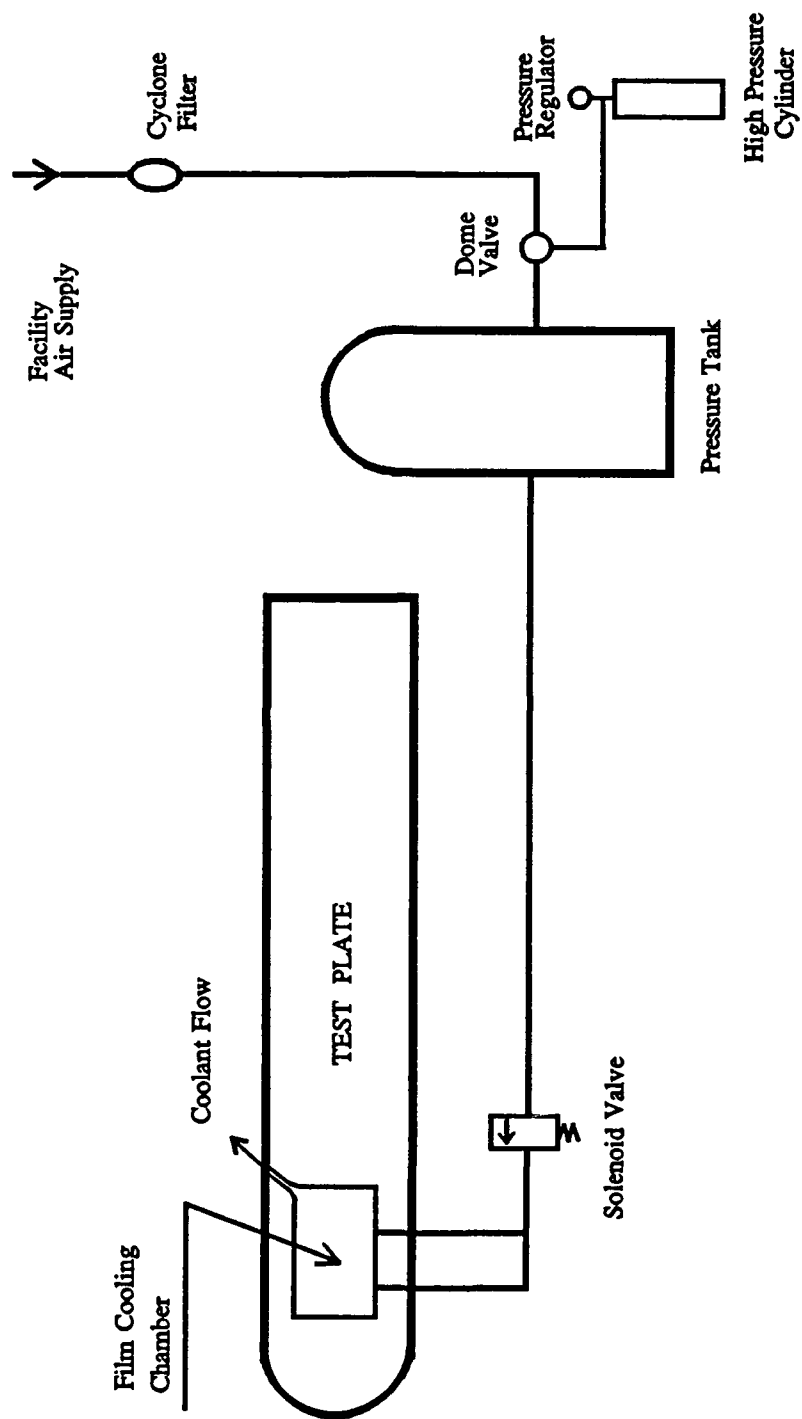
Figure 3.4 Film Cooling Supply and Control System
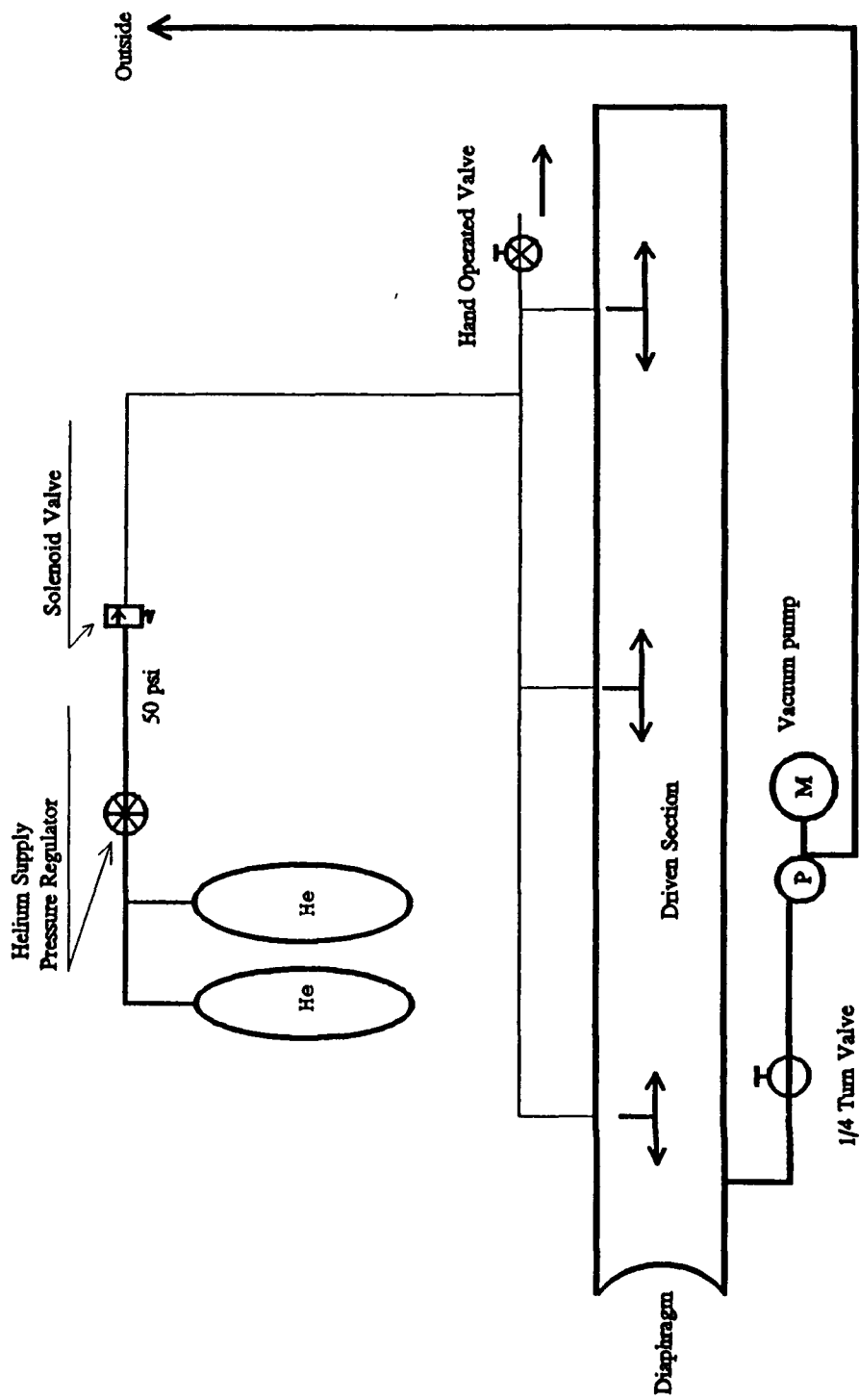
Figure 3.5 Shock Tube Gas Fill and Control System

A.11
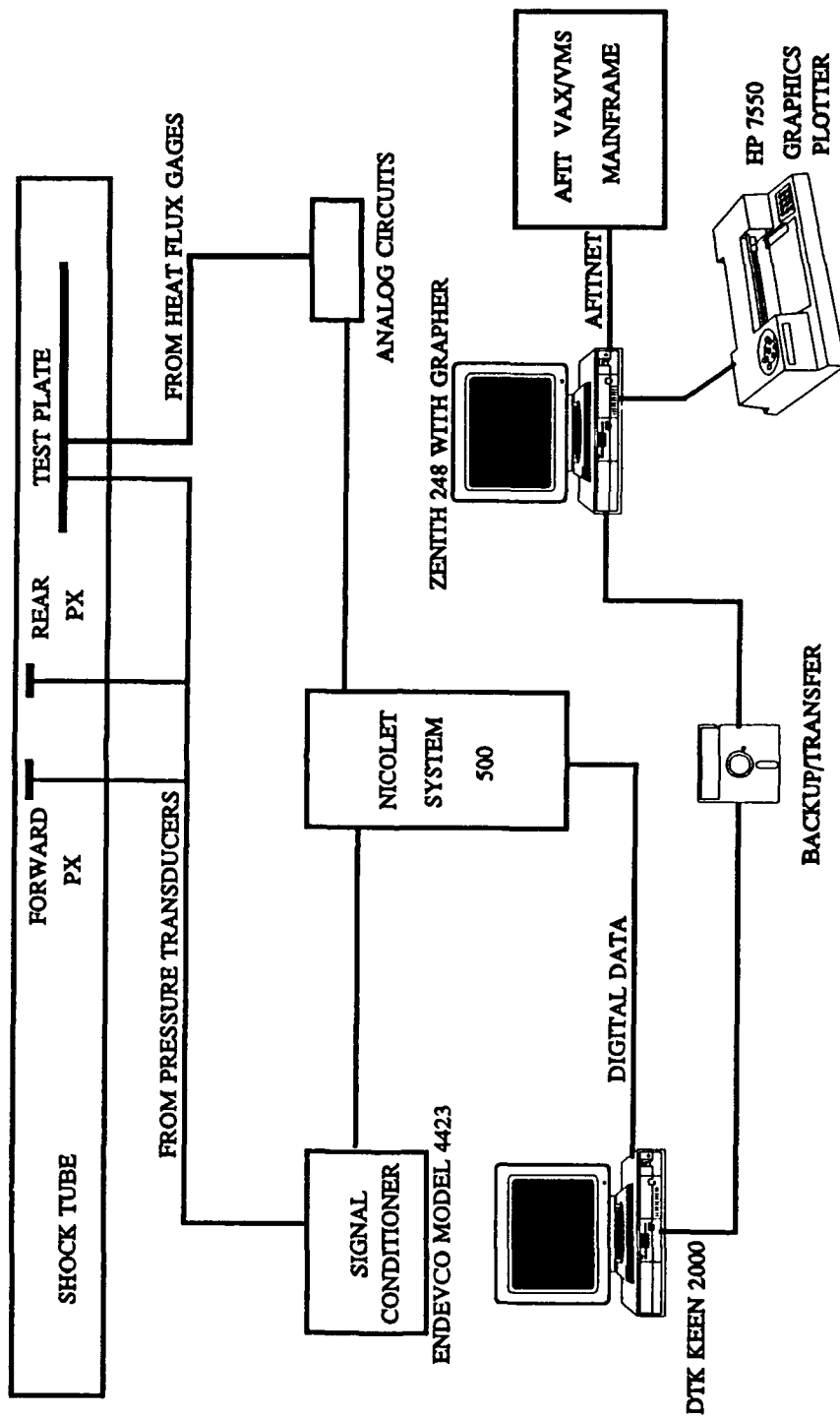
Figure 3.6 Data Acquisition Set-Up
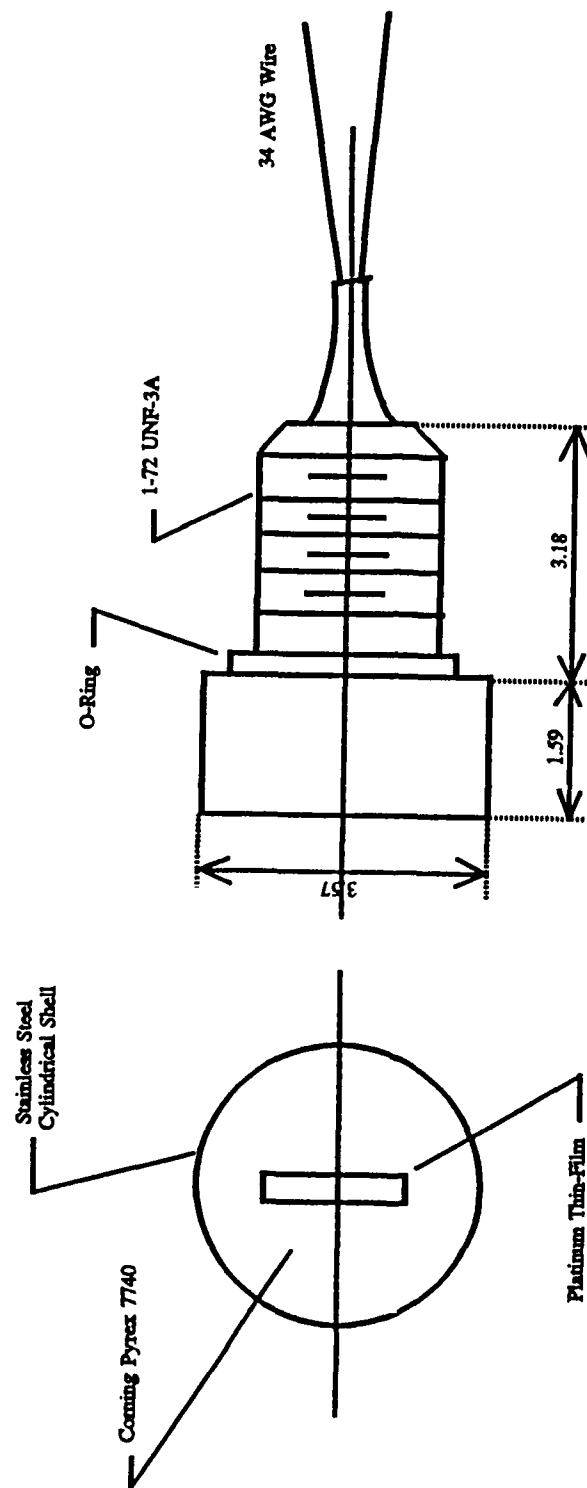
Figure 3.7 Platinum Thin-Film Resistance Heat Transfer Gage, Medtherm Instruments Model PTF-100-20293

A.13
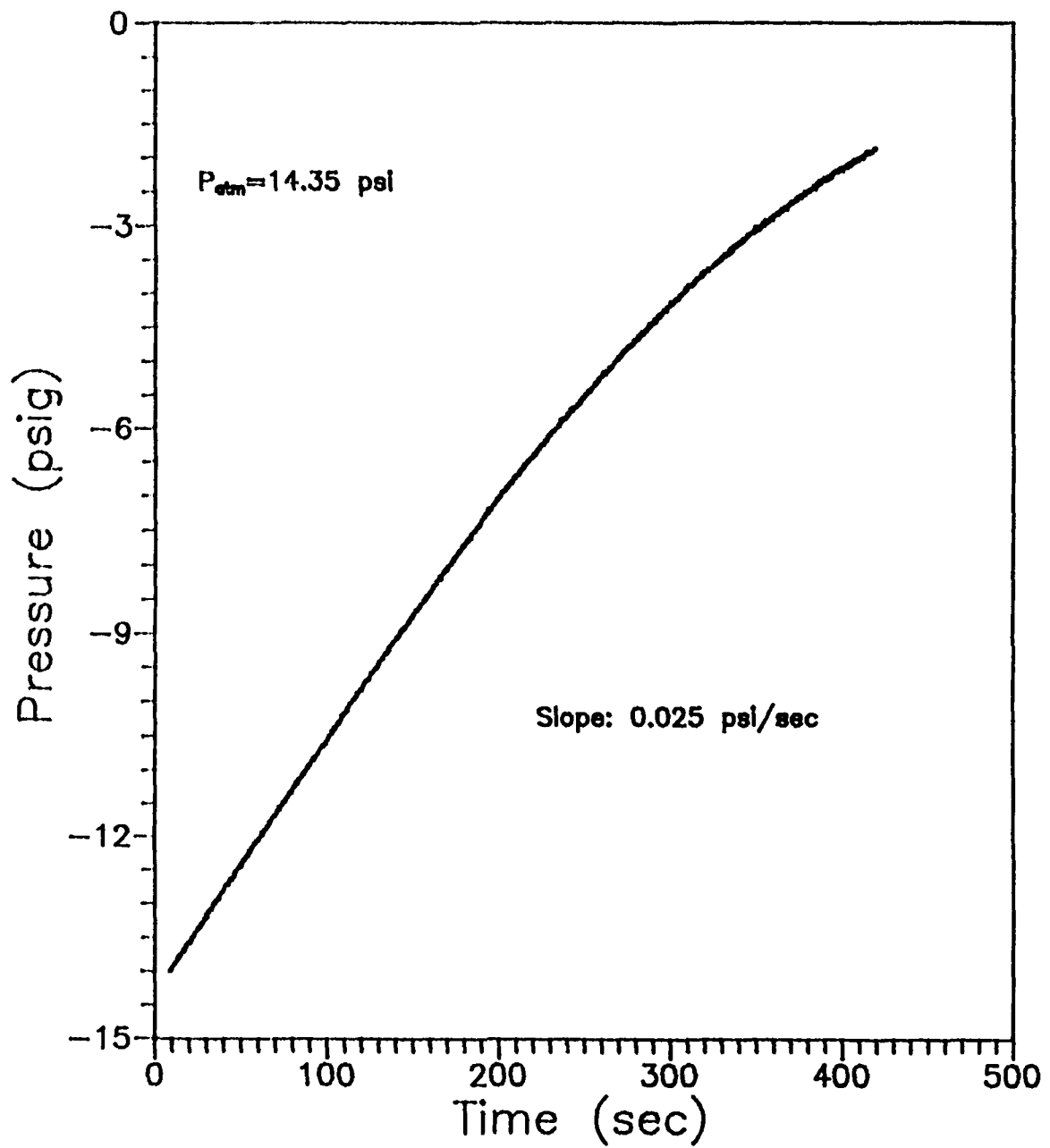
Figure 4.1 Pressure History for the Forward Pressure Transducer, Leakage Test on 10 January 1993

A.14
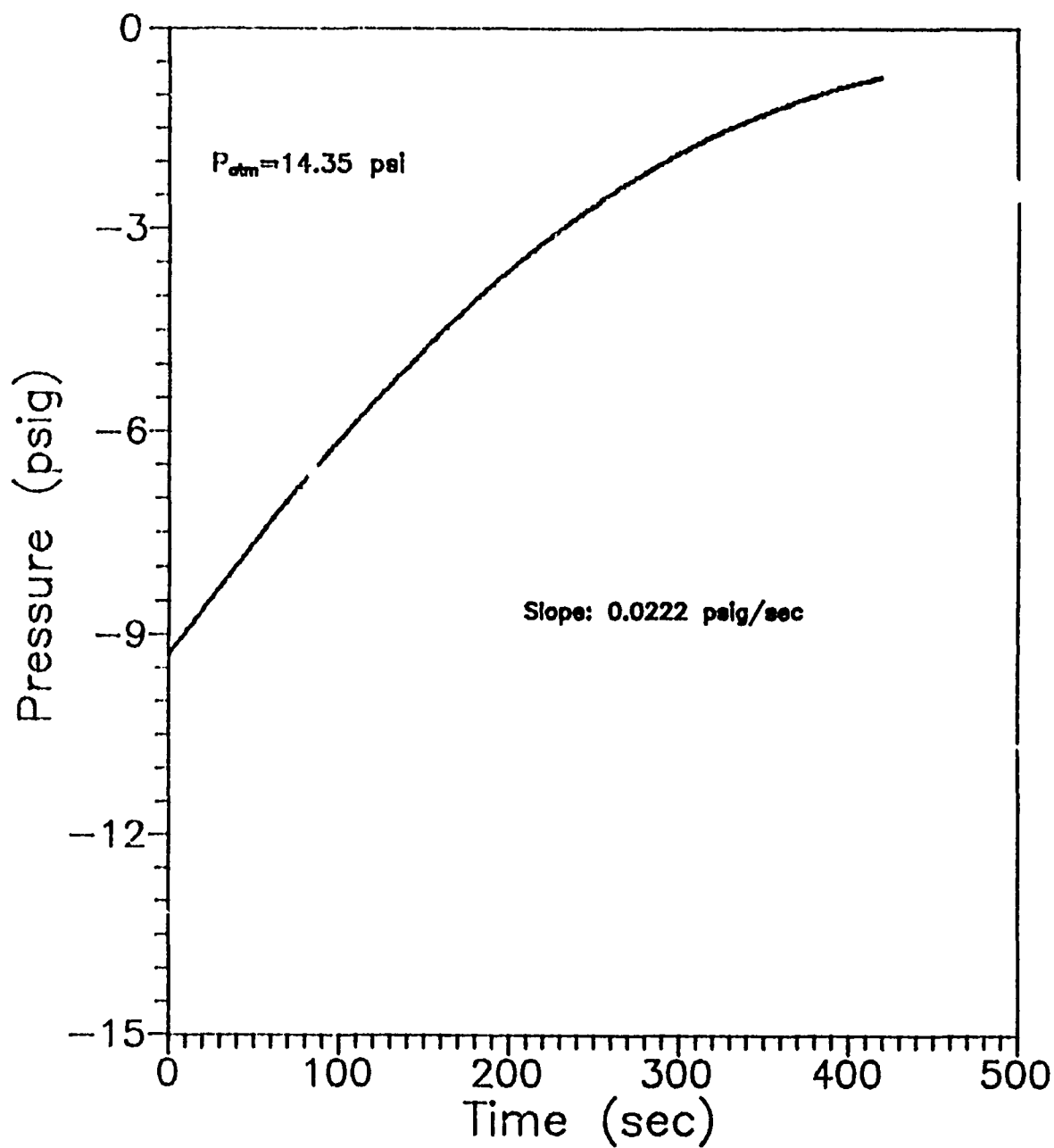
Figure 4.2 Pressure History for the Forward Pressure Transducer, Leakage Test on 15 March 1993

A.15
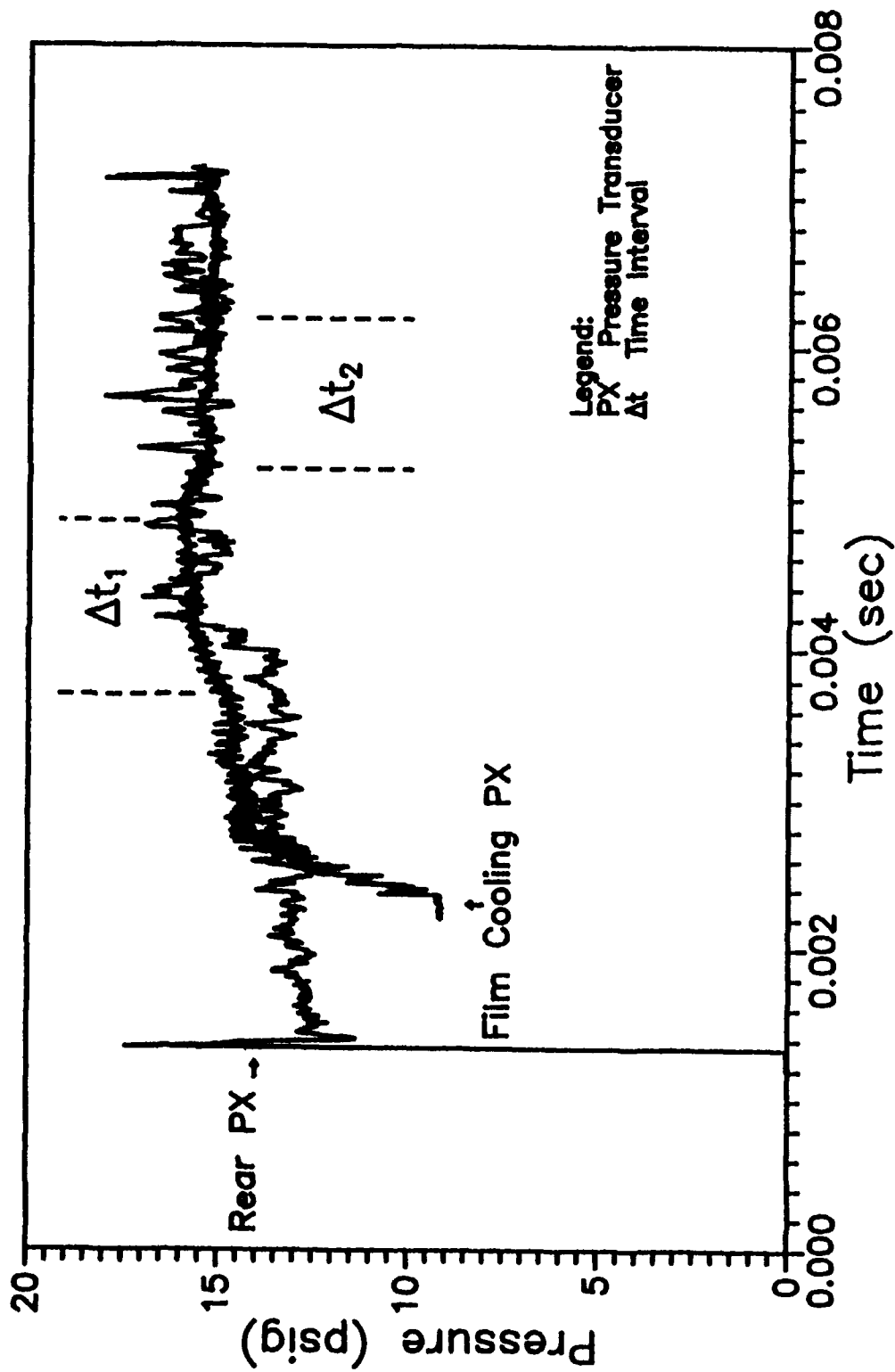
Figure 5.1 Output of Rear PX and Film Cooling PX for Test J22
(Determination of Time Intervals for Averaging)

A.16
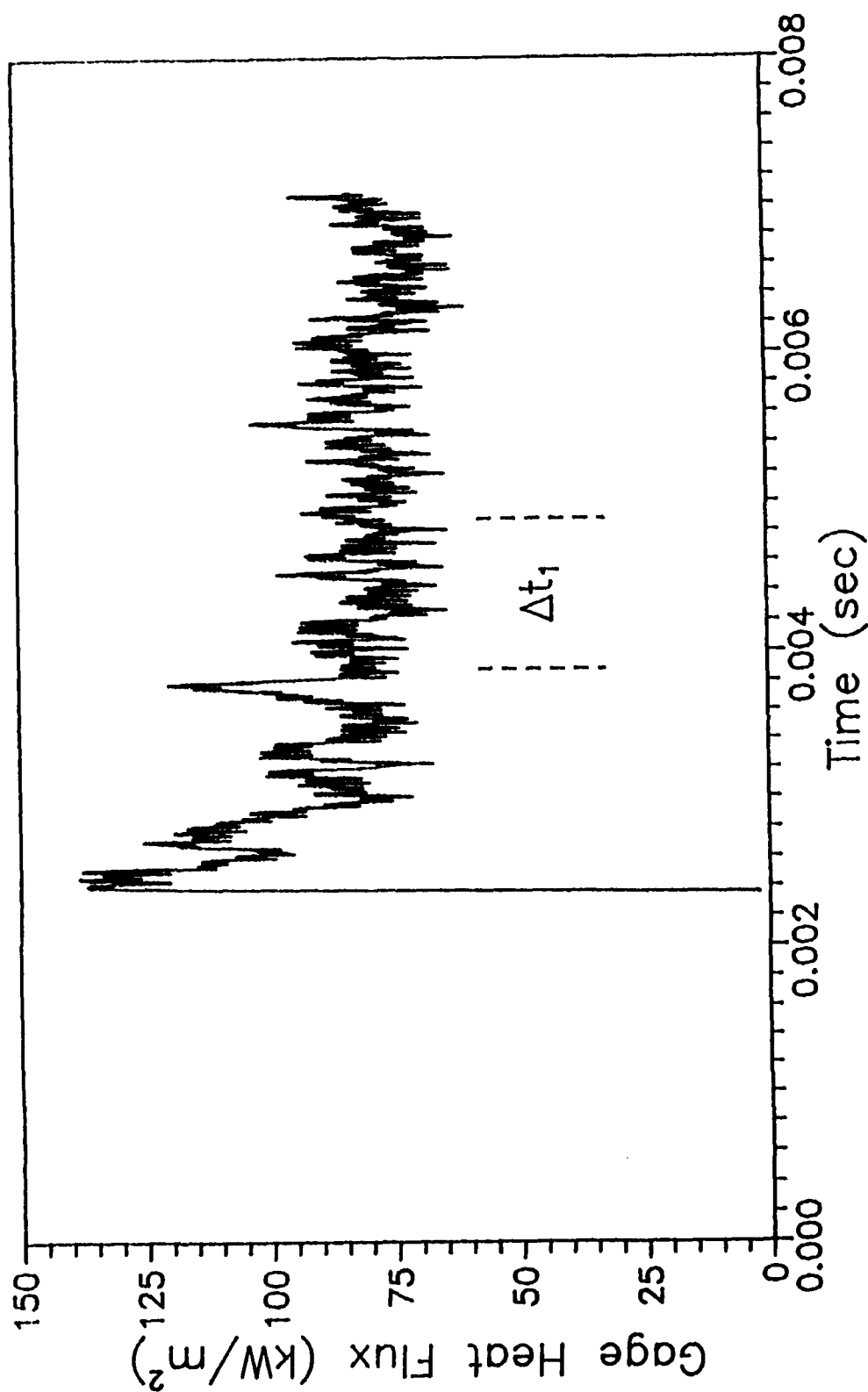
Figure 5.2 Output of Heat Flux Gage for Test J22, X/D=5.9 (Determination of Time Interval for Averaging)

A.17
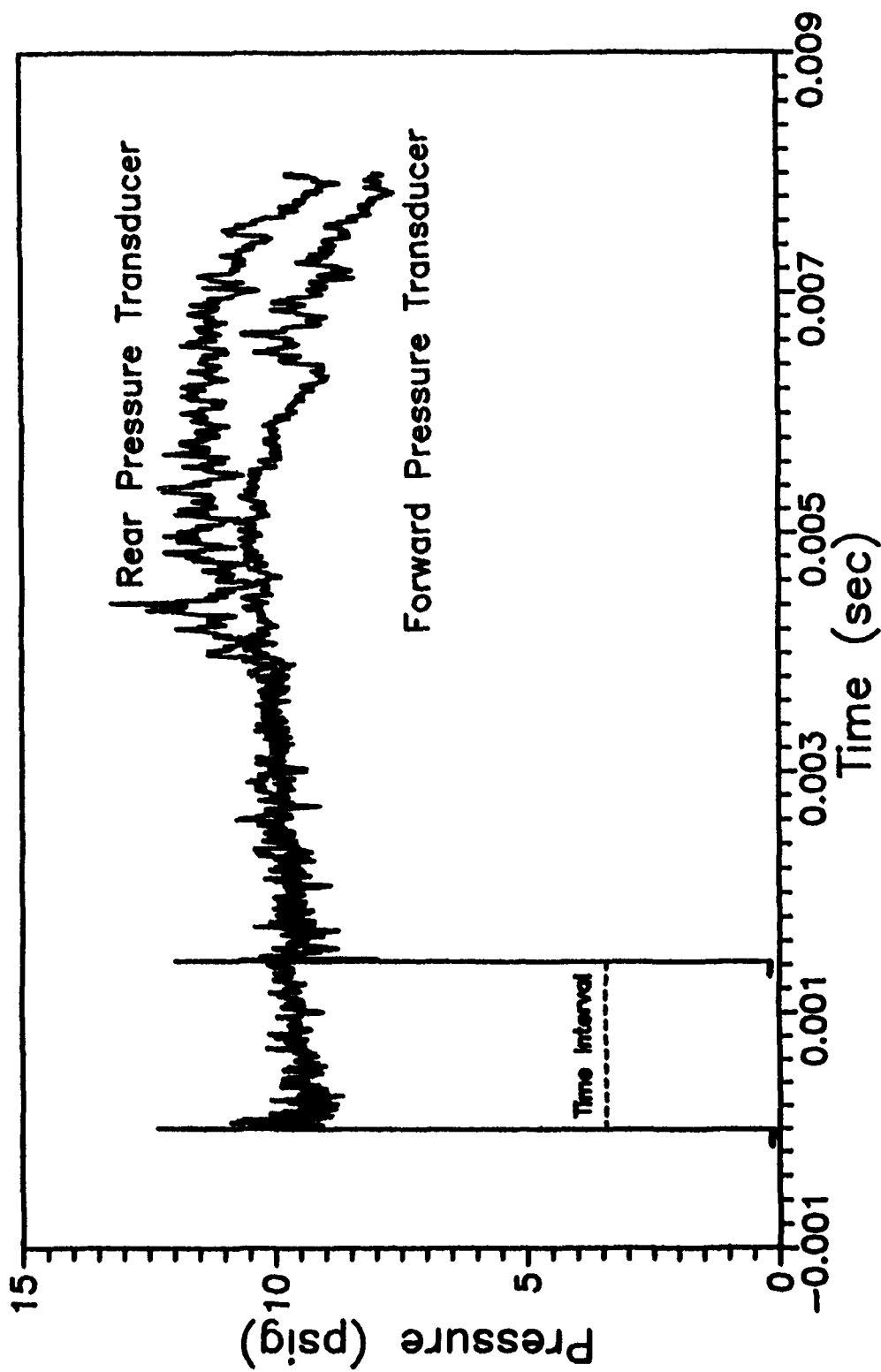
Figure 6.1 Output of Forward PX and Rear PX for Test H03
(Determination of Shock Speed)

A.18
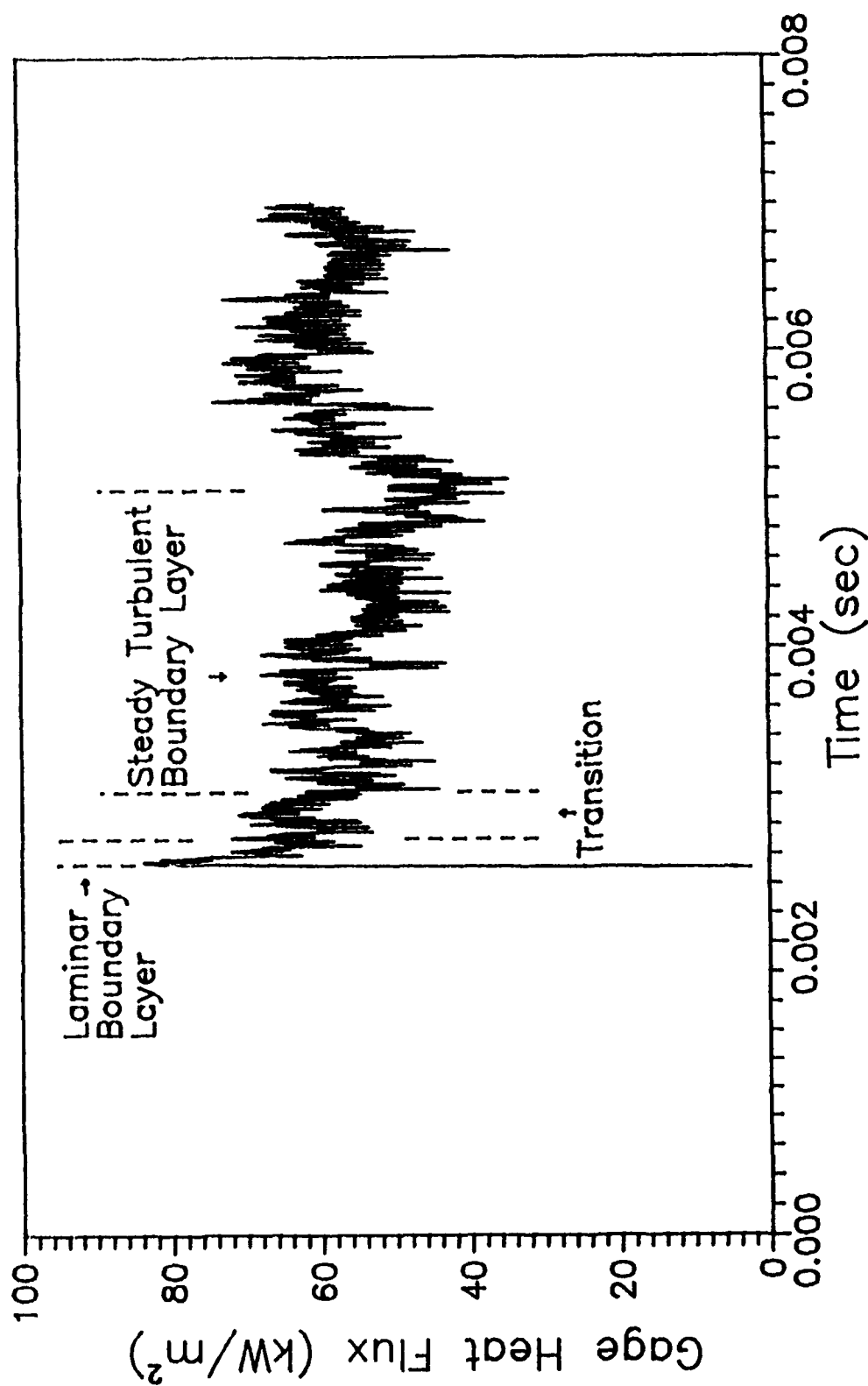
Figure 6.2 Output of Gage Heat Flux for Test H03, X/D=7.8 (Boundary Layer Nature)

A.19
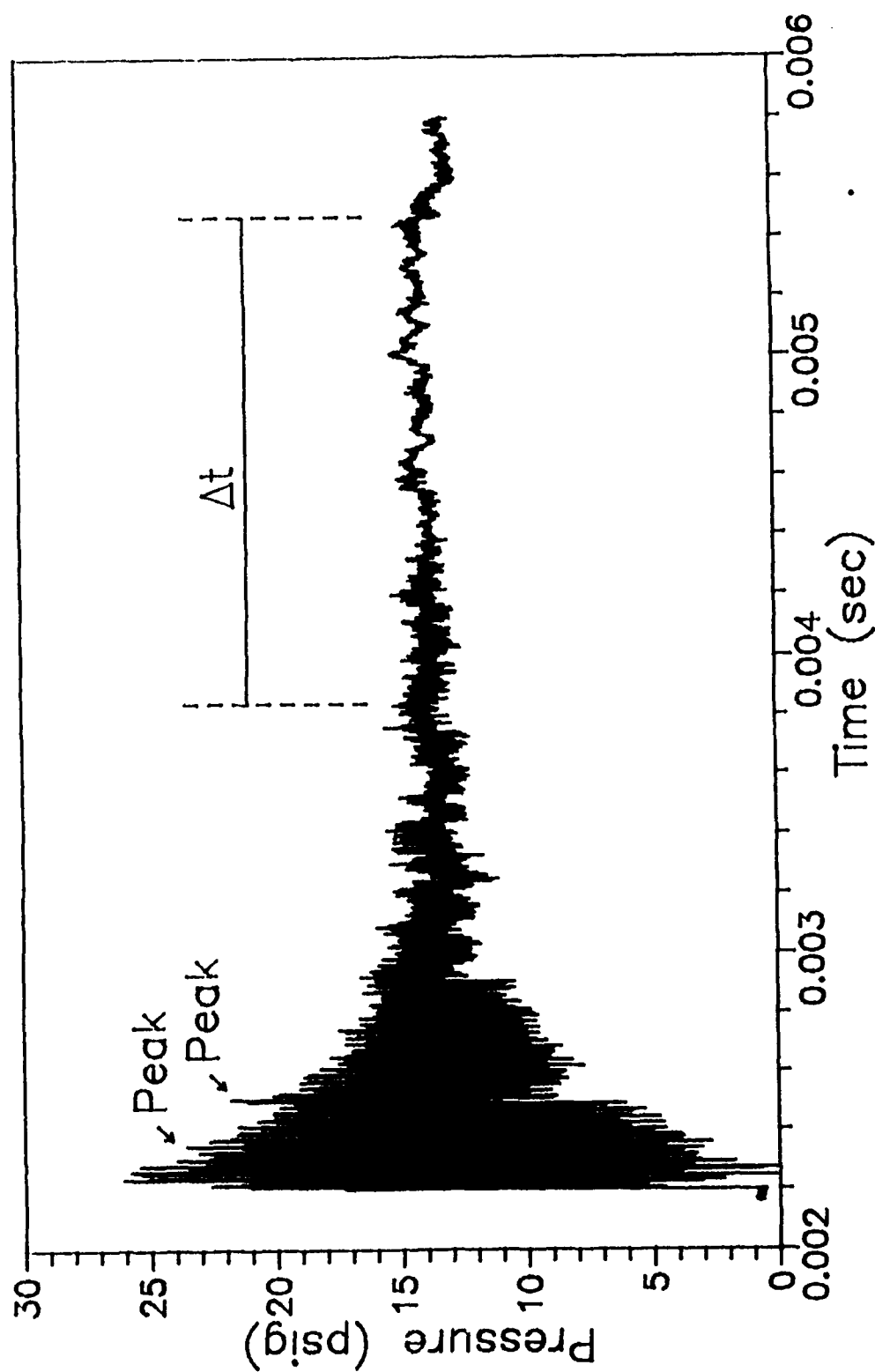
Figure 6.3 Output of Plate Pressure Transducer for Test B12 (Shock Reflections and Time Interval for Averaging)

A.20
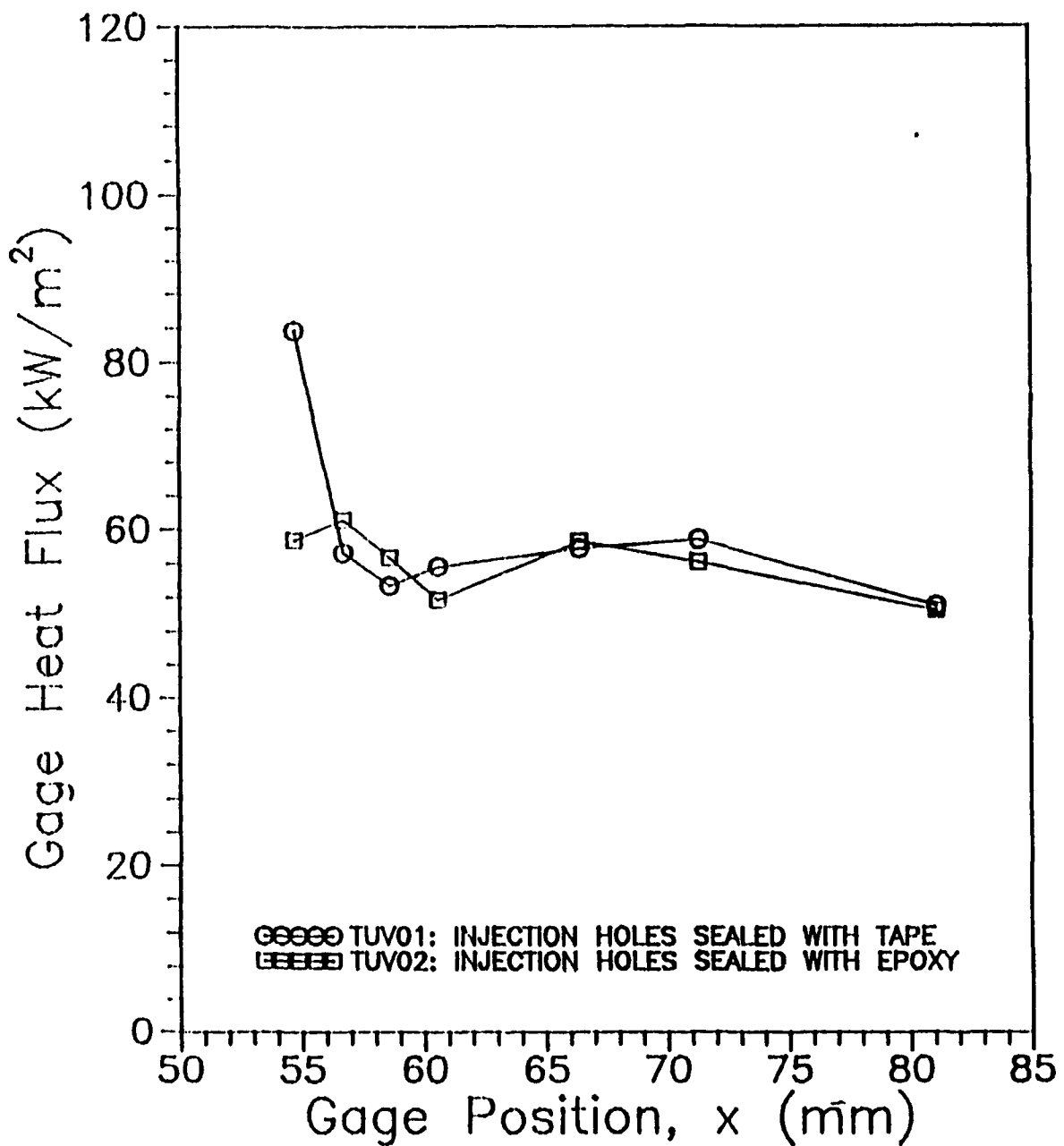
Figure 6.4 Gage Heat Flux for Tests TUV01 and TUV02
(Effect of the Injection Hole Seal)
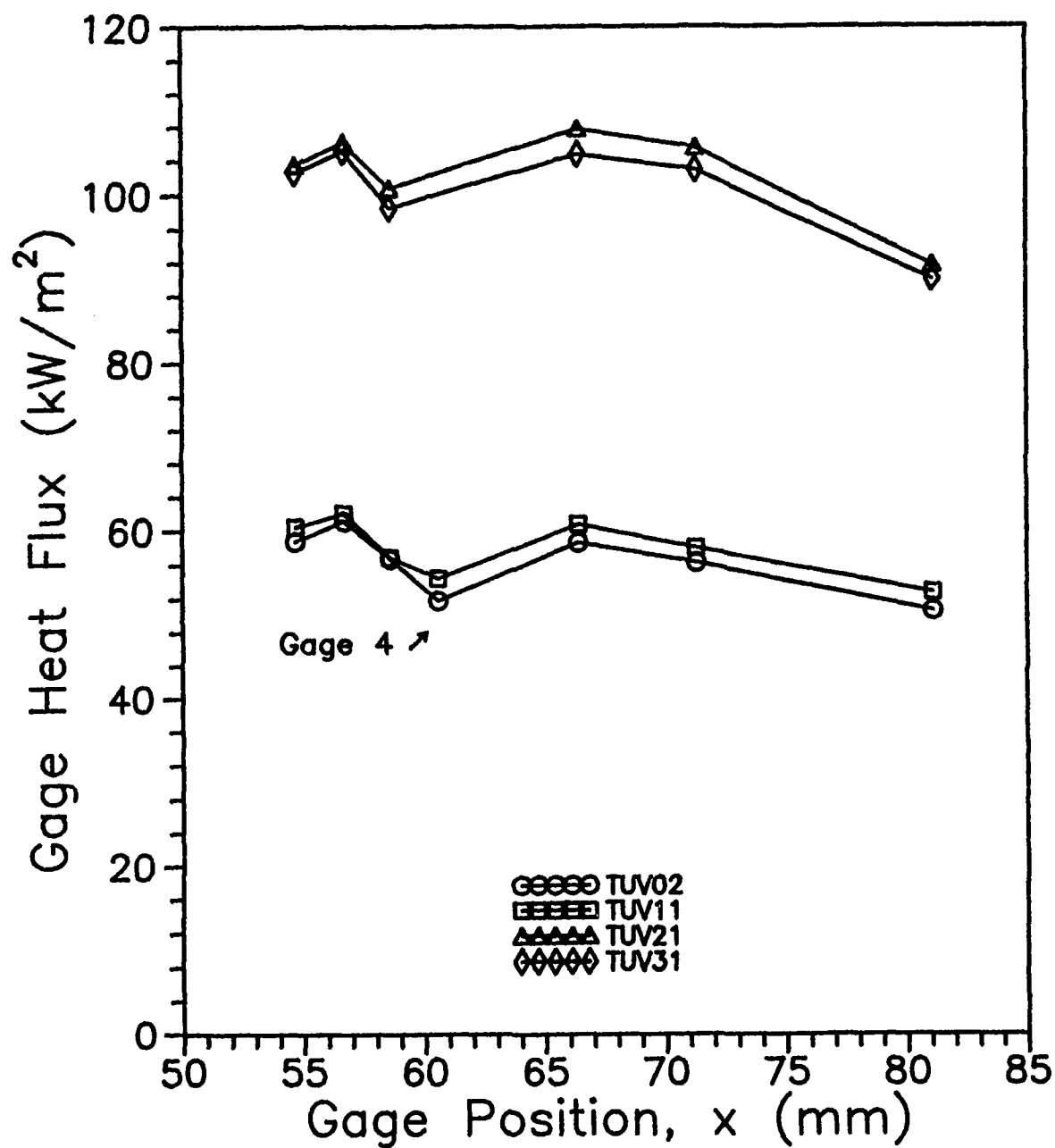
Figure 6.5 Gage Heat Flux for Tests TUV02, TUV11, TUV21, TUV31

A.22
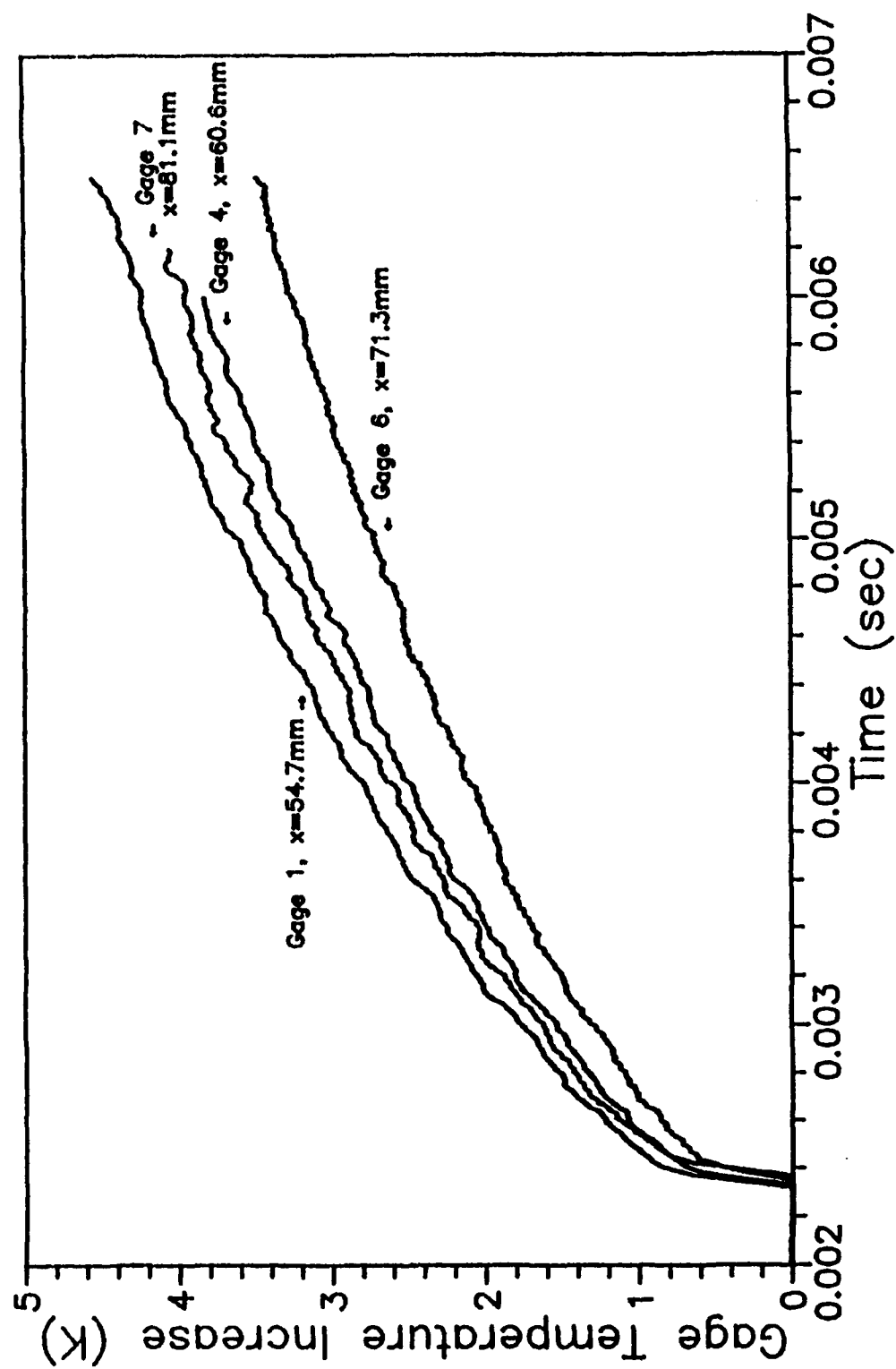
Figure 6.6.1 Gage Temperature Increase for the Aluminum Plate, Test T21

A.23
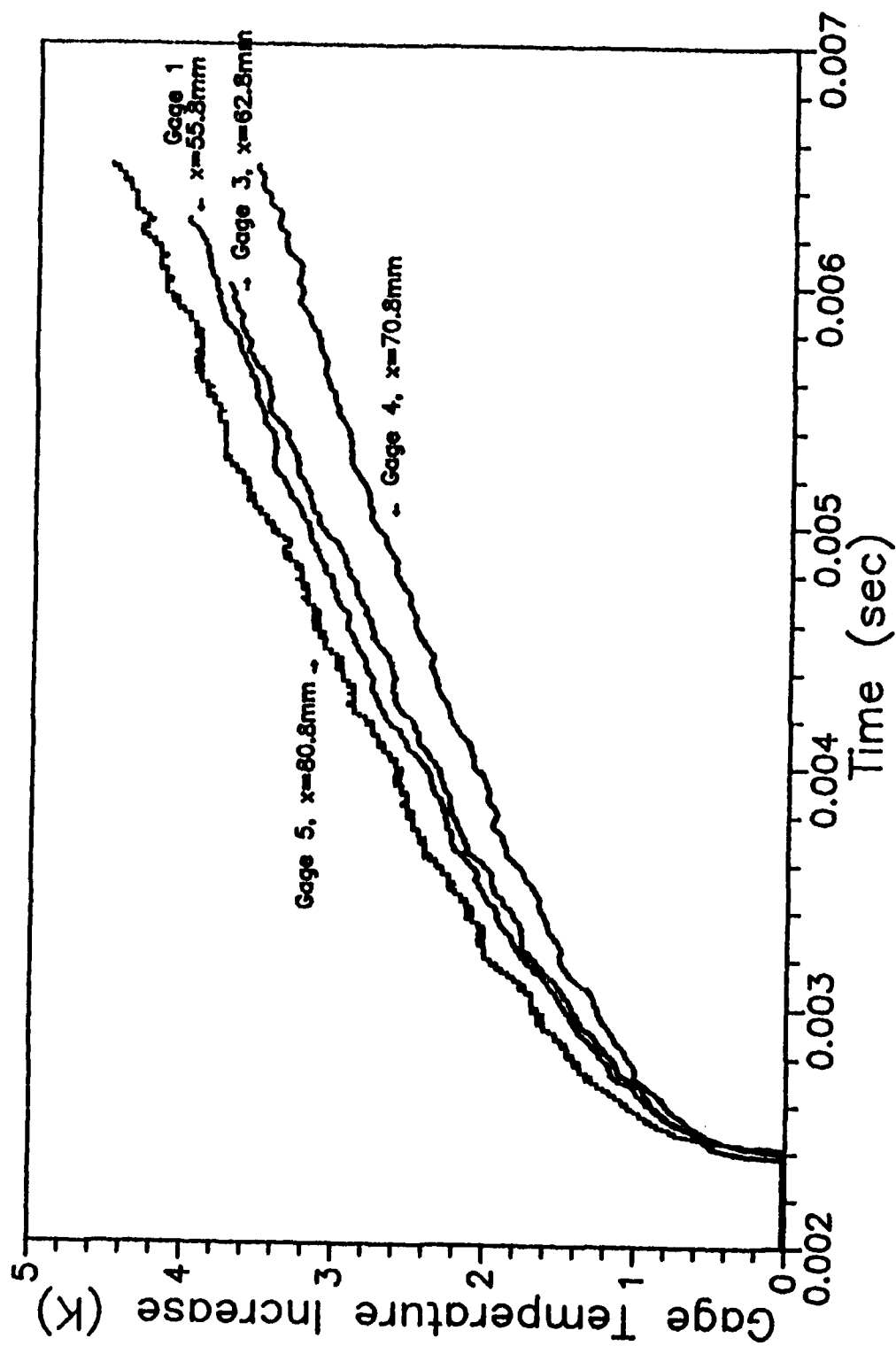
Figure 6.6.2 Gage Temperature Increase for the Corian Plate, Test Q02

A.24
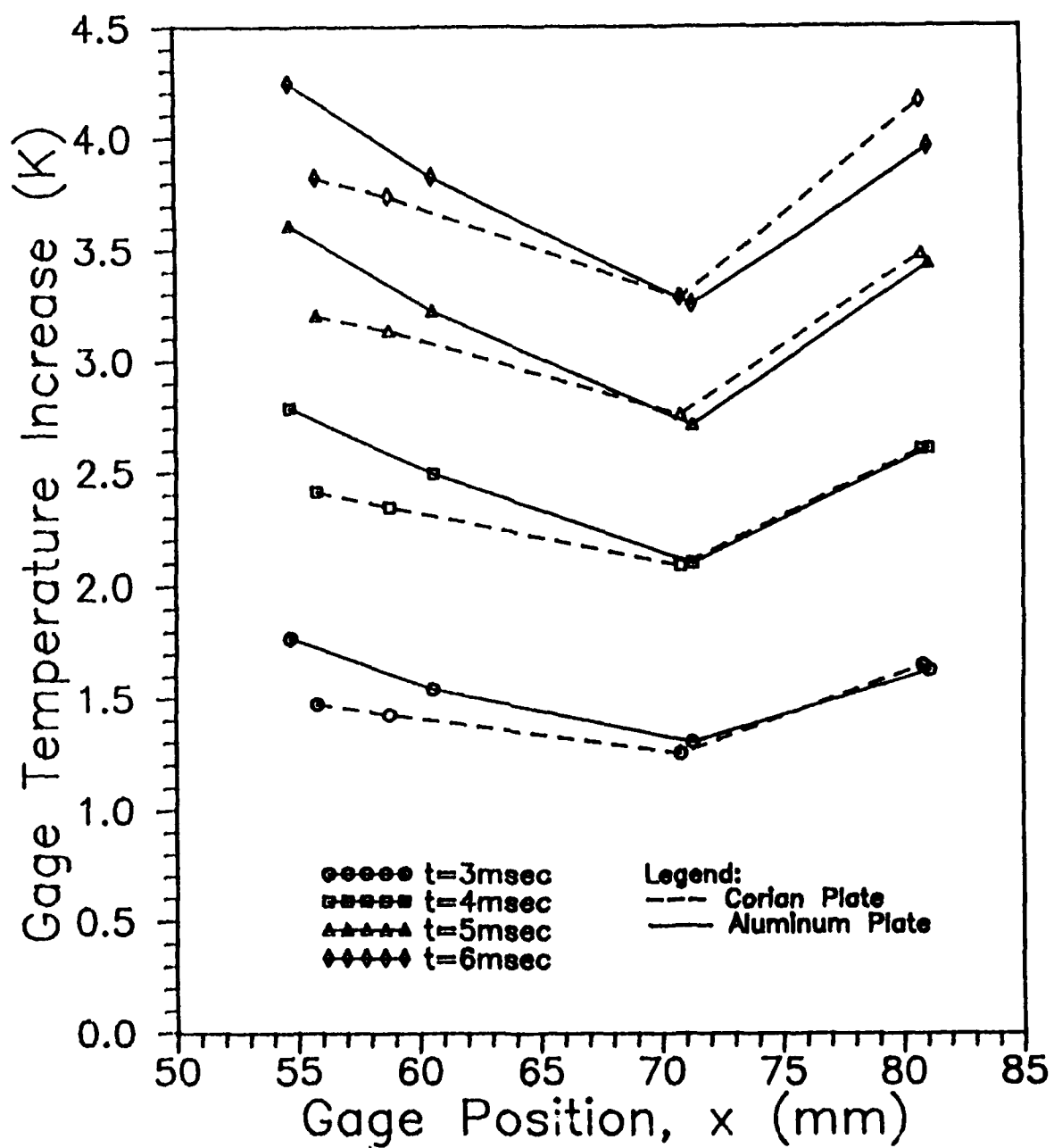
Figure 6.6.3 Gage Temperature Increase Comparison between the Aluminum (Test T21) and Corian (Test Q02) Plates

A.25
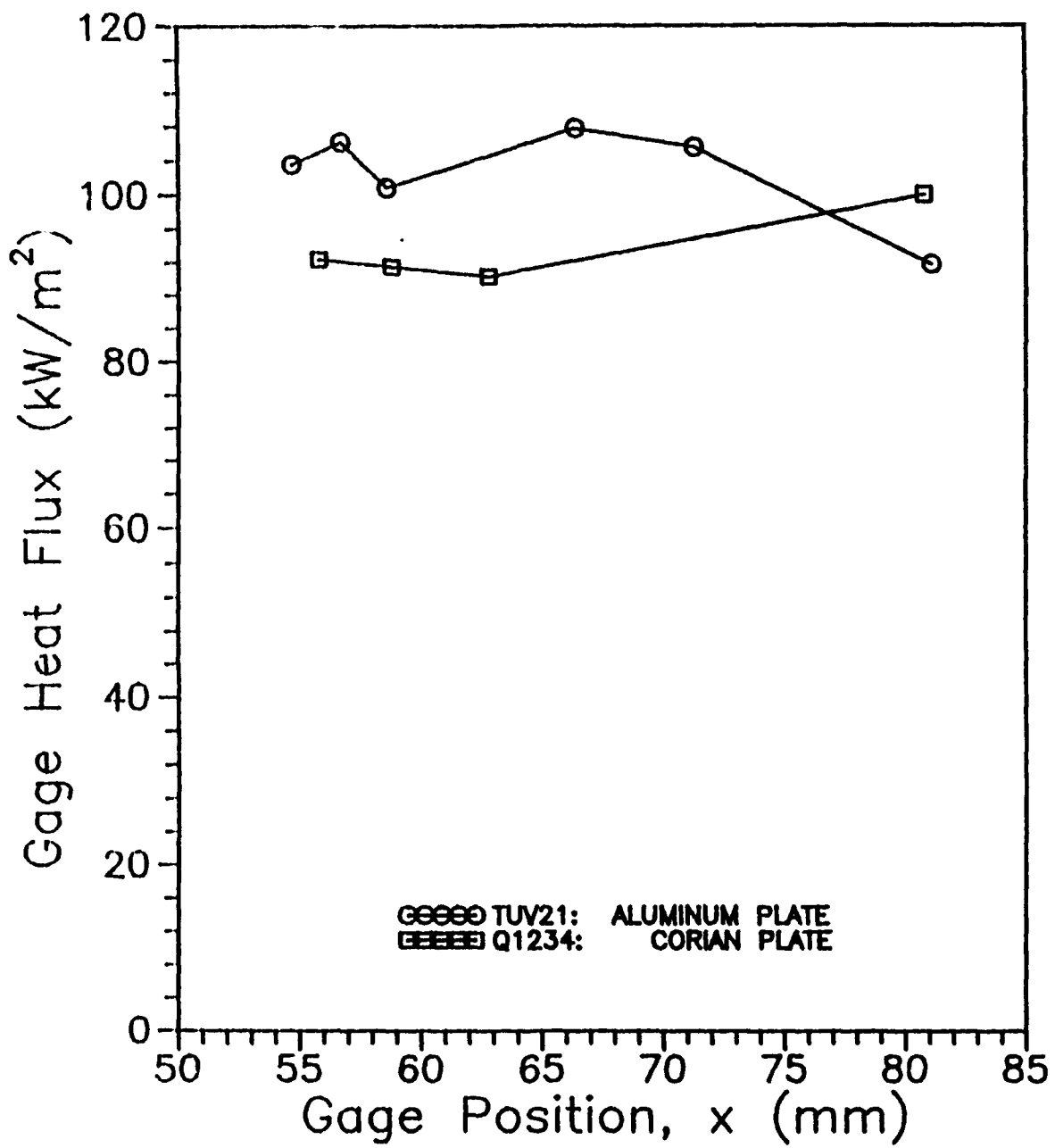
Figure 6.7 Gage Heat Flux Comparison between the Aluminum and Corian Plates for Tests TUV21 and Q1234

A.26
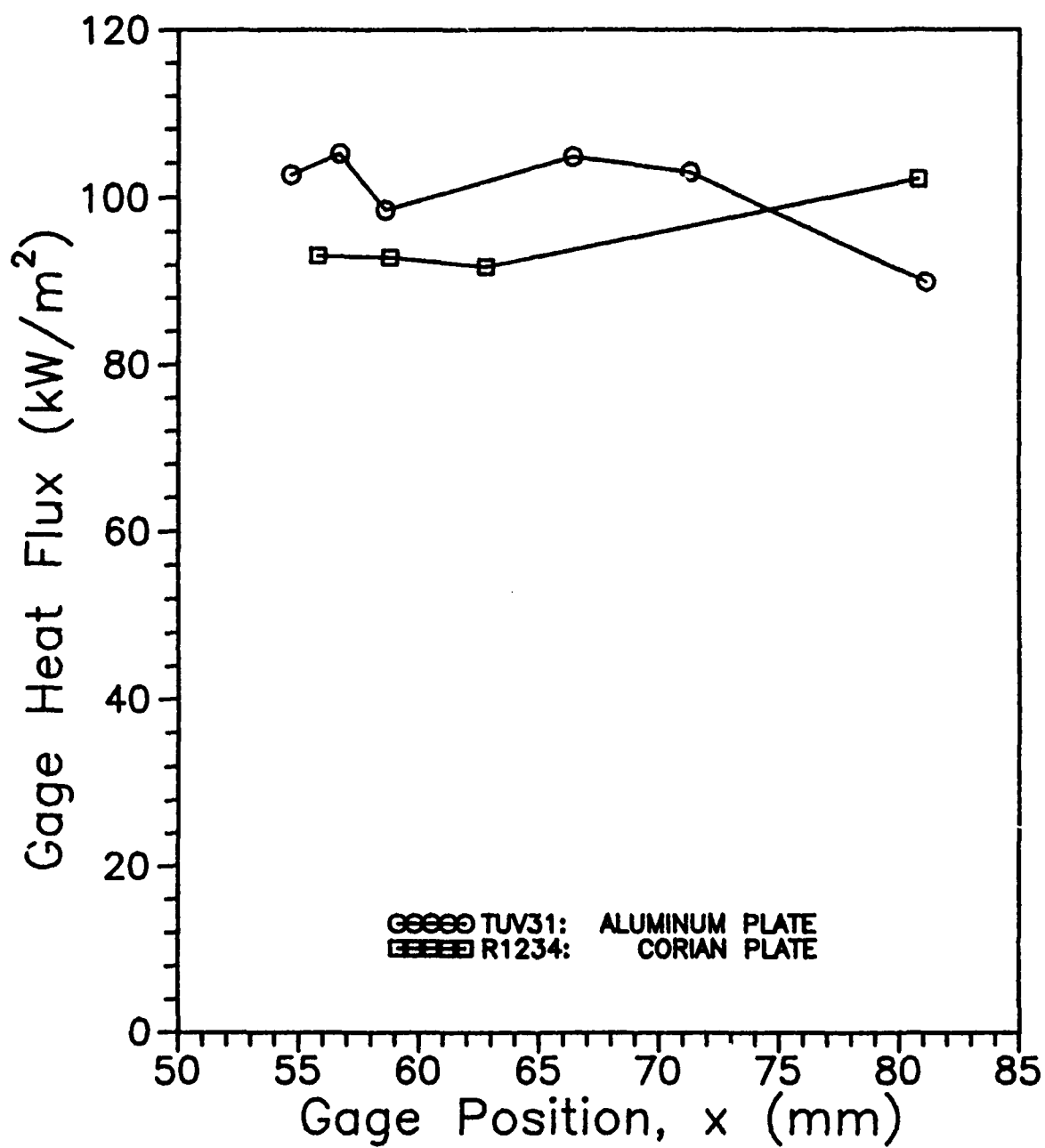
Figure 6.8 Gage Heat Flux Comparison between the Aluminum and Corian Plates for Tests TUV31 and R1234

A.27
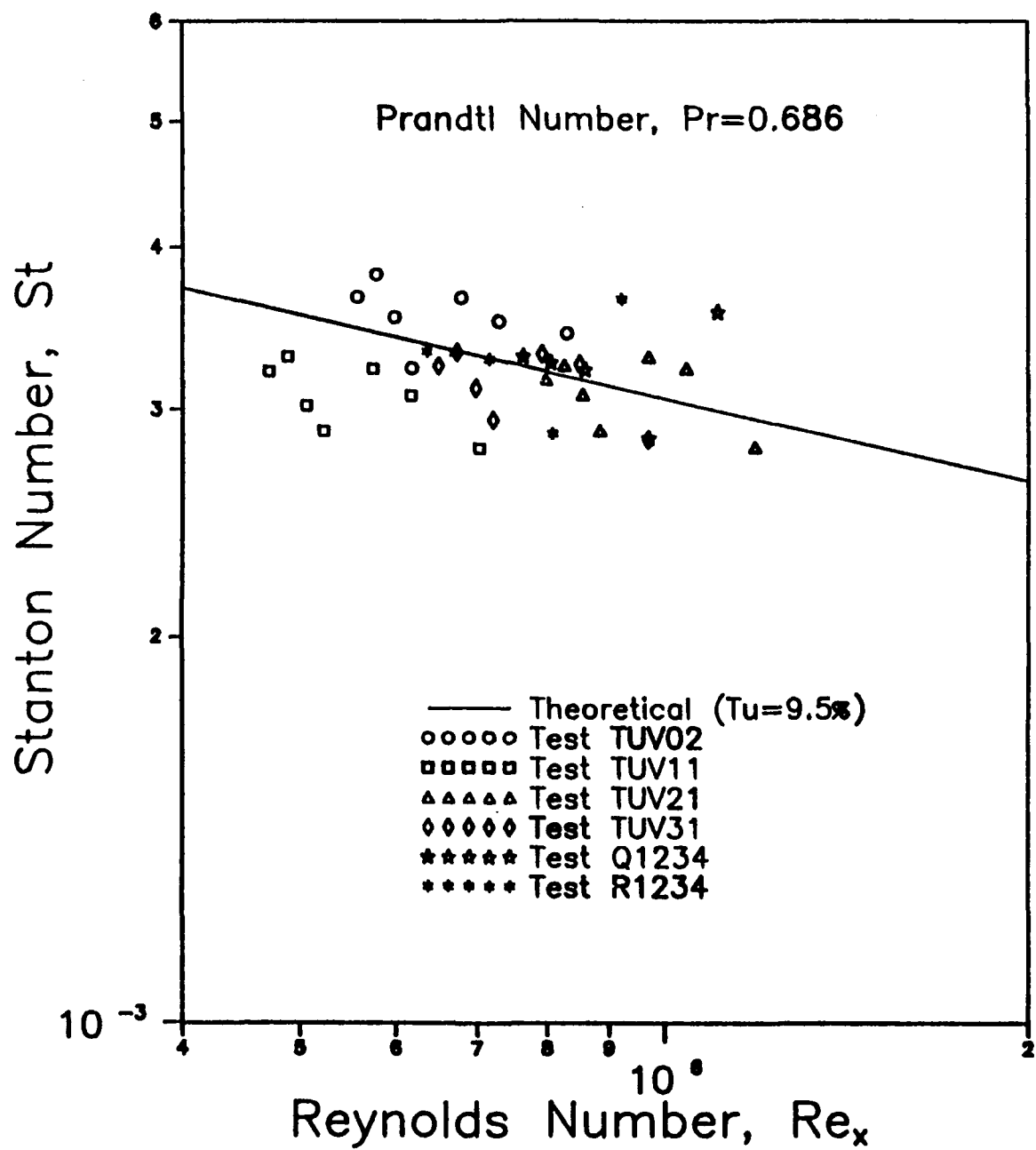
Figure 6.9 Stanton Number vs. Reynolds Number, No Film Cooling

A.28
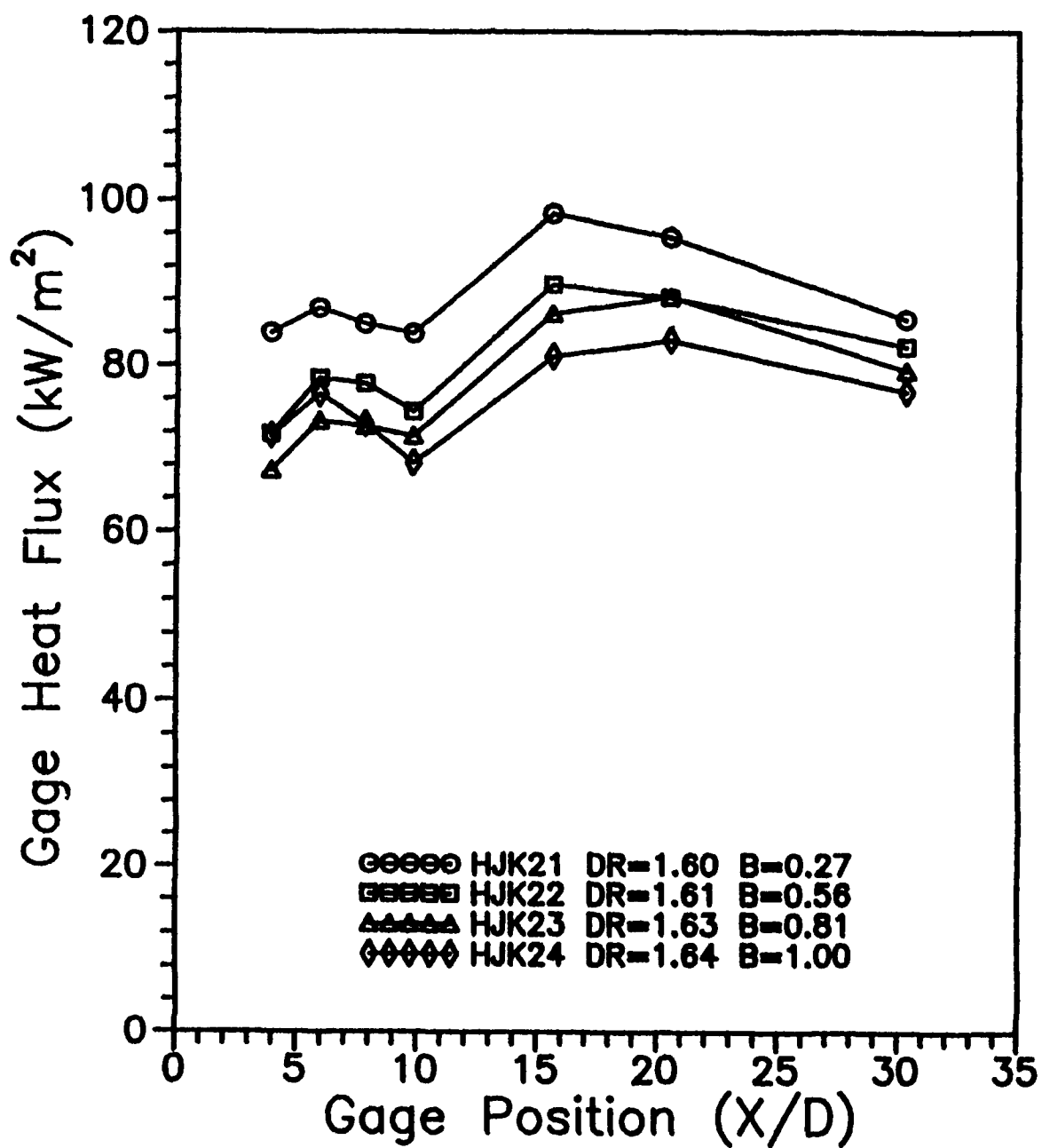
Figure 6.10.1 Gage Heat Flux for the Aluminum Plate in the Weak Injection Regime, $M_2=0.418$

A.29
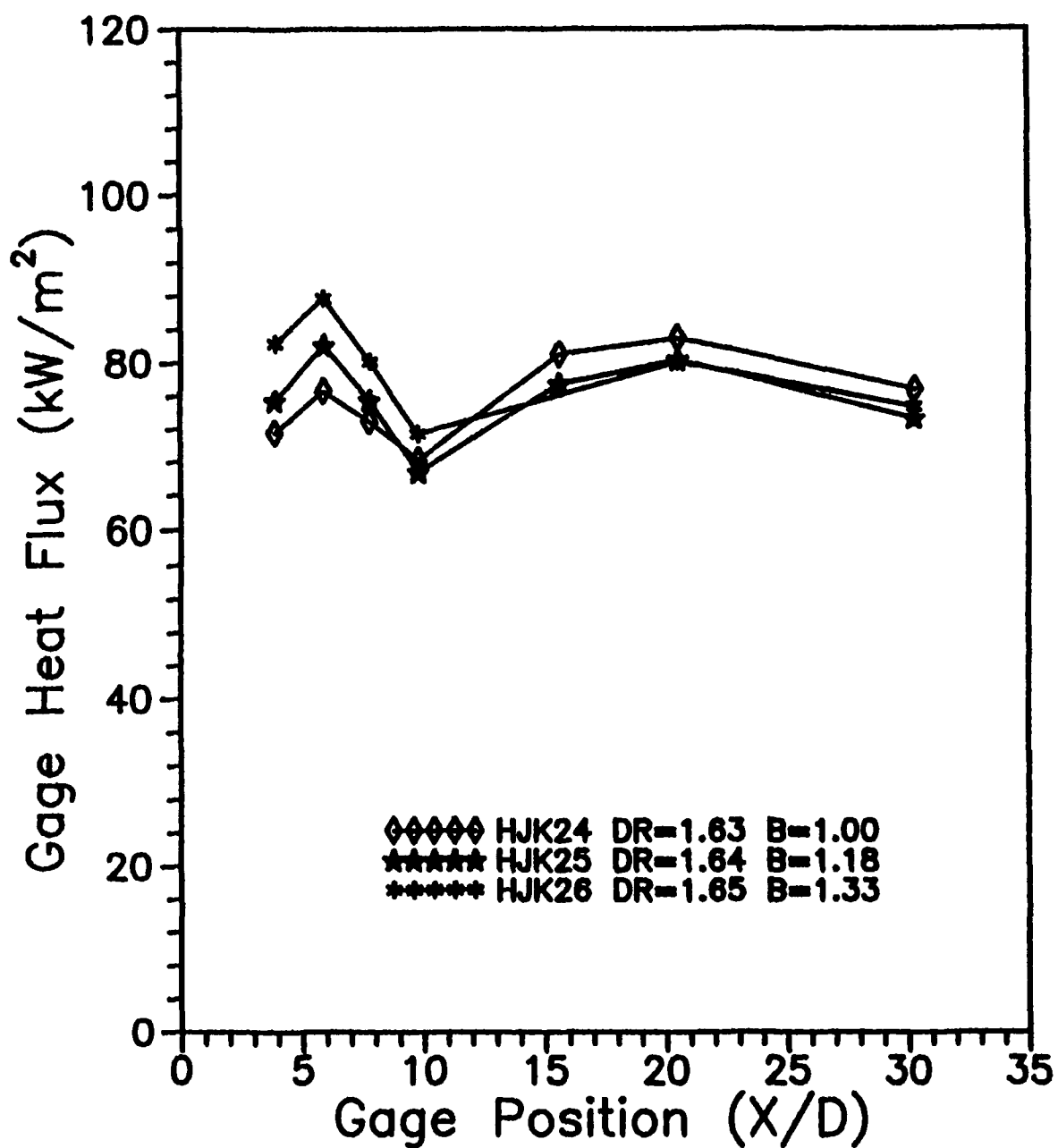
Figure 6.10.2 Gage Heat Flux for the Aluminum Plate in the
Strong Injection Regime, M_2=0.418

A.30
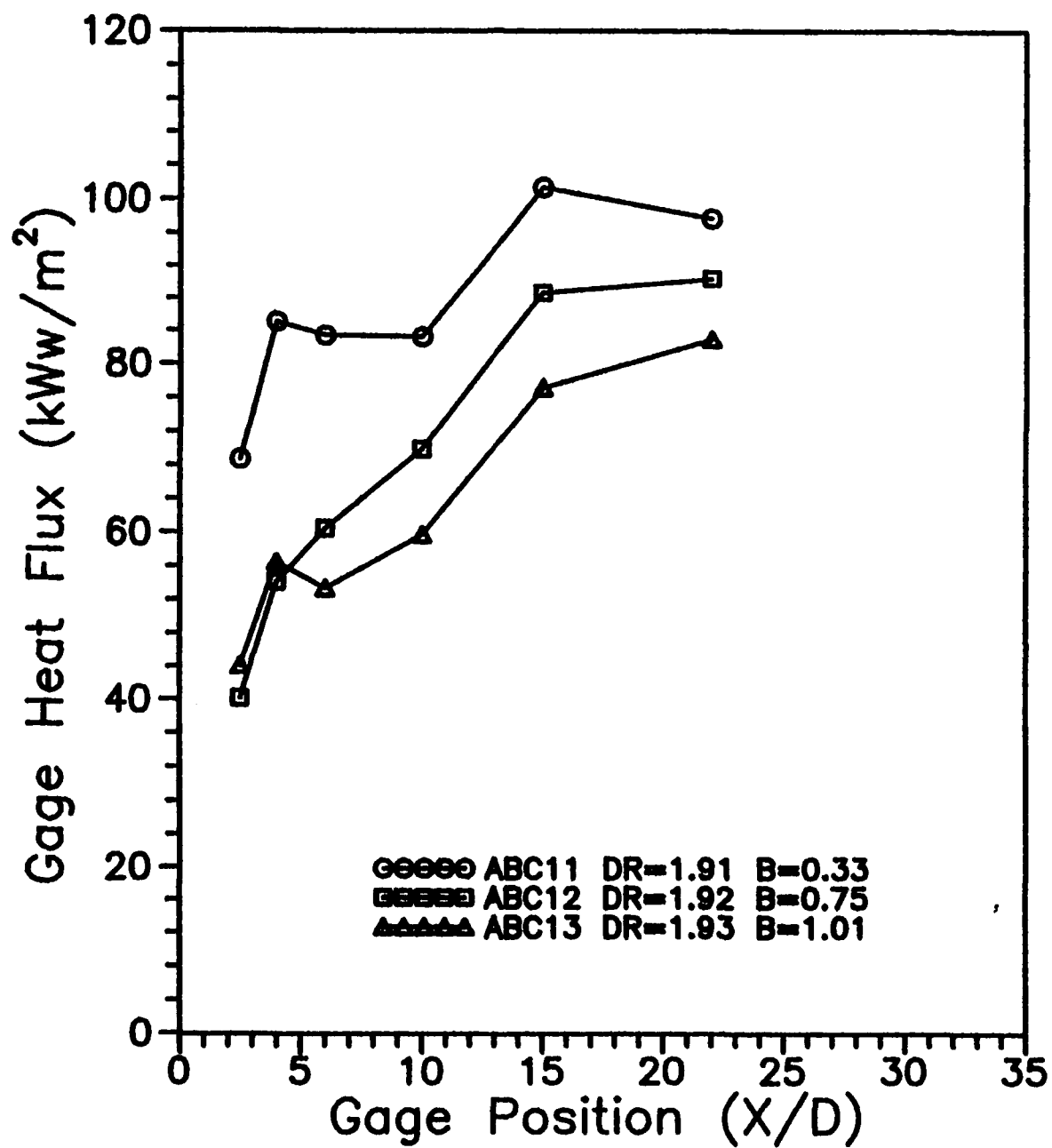
Figure 6.11.1 Gage Heat Flux for the Corian Plate in the Weak Injection Regime, $M_2 = 0.382$

A.31
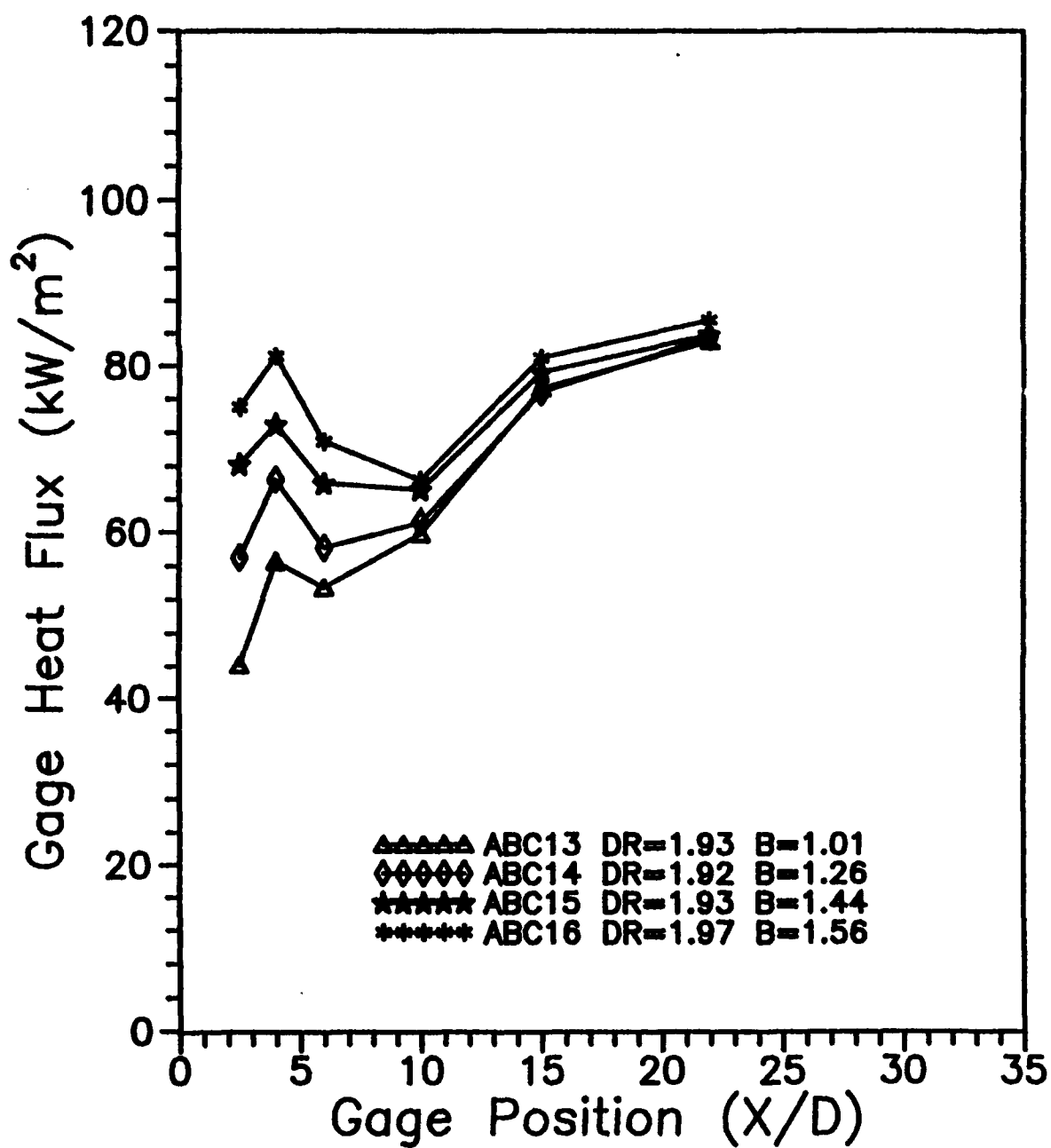
Figure 6.11.2 Gage Heat Flux for the Corian Plate in the Strong Injcetion Regime, M_2=0.382

A.32
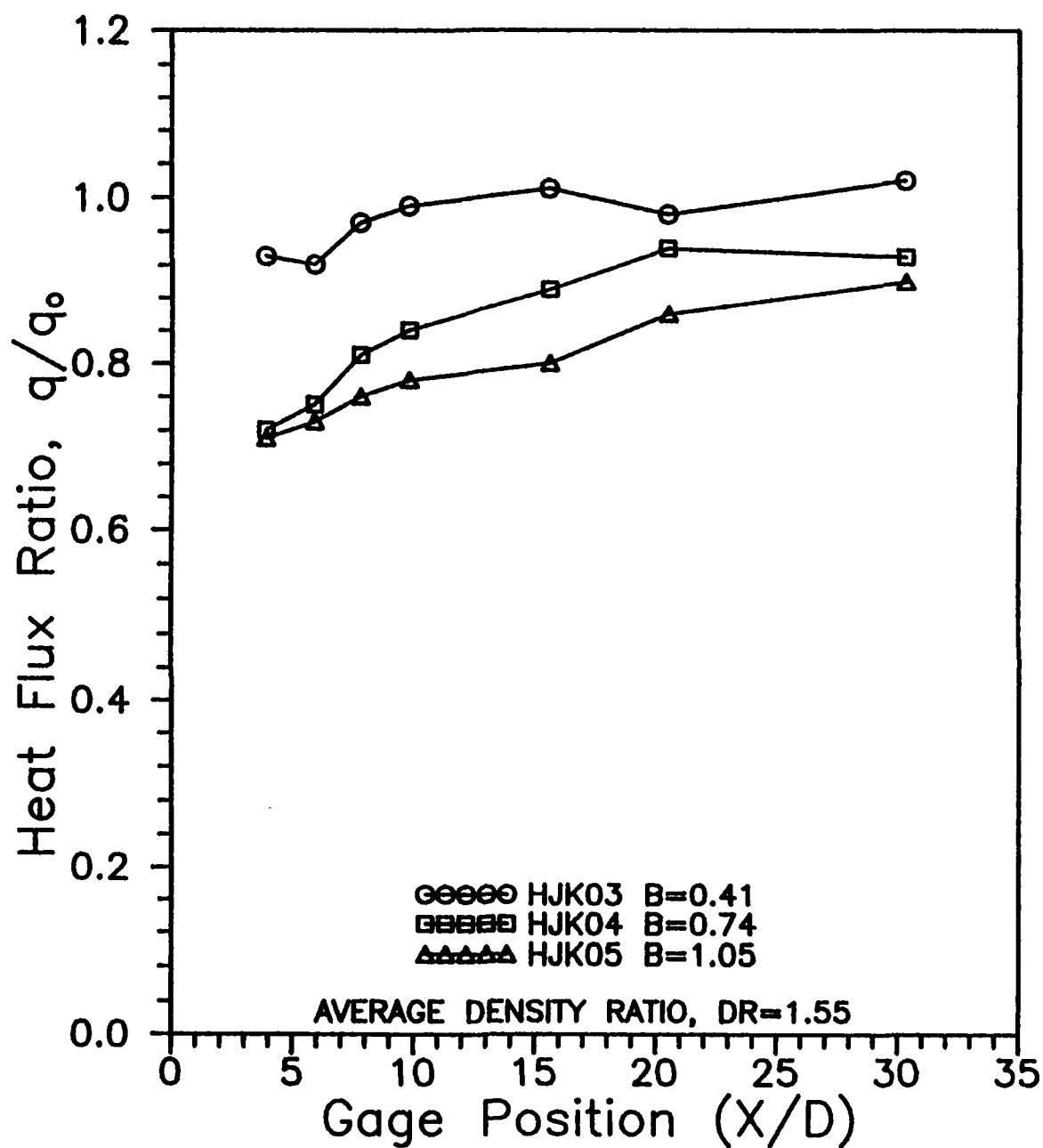
Figure 6.12.1 Gage Heat Flux Ratio for the Aluminum Plate in the
Weak Injection Regime, DR=1.55, M_2=0.324

A.33
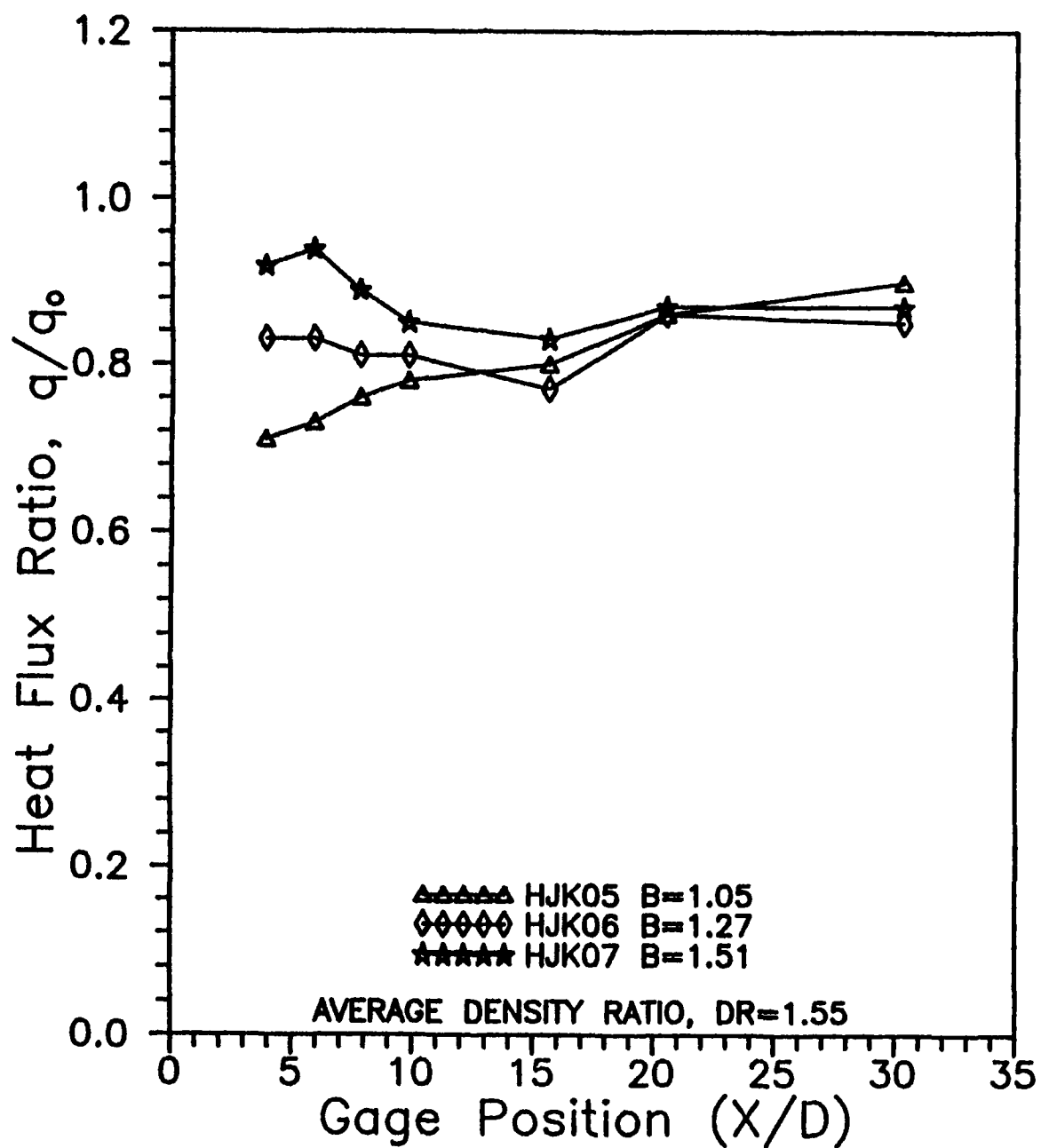
Figure 6.12.2 Gage Heat Flux Ratio for the Aluminum Plate in the Strong Injection Regime, DR=1.55, M₂=0.324

A.34
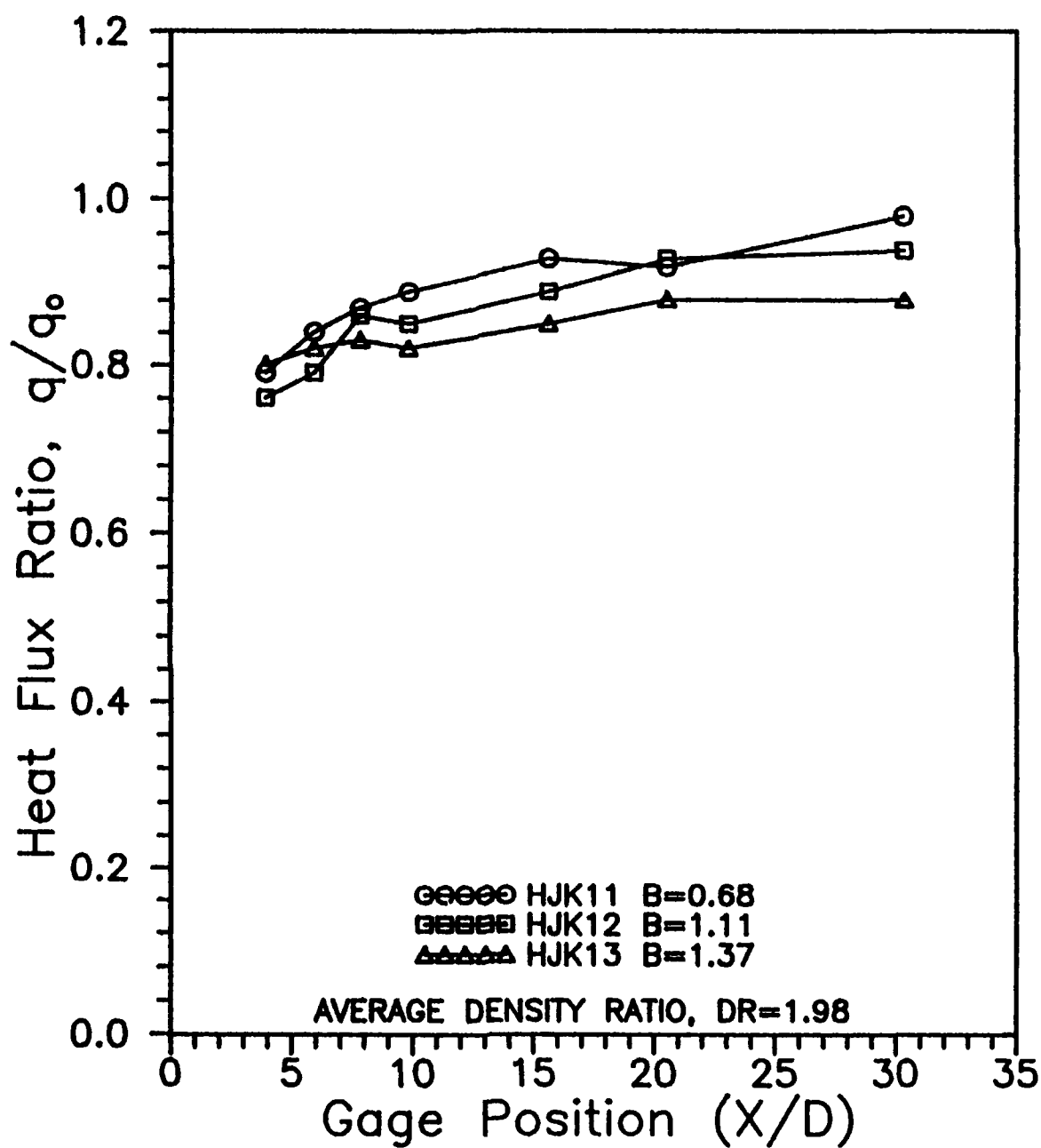
Figure 6.13.1 Gage Heat Flux Ratio for the Aluminum Plate in the Weak Injection Regime, DR=1.98, M$_e$=0.312
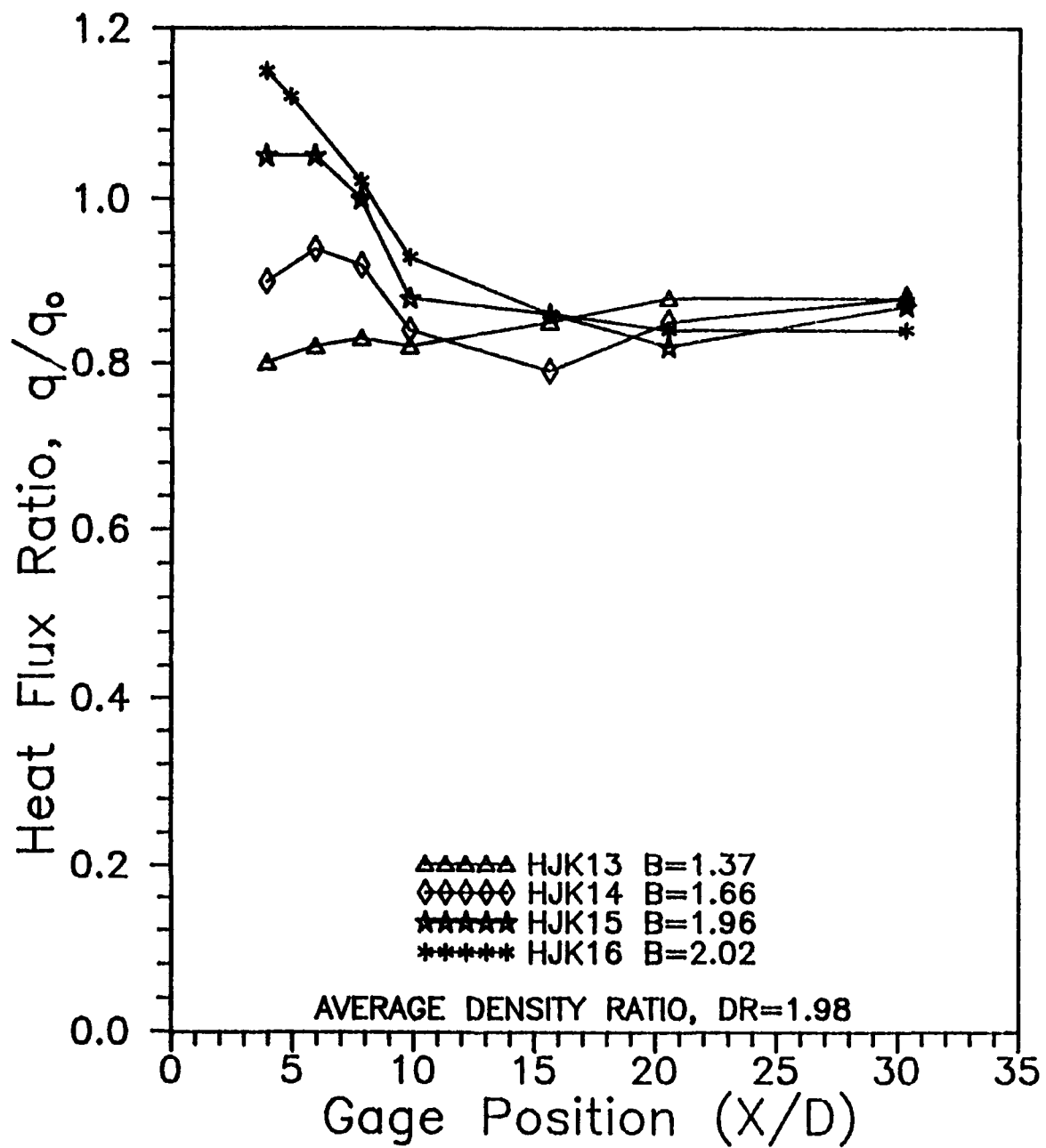
Figure 6.13.2 Gage Heat Flux Ratio for the Aluminum Plate in the
Strong Injection Regime, DR=1.98, M_2=0.312

A.36
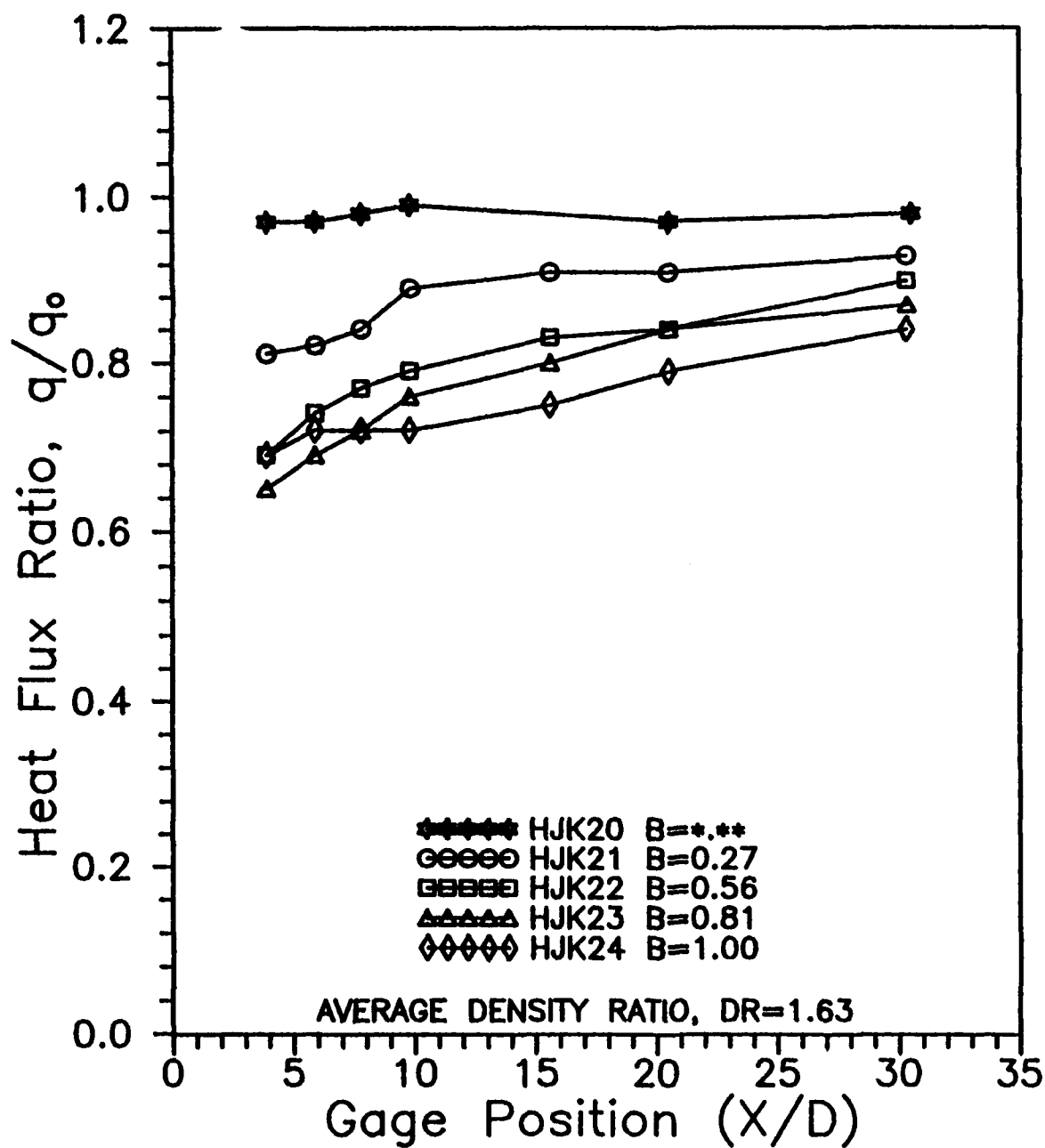
Figure 6.14.1 Gage Heat Flux Ratio for the Aluminum Plate in the Weak Injection Regime, DR=1.63, M_2=0.418
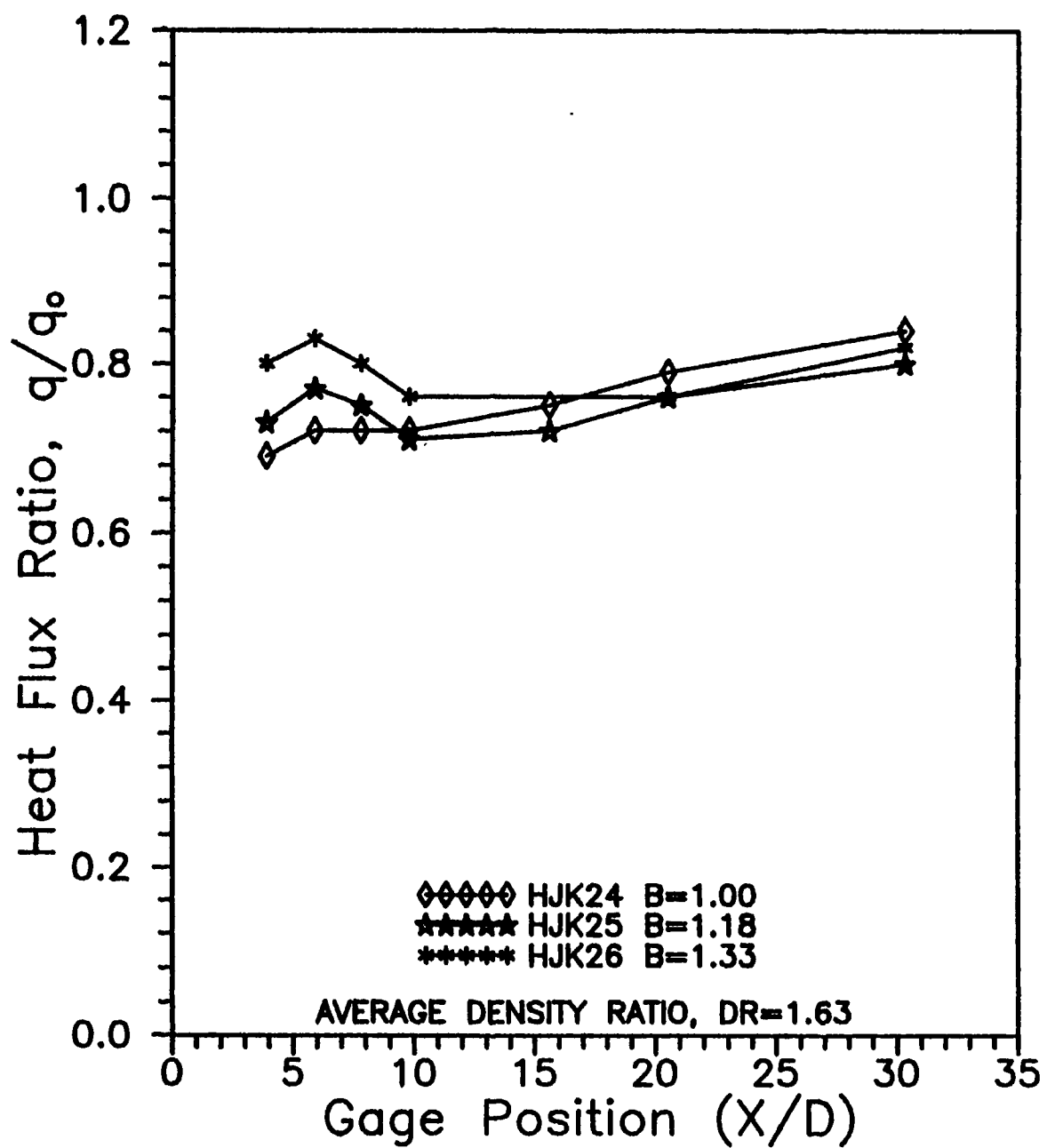
Figure 6.14.2 Gage Heat Flux Ratio for the Aluminum Plate in the Strong Injection Regime, DR=1.63, M_2=0.418

A.38
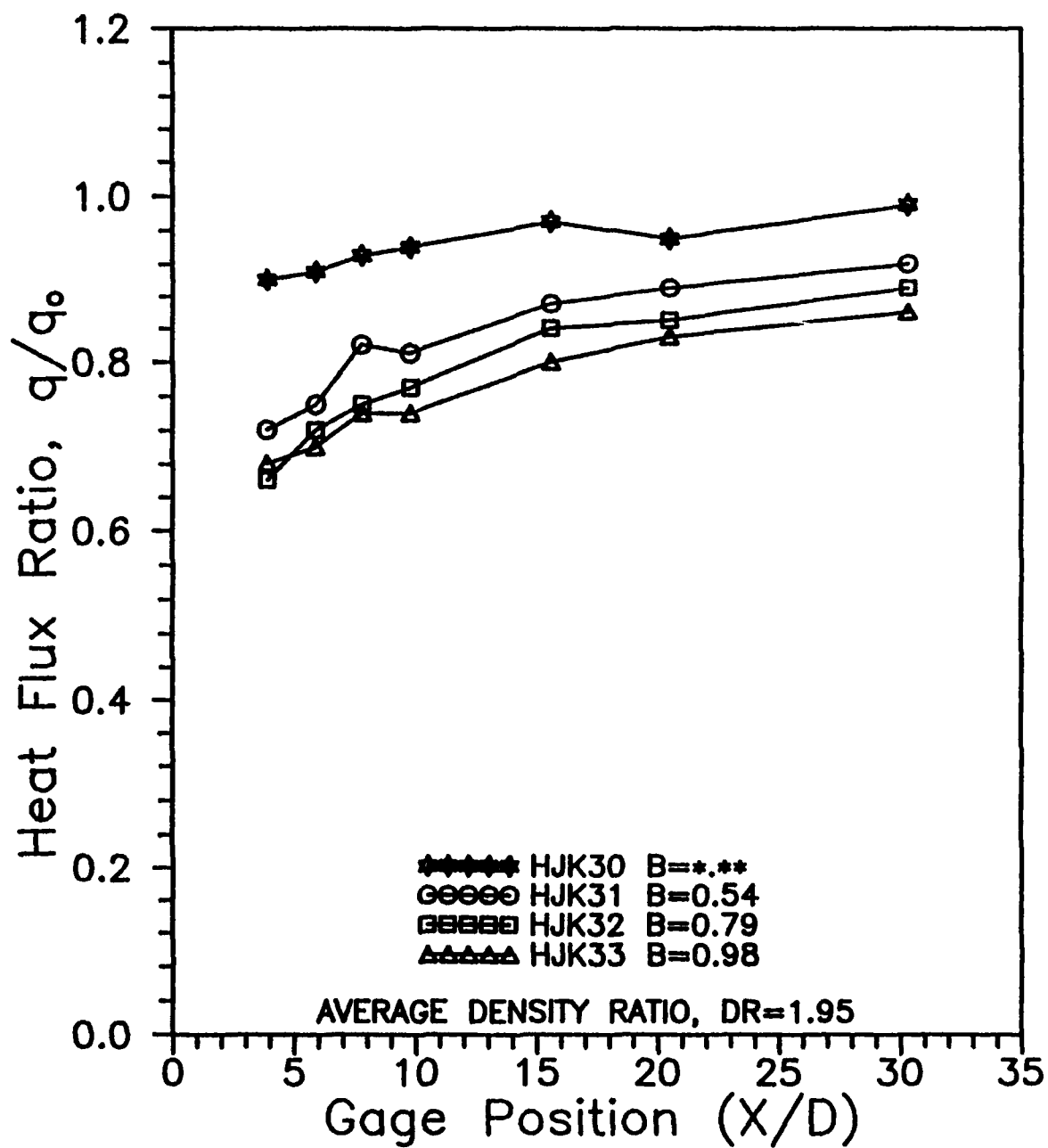
Figure 6.15.1 Gage Heat Flux Ratio for the Aluminum Plate in the Weak Injection Regime, DR=1.95, M_2=0.402

A.39
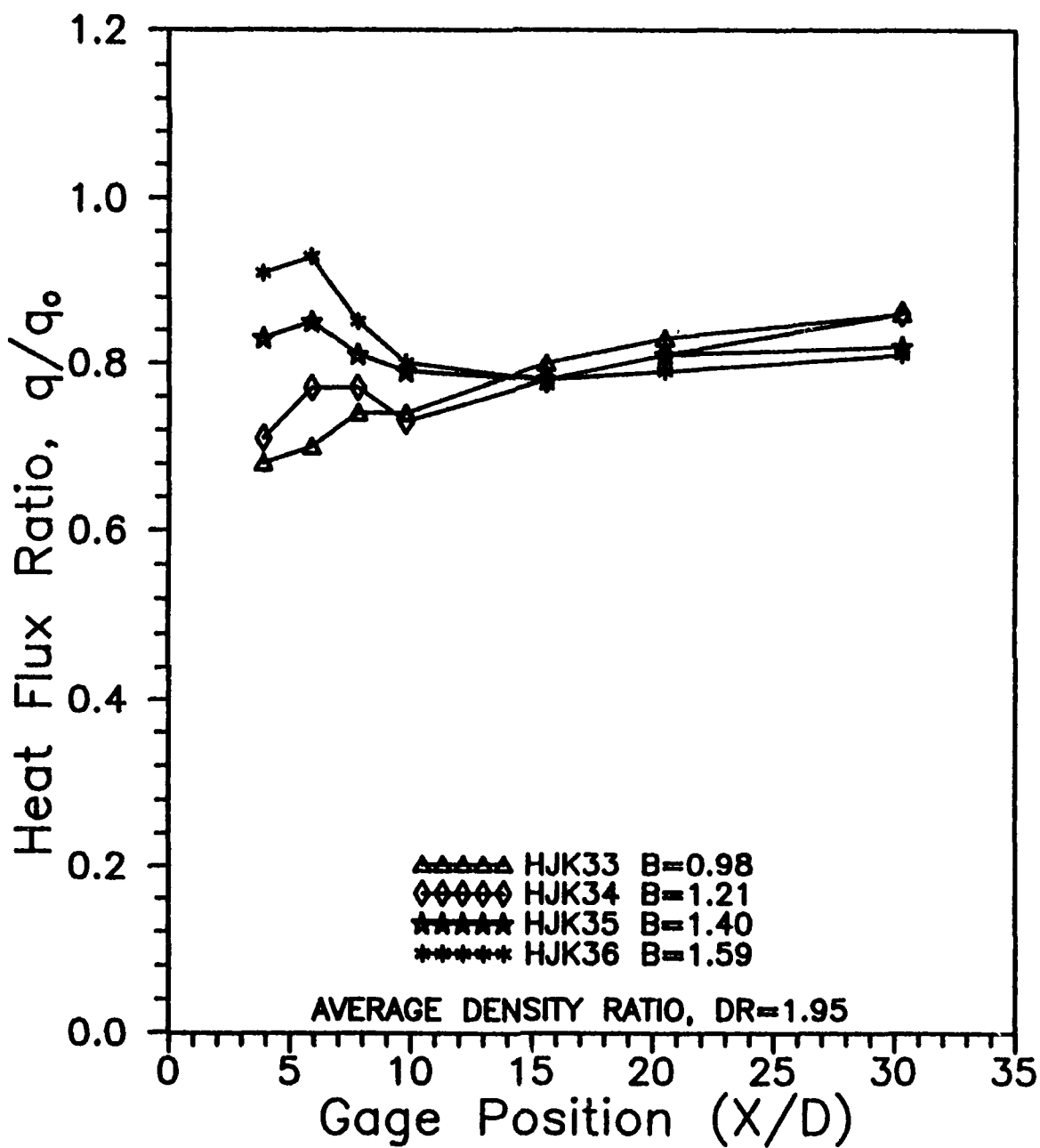
Figure 6.15.2 Gage Heat Flux Ratio for the Aluminum Plate in the Strong Injection Regime, DR=1.95, M_2=0.402

A.40
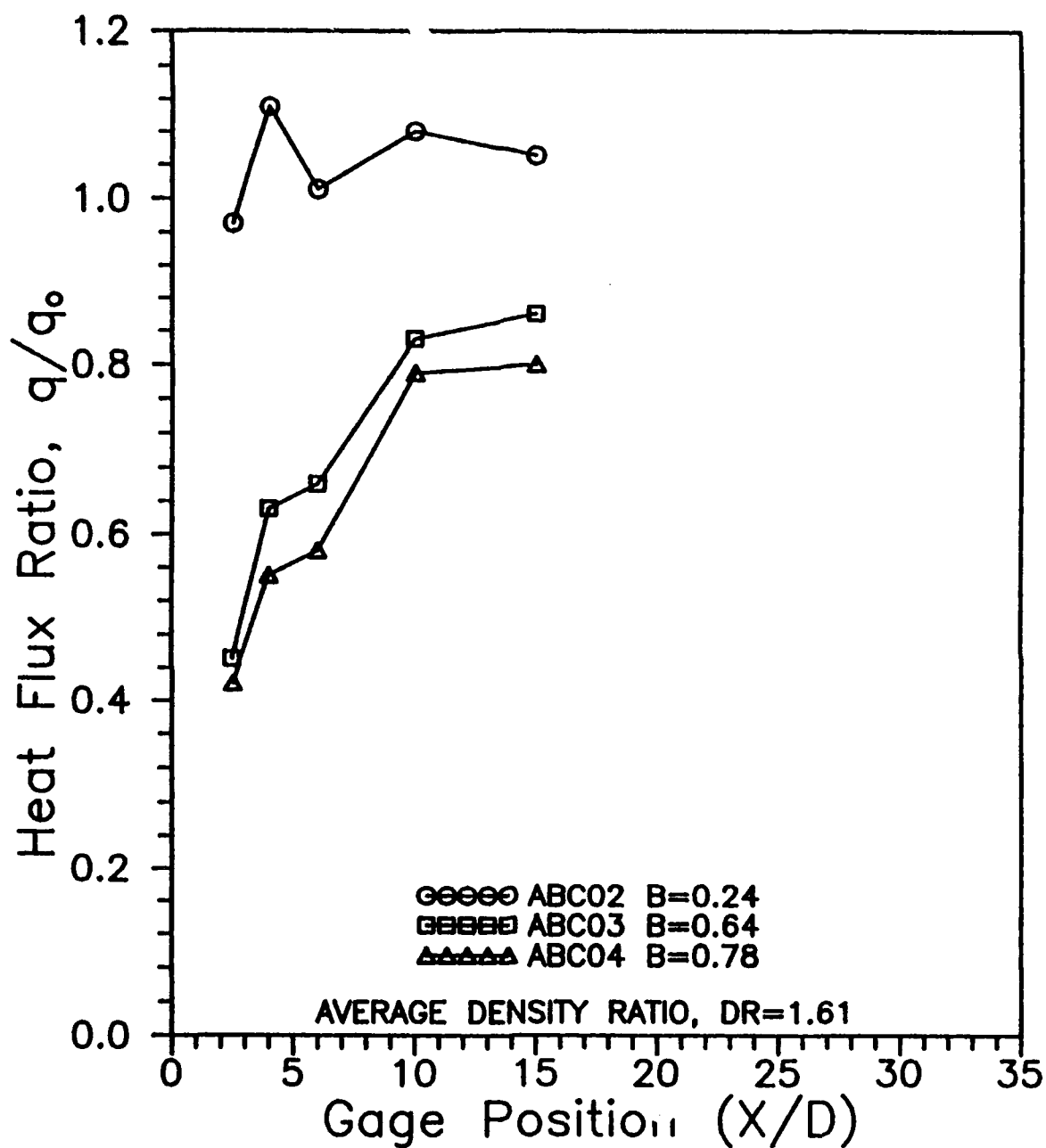
Figure 6.16.1 Gage Heat Flux Ratio for the Corian Plate in the Weak Injection Regime, DR=1.61, M_2=0.426
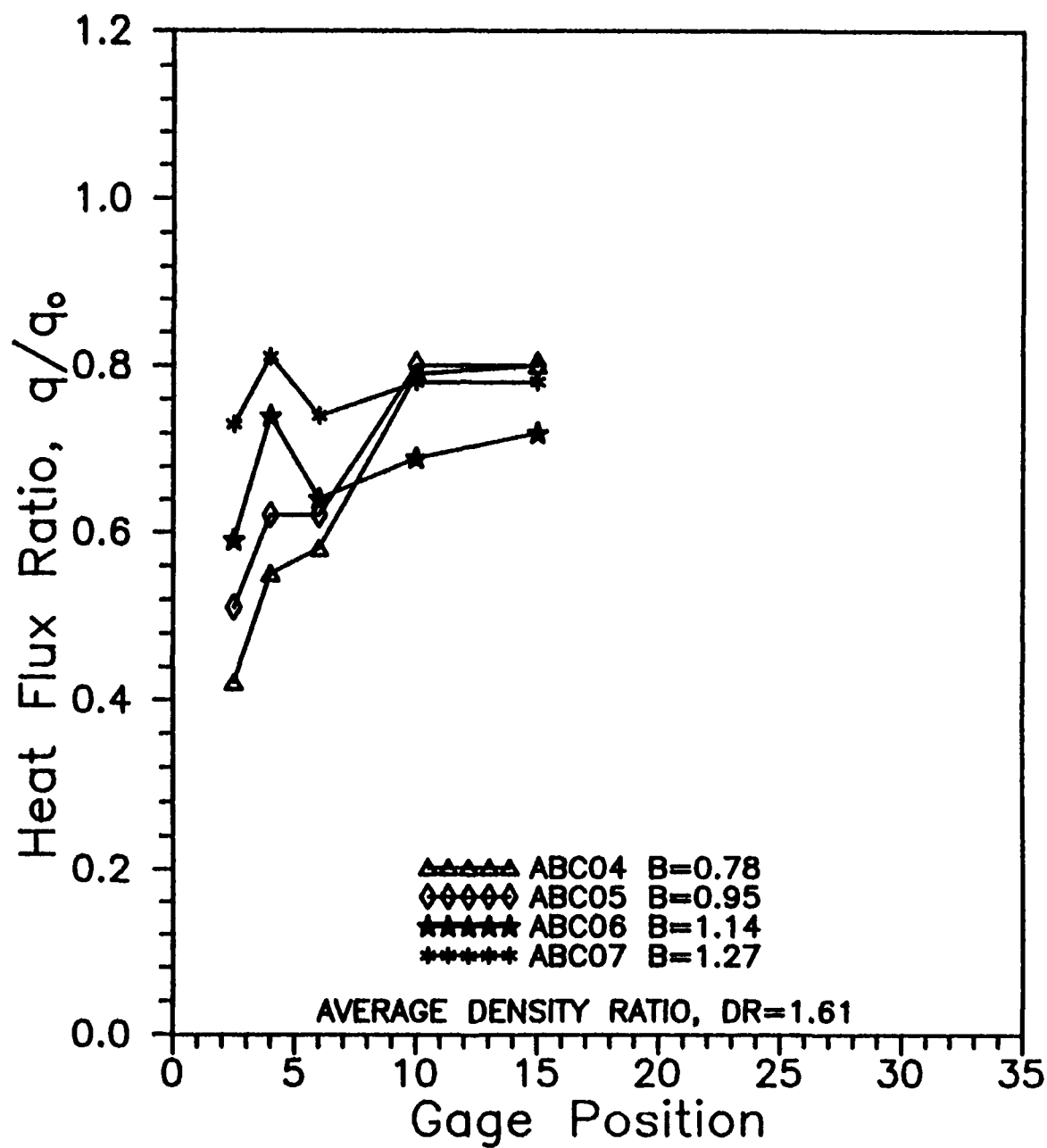
Figure 6.16.2 Gage Heat Flux Ratio for the Corian Plate in the Strong Injection Regime, DR=1.61, M_2=0.426

A.42
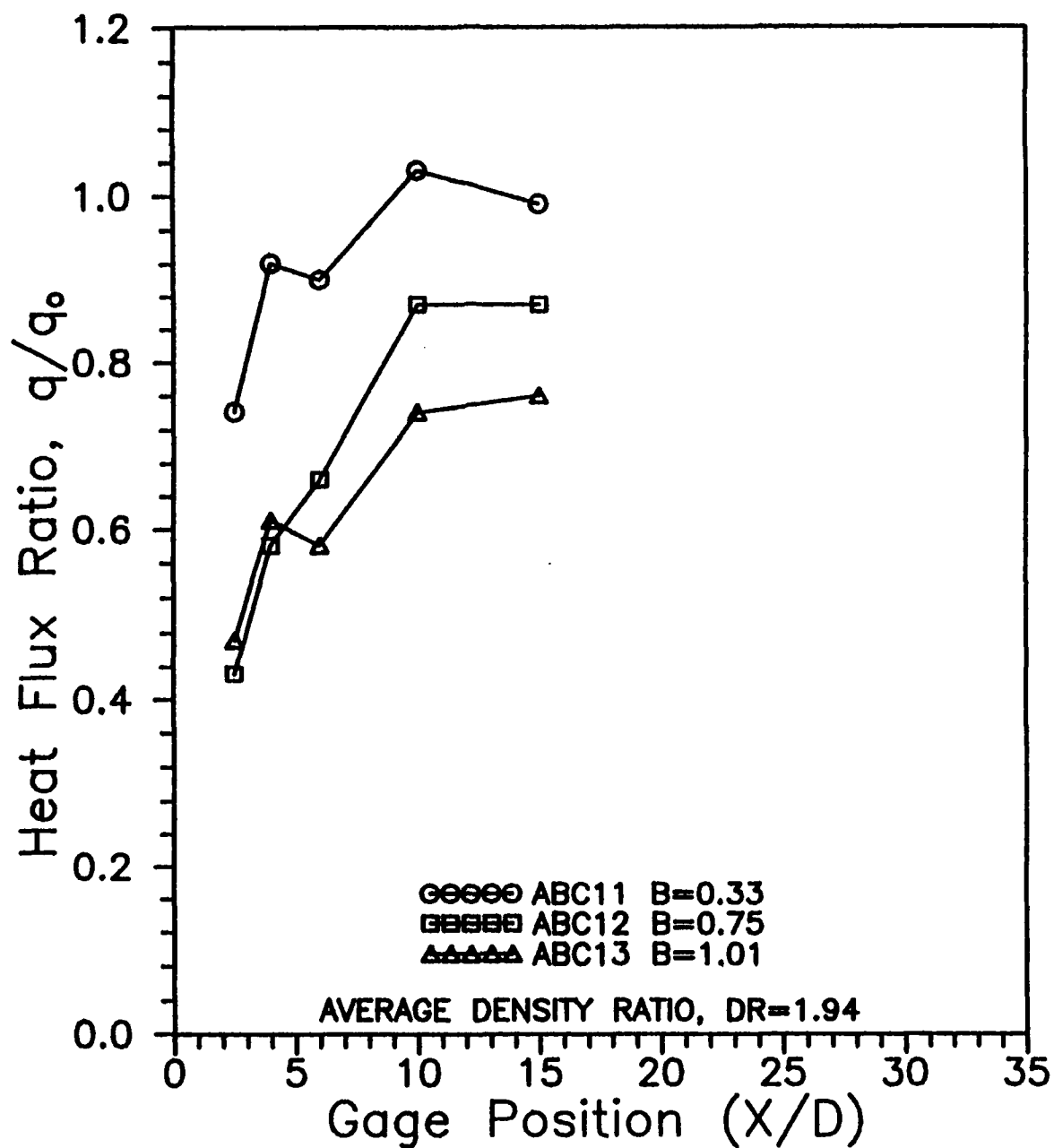
Figure 6.17.1 Gage Heat Flux Ratio for the Corian Plate in the Weak Injection Regime, DR=1.94, M_2=0.382
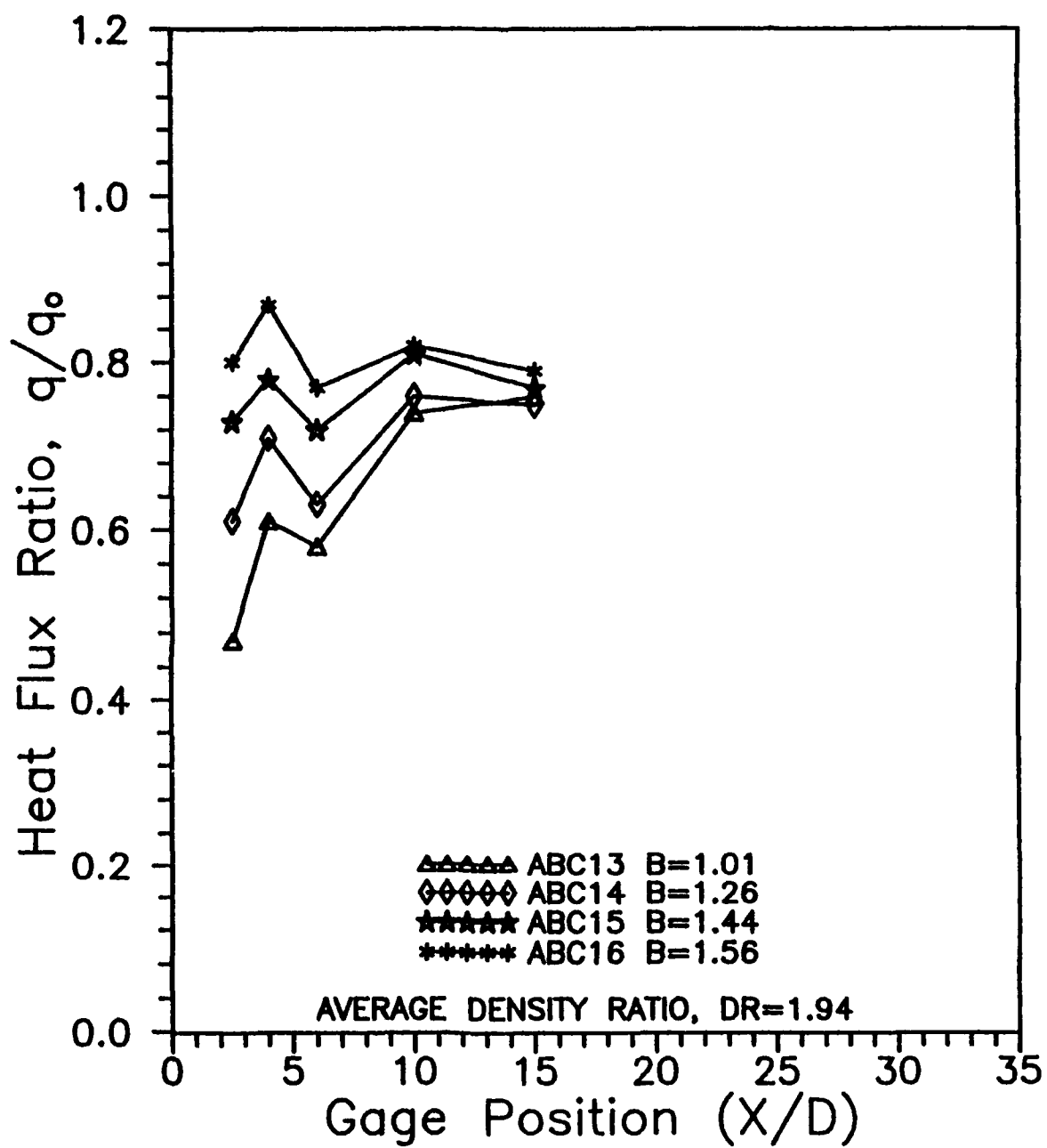
Figure 6.17.2 Gage Heat Flux Ratio for the Corian Plate in the Strong Injection Regime, DR=1.94, M_2=0.382

A.44
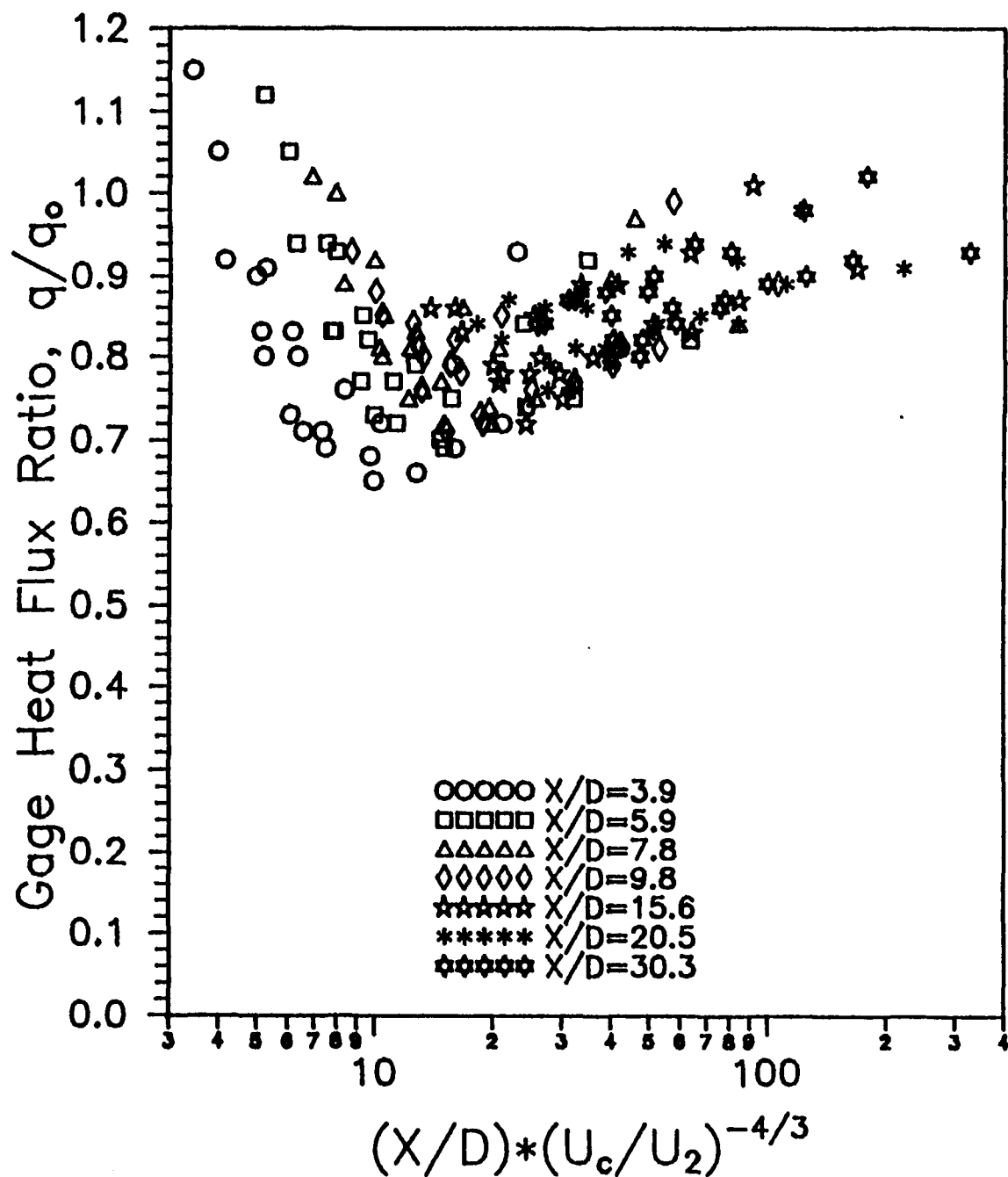
Figure 6.18 Gage Heat Flux Ratio vs. Velocity Ratio
Scaling Parameter for the Aluminum Plate

A.45
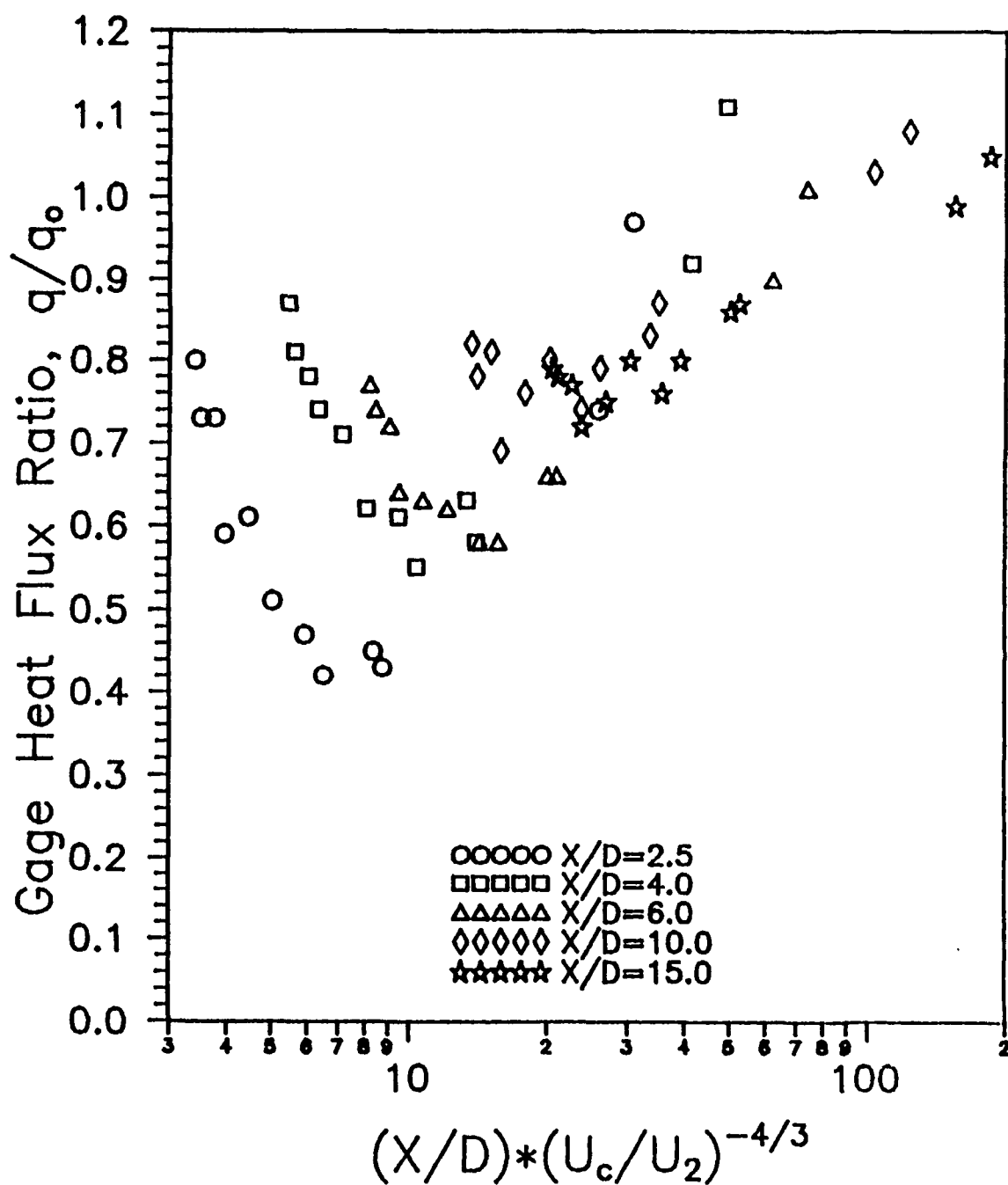
Figure 6.19 Gage Heat Flux Ratio vs Velocity Ratio
Scaling Parameter for the Corian Plate

A.46

Appendix B: Calibration of Pressure Measuring Instruments

The Endevco Model 8530A-100 and Model 8510B-50 pressure transducers were calibrated for positive gage pressure using an AMETEK Model HK-500 Pneumatic Pressure Tester. Each transducer was calibrated with its associated shielded cable and Endevco Model 4423 Signal Conditioner attached as in experimental measurements. Calibration curves for the rear and plate pressure transducers were obtained. Calibration curves for the forward and film cooling pressure transducers were used from Eads (1992: C.3, C.5). The atmospheric pressure was measured using a fortin-type mercury barometer. The data points for each transducer were plotted with a least squares curve fit in Figures A.1 and A.2.
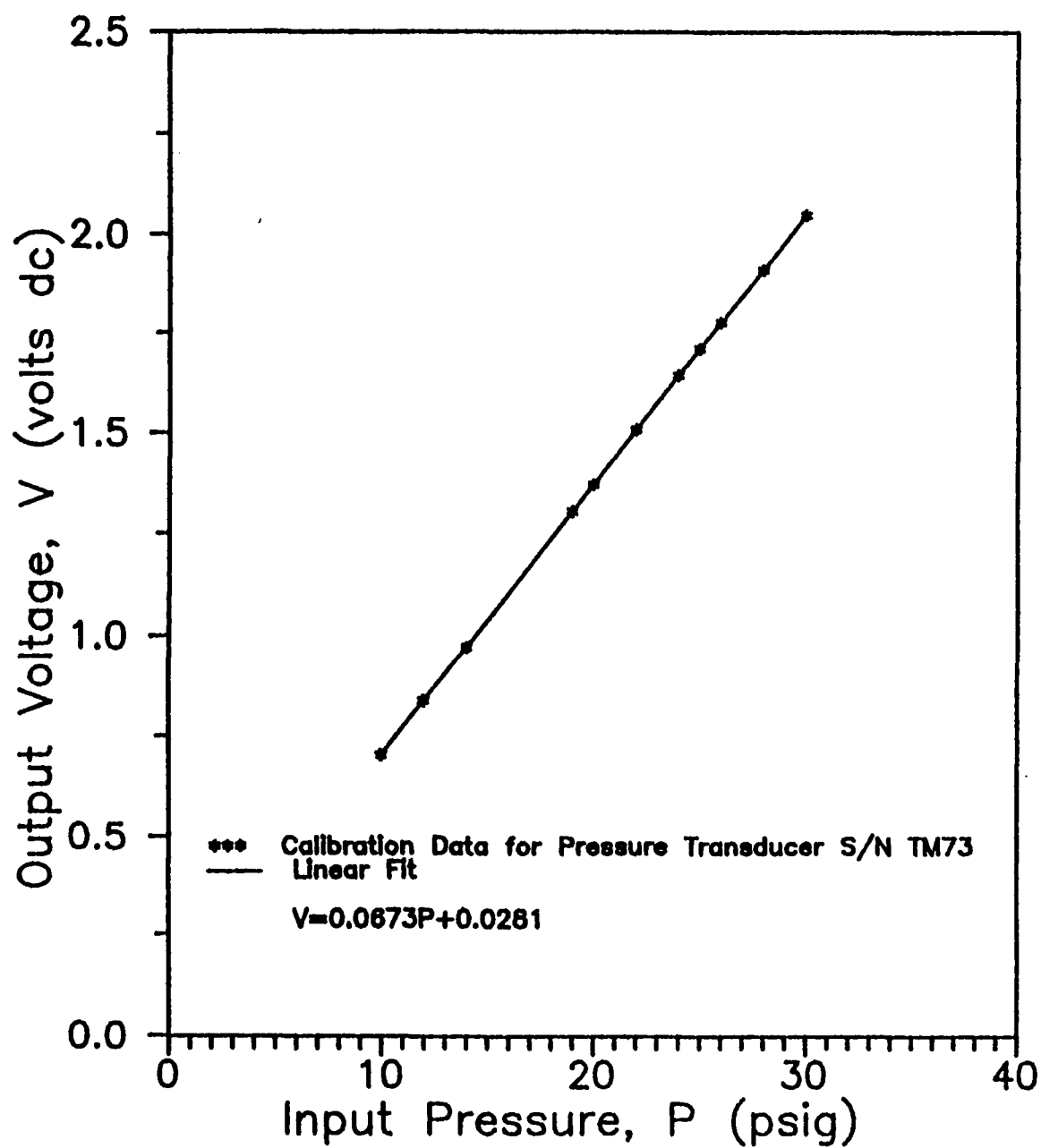
Figure B.1 Calibration Curve for Rear Pressure Transducer

B.2
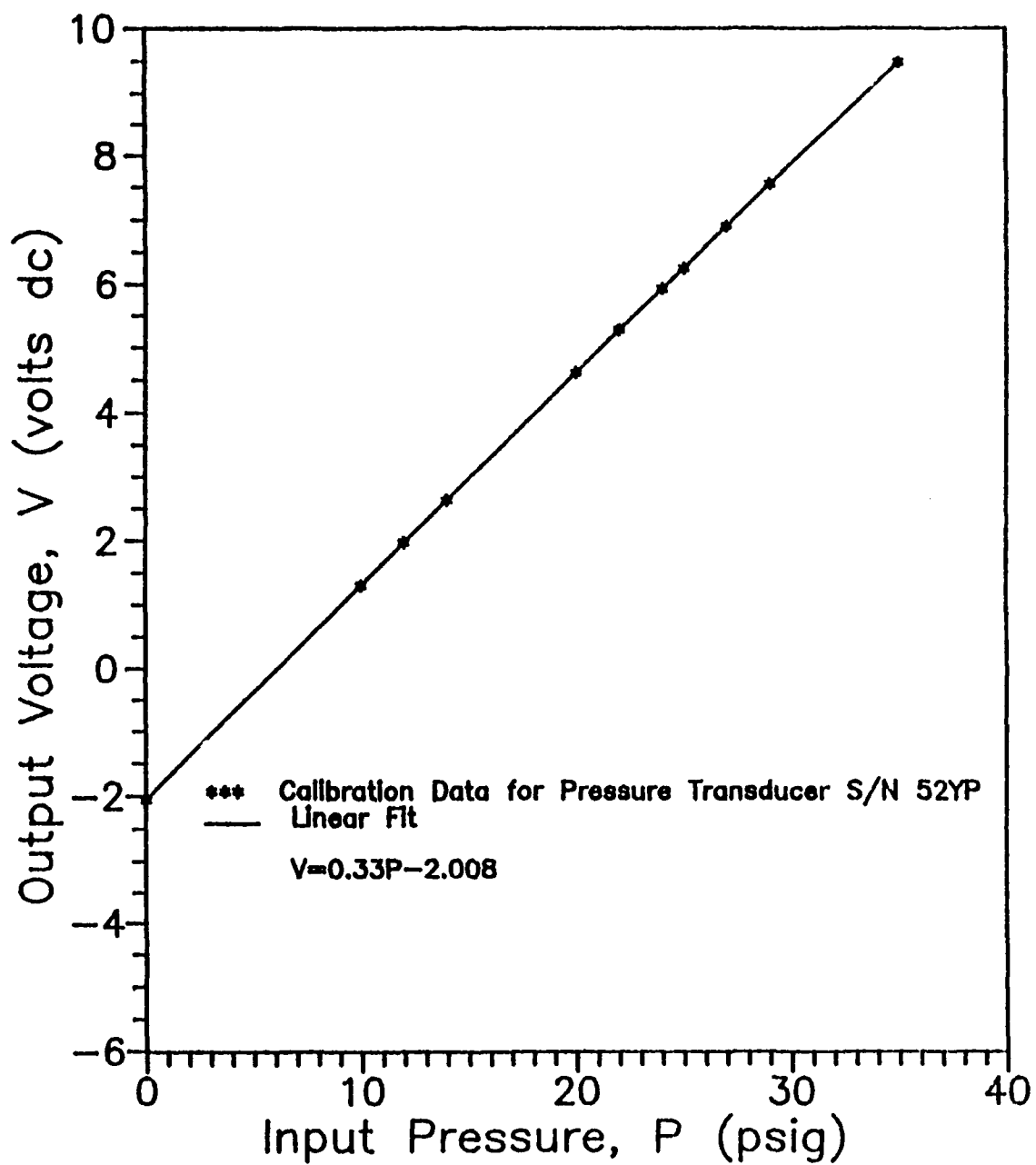
Figure B.2 Calibration Curve for Plate Pressure Transducer

Appendix C: Data Reduction Computer Programs

The programs SHOCK.FOR and AVERAGE.FOR, written in Fortran 77, and compiled on the AFIT VAX/VMS mainframe, were used for data reduction and averaging for all tests, with and without film cooling, incorporating mixtures of air and helium in the shock tube driven section. The program SHOCK.FOR is listed first, followed by the program AVERAGE.FOR.

C.1

```fortran
      PROGRAM SHOCK
C     *****************************************************************
C     WRITTEN BY: MARCO VALENCIA      GAE/93J
C     *****************************************************************
C     THIS PROGRAM COMPUTES SEVERAL PARAMETERS REQUIRED IN THE STUDY OF
C     HEAT TRANSFER TO A FLAT PLATE, USING THE SHOCK TUBE AND THE NIC-500
C     DATA ACQUISITION SYSTEM.
C
C     THE INPUT VARIABLES ARE:
C     - SHOCK TUBE DRIVER PRESSURE (P4)
C     - SHOCK TUBE DRIVEN PRESSURE (P1)
C     - ATMOSPHERIC PRESSURE (PATM)
C     - ROOM TEMPERATURE (T1)
C     - COOLING FLOW STAGNATION TEMPERATURE (Toc)
C     - TIME INTERVAL REQUIRED TO COMPUTE SHOCK MACH NUMBER (DELTAT)
C     - TIME INTERVAL TO AVERAGE A GIVEN PARAMETER (TIN,TFIN)
C     - HELIUM PARTIAL PRESSURE (PHe)
C     - CALIBRATION CONSTANTS (HFC,...)
C
C     THE OUTPUT VARIABLES ARE:
C     - SHOCK TUBE DRIVEN SECTION CONDITIONS (AFTER SHOCK PASSES):
C         - TEMPERATURE (T2)
C         - PRESSURE (P2)
C         - VELOCITY (U2)
C         - MACH NUMBER (M2)
C         - DENSITY (RHO2)
C         - SHOCK MACH NUMBER (Ms)
C     - COOLING FLOW PRESSURES (Pc,Poc)
C     - COOLING FLOW DENSITY (RHOc)
C     - COOLING FLOW EXIT VELOCITY (Uc)
C     - DENSITY RATIO (DR=RHOc/RHO2)
C     - VELOCITY RATIO (VR=Uc/U2)
C     - BLOWING RATIO (B=DR*VR)
C     - MOMENTUM RATIO (I=B*VR)
C     - HEAT FLUX FOR A GIVEN HEAT FLUX GAGE
C
C     IN THE CALCULATION OF THE SHOCK TUBE DRIVEN SECTION CONDITIONS,
C     PARAMETERS SUCH AS SPEED OF SOUND, GAS CONSTANT, SPECIFIC HEAT AT
C     CONSTANT PRESSURE, AND RATIO OF SPECIFIC HEATS ARE ALSO CALCULATED.
C
C     IN THE CALCULATION OF THE HEAT FLUX, PARAMETERS SUCH AS HEAT
C     TRANSFER COEFFICIENT, THERMAL CONDUCTIVITY, DYNAMIC VISCOSITY,
C     PRANDTL NUMBER, LOCAL REYNOLDS NUMBER, RECOVERY FACTOR, AND
C     STANTON NUMBER ARE ALSO CALCULATED.
C
C     IN SUMMARY, THE VARIABLES ARE:
C         A             SPEED OF SOUND
C         CP            SPECIFIC HEAT, CONSTANT PRESSURE
C         DR            FILM COOLING-TO-MAINSTREAM DENSITY RATIO
C         H             HEAT TRANSFER COEFFICIENT
C         K             THERMAL CONDUCTIVITY
C         B             MASS FLUX (BLOWING) RATIO
C         GAM           RATIO OF SPECIFIC HEATS
C         M             MACH NUMBER
C         I             MOMENTUM FLUX RATIO
C         MU            DYNAMIC VISCOSITY
C         P             PRESSURE
C         PR            PRANDTL NUMBER
C         Q             HEAT TRANSFER/UNIT AREA
C         REX           LOCAL REYNOLDS NUMBER
C         R             GAS CONSTANT
C         RC            RECOVERY FACTOR
C         RHO           DENSITY
C         ST            STANTON NUMBER
C         T             TEMPERATURE
```

```
C       TU              TURBULENCE
C       U               VELOCITY
C       VR              FILM COOLING-TO-MAINSTREAM VELOCITY RATIO
C       X               DISTANCE FROM PLATE LEADING EDGE
C
C       SUBSCRIPTS:
C       A               AIR
C       AW              ADIABATIC WALL
C       He              HELIUM
C       E               ENGLISH UNITS
C       C               COOLING
C       TH              THEORETICAL
C       W               WALL
C       x               LOCAL
C       0               STAGNATION
C       1               DRIVEN SECTION
C       2               FREESTREAM (FOLLOWING SHOCK)
C       4               DRIVER SECTION
C
        IMPLICIT NONE
        REAL A1,A4,A14,CPA,CPHE,CP1,DR,GAM1,GAM4,MB,MS,MSOLD,MWA,MWHE,MW1
        REAL PA,PC,PCE,P1,P1E,P2,P4,P4E,P41,PHE,PHE1,PHE2,PHE1E,PHE2E
        REAL R,RA,R1,R2,R4,RHOC,RHO1,RHO2,TC,T1,T2,T4,TOC,U2,UC,A2,M2,MU,K
        REAL PATM,POC1,PR,RC,X,TR,TU,REX,STTH,HTH,TAW,TW,QTH,MM,JJ,NPHE2
        REAL CP,RHO,QW,H,ST,DRMIN,VR,IR,TOC,MUHE,KHE,MUA,KA,IFLAG,IFLAG2
        REAL IFLAG3,IFLAG4,IFLAG5,DELTAT,TT1,TT2,TT3,TT4,TT5,TT6,TT7,MS2
        REAL CNTR,TOLERR,MS1,G4,NMAX,POC
        INTEGER NG,NS,I
        CHARACTER*1 ANS
        CHARACTER*13 OUTPUT
        CHARACTER*3 INPUT1
        WRITE(6,1)
1       FORMAT(///////////)
        PRINT*,'**********************************************************'
        PRINT*,'**********************************************************'
        PRINT*,'THIS IS THE COMPUTER PROGRAM  SHOCK.FOR'
        PRINT*,'**********************************************************'
        PRINT*,'FOR FURTHER INFORMATION ABOUT THIS PROGRAM, PLEASE GET'
        PRINT*,'A COPY OF THE FILE....  SHOCK.DOC'
        PRINT*,'**********************************************************'
        PRINT*,'**********************************************************'
        DO 3 I=1,200
3       CONTINUE
        WRITE(6,2)
2       FORMAT(///////////)
5       WRITE(6,'(/,A)')' ENTER NAME OF OUTPUT FILE:'
        READ(5,'(A13)') OUTPUT
        OPEN(10,FILE=OUTPUT,STATUS='UNKNOWN')
        PRINT*
        PRINT*
10      WRITE(6,*)'********************************************************'
        WRITE(6,*)'ENTER NUMBER FOR CALCULATION FROM THE FOLLOWING:'
        WRITE(6,*)'********************************************************'
        PRINT*
        WRITE(6,*)'1.- CALCULATE DRIVEN SECTION CONDITIONS'
        WRITE(6,*)'2.- CALCULATE AVERAGE WALL HEAT FLUX'
        WRITE(6,*)'3.- CALCULATE REYNOLDS NUMBER, STANTON NUMBER, ETC'
        WRITE(6,*)'4.- CALCULATE :'
        WRITE(6,*)'    DENSITY RATIO (DR)      VELOCITY RATIO (VR)'
        WRITE(6,*)'    BLOWING RATIO (B)       MOMENTUM RATIO (I)'
        WRITE(6,*)'5.- CHANGE OUTPUT FILE NAME'
        WRITE(6,*)'6.- EXIT PROGRAM'
        READ(5,*) NS
        IF (NS.EQ.4) IFLAG=1.
        GO TO (100,200,300,100,5,500) NS
```

```
**********************************************************************
*      INPUT VARIABLES
**********************************************************************
100   IFLAG5=1.
      WRITE(6,*)'ENTER DRIVER PRESSURE P4 (in Hg, gauge)'
         READ(5,*) P4E
      WRITE(6,*)'ENTER DRIVEN PRESSURE P1 (psi)'
         READ(5,*) P1E
      WRITE(6,*)'ENTER ATMOSPHERIC PRESSURE (in Hg)'
         READ(5,*) PATM
      WRITE(6,*)'ENTER TEMPERATURE T1 (K)'
         READ(5,*) T1
      WRITE(6,*)'DO YOU WANT TO USE THE MEASURED MACH NUMBER (Y/N)'
         READ(5,'(A1)') ANS
      IF (ANS.EQ.'y'.OR.ANS.EQ.'Y') THEN
      WRITE(6,*)'ENTER MEASURED TIME (MILISECONDS)'
         READ(5,*) DELTAT
      IFLAG4=1.
      ENDIF
         IF (IFLAG.NE.1.) GOTO 190
      WRITE(6,*)'ENTER STAGNATION COOLING AIR TEMEPRATURE TOC (K)'
         READ(5,*) TOC
      WRITE(6,*)'ENTER STAGNATION COOLING AIR PRESSURE POC (psig)'
         READ(5,*) POC1
190   WRITE(6,*)'SELECT ONE OF THE FOLLOWING:'
      WRITE(6,*)'1. EXECUTE PROGRAM FOR A GIVEN He PARTIAL PRESSURE'
      WRITE(6,*)'2. EXECUTE PROGRAM FOR A RANGE OF He PARTIAL PRESSURES'
      READ(5,*) NS
      IF (NS.EQ.1) THEN
      WRITE(6,*)'ENTER HELIUM PARTIAL PRESSURE (psi)'
      READ(5,*) PHE
      IFLAG3=1.
      ELSE
      WRITE(6,*)'ENTER RANGE OF HELIUM PARTIAL PRESSURES'
      WRITE(6,*)'[PHe1,PHe2]   (psi)'
         READ(5,*) PHE1E, PHE2E
      ENDIF
      IF (IFLAG.NE.1.) THEN
      WRITE(10,890) P4E,P1E,T1,PATM
890   FORMAT(/,'For P4=',F7.2,' in Hg gauge',3X,'P1=',F6.2,' psi',/,
     &'     T1=',F7.2,' K',13x,'Patm=',f6.2,' in Hg',//,2x,'PHe(psi)',
     &2X,'P2(psi)',2X,'T2(K)',2X,'RHO2(Kg/m3)',4X,'M2',6X,'MS',3X,
     &'A1 (m/s)',2X,'GAM1')
      ELSE
      WRITE(10,895) P4E,P1E,T1,TOC,POC1+(PATM*0.4912)
895   FORMAT(/,'For P4=',f7.2,' in Hg gauge',3x,'P1=',f6.2,' in Hg',/,
     &'     T1=',f7.2,' K',3x,'TOC=',f7.2,' K',3x,'POC=',f6.2,'
     &psi',//,2x,'PHe (psi)',11x,'DR',11x,'VR',11x,'B',11X,'I')
      ENDIF
**********************************************************************
*      PRELIMINARY CALCULATIONS
**********************************************************************
      P4= (P4E+PATM) * 3386.388158
      P1= P1E * 6894.7573
      P41=P4/P1
      CPA=1005.
      CPHE=5193.
      R=8314.34
      MWA=28.966
      MWHE=4.003
      RA=R/MWA
      GAM4=1.4
      G4=GAM4/(GAM4-1.)
      R4=RA
      T4=T1
      PHE1= PHE1E * 6894.757293
```

C.4

```
          PHE2= PHE2E * 6894.757293
          PHE=PHE*6894.76
          NPHE2=PHE2
          JJ=(NPHE2-PHE1)/100.
          IF (IFLAG3.EQ.1.) GOTO 205
          DO 250 PHE=PHE1, NPHE2, JJ
205       PA=P1-PHE
          MW1=(PA/P1*MWA)+(PHE/P1*MWHE)
          CP1=((PA*MWA*CPA)+(PHE*MWHE*CPHE))/P1/MW1
          R1=R/MW1
          GAM1=CP1/(CP1-R1)
          A1=(GAM1*R1*T1)**.5
          A4=(GAM4*R4*T4)**.5
          A14=A1/A4
          NMAX=100
          CNTR=0
          TOLERR=0.000001
          MS=1.1
      IF (IFLAG4.NE.1.) GOTO 210
          MM=(711.2/DELTAT)/A1
      MSOLD=MM
      GOTO 220
******************************************************************
*     THEORETICAL SHOCK SPEED CALCULATED BY THE METHOD OF NEWTON-RAPHSON
******************************************************************
210       MSOLD=MS
          CNTR=CNTR+1
          TT2=(1.-3.*GAM4)/(GAM4-1.)
          TT1=(2.*GAM4)/(1.-GAM4)
          TT3=A14*(GAM4-1.)*(MSOLD-1./MSOLD)/(GAM1+1.)
          TT4=((2*GAM1*MSOLD*MSOLD)-GAM1+1.)/(GAM1+1.)
          TT5=(1-TT3)**TT1
          MS1=(TT4*TT5)-P41
          TT6=((4.*GAM1*MS)/(GAM1+1.))
          TT7=A14*(1.-GAM4)*(1.+(1./(MSOLD*MSOLD)))/(GAM1+1.)
          MS2=(TT6*TT5)+TT4*TT1*TT7*(1.-TT3)**TT2
          MS=MSOLD-(MS1/MS2)
          IF (ABS(MS-MSOLD).LT.TOLERR) GOTO 220
          IF (CNTR.LT.NMAX) GOTO 210
              WRITE(6,*)'NO CONVERGENCE FOR Ms'
              PAUSE
              GOTO 10
220       MS=MSOLD
          P2=P1*(2.*GAM1*MS**2.-GAM1+1.)/(GAM1+1.)
          T2=T1*(1+(GAM1-1.)/2.*MS**2.)*(2.*GAM1*MS**2./(GAM1-1.)
      &-1.)/MS**2./(2*GAM1/(GAM1-1.)+(GAM1-1.)/2.)
          RHO2=P2/R1/T2
          A2=(GAM1*R1*T2)**0.5
          U2=(2.*A1)*(MS-1./MS)/(GAM1+1.)
          M2=U2/A2
          IF (IFLAG.NE.1.) THEN
          WRITE(10,900) PHE/6894.76,P2/6894.76,T2,RHO2,M2,MS,A1,GAM1
900       FORMAT(3X,F5.2,5X,F5.2,3X,F5.1,5X,F5.3,5X,F5.3,3X,F5.3,3X,F6.2,
      &3X,F4.2)
          ELSE
          POC=(POC1*6894.76)+(PATM*3386.88)
          IF (POC.LT.P2) THEN
              WRITE(6,*)'WARNING!  POC<P2, NO COOLING FLOW'
              PAUSE
              GOTO 10
          ELSE
              IF (P2.LT.0.52828*POC) THEN
          WRITE(6,*)' COOLING FLOW IS CHOKED!'
          UC=(2.*GAM4*RA*TOC/(GAM4+1.))**0.5
          RHOC=POC/RA/TOC*(2./(GAM4+1.))**(1./(GAM4-1.))
          TC=0.8333*TOC
```

C.5

```fortran
                IFLAG2=1.
                  ELSE
                UC=(2.*RA*TOC*GAM4/(GAM4-1.)*(1-(P2/POC)**((GAM4-1.)/GAM4)))**.5
                RHOC=POC/RA/TOC*(P2/POC)**(1./GAM4)
                TC=TOC*(P2/POC)**((GAM4-1.)/GAM4)
                  ENDIF
                DR=RHOC/RHO2
                VR=UC/U2
                MB=DR*VR
                IF (IFLAG2.EQ.1.) THEN
                WRITE(10,902) PHE/6894.757,DR,VR,MB,MB*VR,'*****'
902        FORMAT(3X,F5.2,12X,F5.3,8X,F5.3,8X,F5.3,8X,F5.3,A)
                  ELSE
                WRITE(10,901) PHE/6894.757,DR,VR,MB,MB*VR
901        FORMAT(3X,F5.2,12X,F5.3,8X,F5.3,8X,F5.3,8X,F5.3)
                  ENDIF
              ENDIF
            ENDIF
            IF (IFLAG3.EQ.1.) GOTO 255
250     CONTINUE
*****************************************************************************
*       INPUT WALL TEMPERATURE
*       CALCULATE   REFERENCE TEMPERATURE, RECOVERYFACTOR, Taw
*****************************************************************************
255     WRITE(6,907)' WALL TEMPERATURE Tw=T1= ',T1,'K  Change? (Y/N)'
907     FORMAT(A,F5.1,A)
        READ(5,'(A1)') ANS
          IF (ANS.EQ.'Y'.OR.ANS.EQ.'y') THEN
        WRITE(6,*)'ENTER WALL TEMPERATURE (C) FOR TIME INTERVAL OF
     &AVERAGING'
        READ(5,*)TW
        TW=TW+273.15
          ELSE
        TW=T1
        ENDIF
*****************************************************************************
*       APPROXIMATE PRANDTL NUMBER FROM (WHITE, 1991:31)
*****************************************************************************
        PR=4.*GAM1/(7.08*GAM1-1.8)
*****************************************************************************
*       REFERENCE TEMPERATURE
*****************************************************************************
        TR=0.5*(T2+TW) + PR**(1./3.)*(GAM1-1.)/2.*M2**2.*T2
        WRITE(6,'(A,F6.2,A)')' REFERENCE TEMPERATURE.... ',TR,' K'
*****************************************************************************
*       DENSITY
*****************************************************************************
        RHO=P2/R1/TR
*****************************************************************************
*       OPTION FOR MORE ACCURATE SPECIFIC HEAT (Cp)
*****************************************************************************
        WRITE(6,908)' SPECIFIC HEAT... Cp= ',CP1,' J/Kg-K.  Change? (Y/N)'
908     FORMAT(A,F7.1,A)
        READ(5,'(A1)') ANS
        IF (ANS.EQ.'Y'.OR.ANS.EQ.'y') THEN
          WRITE(6,*)'ENTER Cp (J/Kg-K)'
          READ(5,*) CP
        ELSE
          CP=CP1
        ENDIF
*****************************************************************************
*       EVALUATE VISCOSITY AND THERMAL CONDUCTIVITY
*****************************************************************************
        CALL MUMIX(TR,P1,PA,PHE,MWA,MWHE,MU)
        CALL KMIX(TR,P1,PA,PHE,MWA,MWHE,K)
```

C.6

```fortran
**********************************************************************
*      PRANDTL NUMBER FOR AIR (He/AIR MIXTURE APROXIMATED ABOVE)
**********************************************************************
       IF(PHE.LE.1) PR=MU*CP/K
**********************************************************************
*      RECOVERY FACTOR FOR TURBULENT FLOW
**********************************************************************
       RC=PR**(1./3.)
**********************************************************************
*      ADIABATIC WALL TEMPERATURE (Taw)
**********************************************************************
       TAW=T2*(1+RC*(GAM1-1.)*M2**2/2.)
       WRITE(10,909) TW,PR,TR,RHO,TR,CP,MU,K,RC,TAW
 909   FORMAT(//,'WALL TEMPERATURE Tw= ',F5.1,' K',/,'PRANDTL NUMBER
      & Pr= ',F5.3,/,'REFERENCE TEMPERATURE Tr= ',F5.1,' K',/,'DENSITY
      & RHO2= ',F5.3,' Kg/m3  (EVALUATED AT ',F5.1,' K)',/,'SPECIFIC HEAT
      & Cp= ',F6.1,' J/Kg-K',/,'VISCOSITY MU= ',F7.5,' Pa-sec',/,
      &'THERMAL CONDUCTIVITY K= ',F5.3,' W/m2-K',/,'RECOVERY FACTOR
      & Rc= ',F5.3,/,'ADIABATIC WALL TEMPERATURE Taw= ',F5.1,' K')
       GOTO 10
**********************************************************************
*      COMPUTE AVERAGE HEAT FLUX, MEASURED
**********************************************************************
 200   CALL QAVE(QW)
       GO TO 10
**********************************************************************
*      CALCULATE REYNOLDS NUMBER (Rex), HEAT TRANSFER COEFFICIENT (h)
*      STANTON NUMBER (St)
**********************************************************************
 300   IF (IFLAG5.NE.1) THEN
       WRITE(6,*)' MUST COMPUTE OPTIONS 1 AND 2 FIRST'
       GO TO 10
       ENDIF
       WRITE(6,*)'ENTER TURBULENCE LEVEL   (0.0 or 9.5)'
       READ(5,*) TU
*****************************************************
*      Rex (THEORETICAL AND EXPERIMENTAL)
*****************************************************
       REX=RHO*U2*X(NG)/MU
*****************************************************
*      THEORETICAL St, h, q
*****************************************************
       STTH=(0.0287/REX**.2/PR**.4)*(1.+5.*TU/100.)
       HTH=STTH*RHO*U2*CP
       QTH=HTH*(TAW-TW)
*****************************************************
*      EXPERIMENTAL/MEASURED h, St
*****************************************************
       H=QW/(TAW-TW)
       ST=H/RHO/U2/CP
**********************************************************************
*      OUTPUT RESULTS
**********************************************************************
       WRITE(6,903)NG,REX*1E-6,STTH*1E3,HTH,QTH/1E3,QW/1E3,H,ST*1E3
       WRITE(13,903)NG,REX*1E-6,STTH*1E3,HTH,QTH/1E3,QW/1E3,H,ST*1E3
 903   FORMAT(/,T2,'Gage',T9,'Rex',T17,'St,th',T25,'h,th',T33,'q,th',
      &T41,'qw,avg',T49,'h',T57,'St',/,' No.',T8,' (x1E-6)',T17,
      &' (x1E3)',T25,'W/m^2/K',T33,'kW/m^2',T41,'kW/m^2',T49,'W/m^2',
      &T57,' (x1E3)',//,T2,I1,T9,F6.4,T17,F6.3,T25,F6.1,T33,F6.2,T41,
      &F6.2,T49,F6.1,T57,F6.3,/)
       GO TO 10
 500   WRITE(6,*)'OUTPUT IS IN FILE ',OUTPUT
       STOP
       END
```

```
************************************************************************
************************************************************************
*       FUNCTIONS FOR PROPERTY VALUES
************************************************************************
************************************************************************
      REAL FUNCTION MUA(T)
C     FROM SUTHERLAND-LAW FOR ABSOLUTE VISCOSITY OF AIR (White, 1991:28)
      MUA= 1.716E-5*(T/273.)**(1.5)*(384./(T+111.))
      END
************************************************************************
************************************************************************
      REAL FUNCTION MUHE(T)
C     LINEAR FIT OF VISCOSITY FOR He FROM (KAYS AND CRAWFORD, 1980:391)
      MUHE= 4.4E-8*T + 6.7E-6
      END
************************************************************************
************************************************************************
      REAL FUNCTION KA(T)
C     FROM SUTHERLAND-LAW FOR THERMAL CONDUCTIVITY OF AIR (White,'91:31)
      KA= 0.0241*(T/273.)**1.5*(467./(T+194.))
      END
************************************************************************
************************************************************************
      REAL FUNCTION KHE(T)
C     LINEAR FIT OF THERMAL CONDUCTIVITY FOR He FROM (K&C, 1980:391)
      KHE= 3.4E-5*T + 0.0053
      END
************************************************************************
************************************************************************
C     THESE VALUES DEPEND ON THE THIN-FILM GAGE LOCATION
      REAL FUNCTION X(NG)
      IF (NG.EQ.1) X=0.05477
      IF (NG.EQ.2) X=0.05675
      IF (NG.EQ.3) X=0.05874
      IF (NG.EQ.4) X=0.06072
      IF (NG.EQ.5) X=0.06668
      IF (NG.EQ.6) X=0.07164
      IF (NG.EQ.7) X=0.08156
      END
************************************************************************
************************************************************************
*       SUBROUTINES FOR PROPERTY VALUES
************************************************************************
************************************************************************
      SUBROUTINE MUMIX(TR,P1,PA,PHE,MWA,MWHE,MU)
C     DILUTE MIXTURE VISCOSITY  APPROXIMATION FROM (WHITE, 1991:35)
C     WITH MOLE FRACTION=PARTIAL PRESSURE
      REAL MWA, MWHE, MU, MUA, MUHE
      PHIHA=(1.+(MUHE(TR)/MUA(TR))**.5*(MWA/MWHE)**.25)**2./
     & (8.+8.*MWHE/MWA)**.5
      PHIAH=(1.+(MUA(TR)/MUHE(TR))**.5*(MWHE/MWA)**.25)**2./
     & (8.+8.*MWA/MWHE)**.5
      MU=PHE/P1*MUHE(TR)/(PA/P1*PHIHA+PHE/P1)+PA/P1*MUA(TR)/(PHE/P1*
     &PHIAH+PA/P1)
      RETURN
      END
************************************************************************
************************************************************************
      SUBROUTINE KMIX(TR,P1,PA,PHE,MWA,MWHE,K)
C     DILUTE MIXTURE THERMAL CONDUCTIVITY
      REAL K, KHE, KA, KPHIHA, KPHIAH, MWA, MWHE
      KPHIHA=(1.+(KHE(TR)/KA(TR))**.5*(MWA/MWHE)**.25)**2./
     & (8.+8.*MWHE/MWA)**.5
      KPHIAH=(1.+(KA(TR)/KHE(TR))**.5*(MWHE/MWA)**.25)**2./
     & (8.+8.*MWA/MWHE)**.5
      K=PHE/P1*KHE(TR)/(PA/P1*KPHIHA + PHE/P1)+PA/P1*KA(TR)/(PHE/P1*
```

```
       & KPHIAH + PA/P1)
       RETURN
       END
***********************************************************************
***********************************************************************
*      AVERAGE HEAT FLUX SUBROUTINE
***********************************************************************
***********************************************************************
       SUBROUTINE QAVE(QAVG)
*      WRITTEN TO COMPUTE AN AVERAGE OF THE HEAT FLUX TRANSFERED TO A
*      FLAT PLATE WITH FILM COOLING IN A SHOCK TUBE USING THIN-FILM
*      RESISTANCE GAGES AND HEAT FLUX ELECTRICAL ANALOG OUTPUT VOLTAGE
*
*      LIST OF VARIABLES:
*      COUNT      COUNTER FOR NUMBER OF POINTS TO AVERAGE
*      HFC        HEAT FLUX PROPORTIONALITY COEFFICIENT (W/m² per Volt)
*                 (GAGE/CIRCUIT DEPENDENT, FROM CALIBRATIONS)
*      QAVG       AVERAGE HEAT FLUX   (W/m²)
*      Q(I)       HEAT FLUX AT DATA PT I WITH RESPECT TO AVERAGE REFERENCE
*      TIME(I)    TIME OF DATA POINT I
*      TBEG       BEGINNING TIME FOR QAVG (FROM NICOLET SCREEN)
*      TEND       ENDING TIME FOR QAVG (FROM NICOLET SCREEN)
*      TPP        TIME PER POINT OF DATA ACQUIRED
*      TTOT       TOTAL ACQUISITION TIME
*      VSUM       INITIAL REFERENCE (ZERO HEAT FLUX) VOLTAGE SUM
*      VRAVG      AVERAGE REFERENCE VOLTAGE
*      V(I)       HEAT FLUX VOLTAGE AT DATA PT  I
*      VAVG       AVERAGE HEAT FLUX VOLTAGE (FOR SPECIFIED RANGE)
*
*
       IMPLICIT NONE
       REAL Q(10000), TIME(10000), V(10000), SUM, SUMA, TBEGI, TENDI
       REAL RR, TBEGIA, TENDIA, QU(10000)
       REAL HFC,QAVG,QAVGA,QREF,VAVG,VAVGA,VRAVG,VSUM,TPP,TTOT, TBEG
       REAL TEND, TBEGA,TENDA
       INTEGER I, J, COUNT, COUNTA, NDATA, NG, NREF
       CHARACTER*1 ANS
       CHARACTER*3 INPUT1
       CHARACTER*60 HDR1,HDR2
       CHARACTER*8 INPUT2,OUTPUT1,QOUT1
       CHARACTER*13 INPUT,OUT,QOUT
       WRITE(6,880)
 880   FORMAT(////////////)
       WRITE(6,*)'*****************************************************
      &*****'
       WRITE(6,*)'*****************************************************
      &*****'
       WRITE(6,*)'THIS IS THE DATA REDUCTION PROGRAM FOR AVERAGING HEAT
      & FLUX'
       WRITE(6,*)'     (PROGRAM ASSUMES FIRST 20% OF DATA IS REFERENCE)'
       WRITE(6,*)'*****************************************************
      &*****'
       WRITE(6,*)'*****************************************************
      &*****'
       WRITE(6,881)
 881   FORMAT(/////)
       NG=0
       WRITE(6,*) 'ENTER TEST CODE'
       READ(5,'(A3)') INPUT1
       NDATA=5000
       TPP=2.
       TPP= TPP*1.E-6
       TTOT= REAL(NDATA)*TPP            !Total Time
       WRITE(6,*) 'ENTER FIRST INTERVAL IN MILISECONDS'
       READ(5,*) TBEGI,TENDI
       WRITE(6,881)
```

C.9

```fortran
      TBEG= TBEGI*.001 + TTOT/10.
      TEND= TENDI*.001 + TTOT/10.
10    NG=NG+1
      WRITE(6,881)
      IF (NG.EQ.1) THEN
      INPUT2='001A.FLT'
      OUTPUT1='HF1A.DAT'
      QOUT1='QT1A.DAT'
      ENDIF
      IF (NG.EQ.2) THEN
      INPUT2='001B.FLT'
      OUTPUT1='HF1B.DAT'
      QOUT1='QT1B.DAT'
      ENDIF
      IF (NG.EQ.3) THEN
      INPUT2='001C.FLT'
      OUTPUT1='HF1C.DAT'
      QOUT1='QT1C.DAT'
      ENDIF
      IF (NG.EQ.4) THEN
      INPUT2='001D.FLT'
      OUTPUT1='HF1D.DAT'
      QOUT1='QT1D.DAT'
      ENDIF
      IF (NG.EQ.5) THEN
      INPUT2='002A.FLT'
      OUTPUT1='HF2A.DAT'
      QOUT1='QT2A.DAT'
      ENDIF
      IF (NG.EQ.6) THEN
      INPUT2='002B.FLT'
      OUTPUT1='HF2B.DAT'
      QOUT1='QT2B.DAT'
      ENDIF
      IF (NG.EQ.7) THEN
      INPUT2='002C.FLT'
      OUTPUT1='HF2C.DAT'
      QOUT1='QT2C.DAT'
      ENDIF
      INPUT=INPUT1//INPUT2
      OUT=INPUT1//OUTPUT1
      QOUT=INPUT1//QOUT1
      OPEN(15,FILE=INPUT,STATUS='UNKNOWN')
      OPEN(11,FILE=OUT,STATUS='UNKNOWN')
      OPEN(12,FILE=QOUT,STATUS='NEW')
      WRITE(6,*) 'USE PROGRAMMED VALUES FOR CALIB. COEFF. (Y/N)'
      READ(5,'(A1)') ANS
      IF (ANS.EQ.'y'.OR.ANS.EQ.'Y') THEN
         CALL CAL(HFC,NG)
      ELSE
         WRITE(6,*)'ENTER CALIB. COEFF. FOR GAUGE # ',NG,'W/m2/Volt'
         READ(5,*) HFC
      ENDIF
************************************************************************
*     READ HEADER IN FILENAME.FLT DATA FILE AND WRITE IT TO OUTPUT FILE
************************************************************************
      READ(15,900) HDR1,HDR2
900   FORMAT(2(A60,/))
      WRITE(11,*)'***********************************************'
      WRITE(11,1000) HDR1(:11),HDR1(12:)
1000  FORMAT(5X,' FROM FILE....',A11,/,1X,A30)
      WRITE(11,*)'***********************************************'
      WRITE(6,*)'INPUT FILENAME IS.... ',INPUT
      WRITE(6,*)'DATA USED IS FROM.... ',HDR1(12:)
************************************************************************
*   READ DATA AND CALCULATE AVERAGE HEAT FLUX
```

C.10

```
**********************************************************************
      DO 15 I=1,NDATA-1
      READ(15,*) V(I), TIME(I)
15    CONTINUE
      VSUM = 0.
      COUNT = 0
      NREF = NINT(TTOT/5./TPP)
      DO 20 I= 1, NREF
         COUNT=COUNT+1
         VSUM=VSUM+V(I)
20    CONTINUE
      WRITE(6,'(A,I5)')' NUMBER OF REFERENCE POINTS USED=',COUNT
      VRAVG = VSUM/REAL(COUNT)
      QREF=HFC*VRAVG
      COUNT = 0
      COUNTA = 0
      SUM = 0.
      SUMA = 0.
      DO 30 J= 1, NDATA-1
         IF (TIME(J).GE.TBEG.AND.TIME(J).LE.TEND) THEN
            COUNT=COUNT+1
            SUM=SUM+V(J)
         ELSE
         IF (TIME(J).GE.TBEGA.AND.TIME(J).LE.TENDA) THEN
            COUNTA=COUNTA+1
            SUMA=SUMA+V(J)
         ENDIF
         ENDIF
         Q(J)=HFC*(V(J)-VRAVG)
         QU(J)=Q(J)/1000.
        WRITE(12,*) TIME(J),QU(J)
30    CONTINUE
      VAVG=SUM/REAL(COUNT)-VRAVG
      VAVGA=SUMA/REAL(COUNTA)-VRAVG
      QAVG=VAVG*HFC
      QAVGA=VAVGA*HFC
**********************************************************************
*     OUTPUT RESULTS
**********************************************************************
      WRITE(11,910) HFC,QREF/1000.
910   FORMAT(/,' GAGE/CIRCUIT CALIBRATION COEFFICIENT  HFC= ',F8.1,
     &' W/m2/Volt',/,' Q(REFERENCE)  Qr= ',F7.2,' KW/m2')
      PRINT*
      WRITE(11,55)' FROM ',TBEGI,' MSEC   TO ',TENDI,' MSEC'
55    FORMAT(A,F5.2,A,F5.2,A)
      WRITE(11,902)' FOR GAGE # ',NG,' AVERAGE HEAT FLUX  QAVG= ',
     &QAVG/1000.,' Kw/m2'
      PRINT*
902   FORMAT(A,I1,A,F6.2,A,//)
      WRITE(6,*)'OUTPUT IS IN FILE ',OUT
      WRITE(6,*)'OUTPUT OF TIME vs. Q IS IN FILE ',QOUT
      IF (NG.LT.7) THEN
      REWIND 10
      GOTO 10
      ENDIF
      RETURN
      END
**********************************************************************
**********************************************************************
C     THESE VALUES DEPEND ON THE THIN-FILM GAGES
      SUBROUTINE CAL(HFC,NG)
      IF(NG.EQ.1) HFC=53710.
      IF(NG.EQ.2) HFC=69715.
      IF(NG.EQ.3) HFC=65647.
      IF(NG.EQ.4) HFC=62668.
      IF(NG.EQ.5) HFC=41949.
```

C.11

```
IF(NG.EQ.6) HFC=91732.
IF(NG.EQ.7) HFC=35521.
HFC=HFC*(2.*3.1415926536)**.5
RETURN
END
```

```fortran
      PROGRAM AVERAGE
C     WRITTEN BY: MARCO VALENCIA GAE-9?J
C     THIS PROGRAM COMPUTES AN AVERAGE VALUE FOR AN INPUT FILE
C     FROM THE NICOLET-500 DATA ACQUISITION SYSTEM, GIVEN A
C     TIME INTERVAL AND ASSUMING A 10% PRETRIG SETTING.
C
      IMPLICIT NONE
      REAL TPP,TTO,TIN,TFIN,TINI,TFINA,SUM,VAVER,SUM1,VAVER1,TFINA2
      REAL TFIN2,TIME(10000),V(100000)
      INTEGER NDATA,COUNT,I,COUNT1
      CHARACTER*12 INPUT,UNI
      CHARACTER*60 HEAD1,HEAD2
      PRINT*
      PRINT*
      WRITE(6,*)'****************************************'
      WRITE(6,*)'THIS IS A DATA REDUCTION PROGRAM TO COMPUTE'
      WRITE(6,*)'AN AVERAGE VALUE FOR A GIVEN PARAMETER USING'
      WRITE(6,*)'THE NIC-500 DATA ACQUISITION SYSTEM'
      WRITE(6,*)'****************************************'
      WRITE(6,*)'PROGRAM ASSUMES 10% PRETRIG SETING'
      PRINT*
      PRINT*
      WRITE(6,*)'ENTER FILENAME OF DATA TO READ (FILENAME.FLT):'
      READ(5,'(A12)') INPUT
      OPEN(10,FILE=INPUT,STATUS='UNKNOWN')
      WRITE(6,*)'ENTER UNITS OF PARAMETER BEING AVERAGED'
      READ(5,'(A10)') UNI
      UNI='psig'
      WRITE(6,*)'ENTER NUMBER OF DATA POINTS ACQUIRED (5000?)'
      READ(5,*) NDATA
      WRITE(6,*)'ENTER TIME PER POINT IN MICROSECONDS (2?)'
      READ(5,*) TPP
      NDATA=5000.
      TPP=2.
      TPP=TPP*1.E-6
      TTO=REAL(NDATA)*TPP            !SWEEP TIME
      WRITE(6,*)'ENTER TIME INTERVAL IN MILISECONDS'
      READ(5,*) TINI,TFINA
      TIN=(TINI*0.001)+(TTO/10.)
      TFIN=(TFINA*0.001)+(TTO/10.)
      READ HEADER IN FILENAME.FLT DATA FILE
      READ(10,900) HEAD1,HEAD2
900   FORMAT(2(A60,/))
      DO 10 I=1,NDATA-1
      READ(10,*) V(I), TIME(I)
10    CONTINUE
      COUNT=0
      SUM=0
      SUM1=0
      DO 20 I=1,NDATA-1
      IF (TIME(I).GE.TIN.AND.TIME(I).LE.TFIN) THEN
      COUNT=COUNT+1
      SUM=SUM+V(I)
      ENDIF
      ELSE
20    CONTINUE
      VAVER=SUM/REAL(COUNT)
*     RESULTS
      PRINT*
      PRINT*
      WRITE(6,*)'****************************************
     &*******************'
      WRITE(6,903)'  FOR THE DATA FROM THE...',HEAD1(12:)
903   FORMAT(A,A40)
      WRITE(6,905)'  FROM ',TINI,' MSEC  TO ',TFINA,' MSEC'
905   FORMAT(A,F5.2,A,F5.2,A)
```

C.13

```
        WRITE(6,910)'  MEAN VALUE IS.....',VAVER,UNI
910     FORMAT(A,F6.2,1X,A12)
        WRITE(6,*)'***********************************************
     &********************'
        END
```

Appendix D: Test Conditions

The information presented in this appendix was measured and calculated according to the procedure described in Section 5.2. Pressure data units are distinct because they correspond to the measured value from the respective gage. To convert these units to the SI system, conversion factors must be used, i.e., 1 psi is equal to 6894.76 Pa, and 1 inHg is equal to 3386.39 Pa.

Aluminum Plate with Film Cooling, P_4=80 inHg

Test Code	P_1 (psi)	P_{atm} (inHg)	T_1 (K)	P_{He} (psi)
H03	14.21	29.02	296.0	3.90
J03	14.34	29.24	296.0	3.98
K03	14.30	29.20	296.0	3.86
H04	14.21	29.02	296.0	3.83
J04	14.34	29.24	296.0	3.87
K04	14.30	29.20	296.0	3.95
H05	14.21	29.02	296.0	3.83
J05	14.34	29.24	296.0	4.05
K05	14.30	29.20	296.0	3.89
H06	14.21	29.02	296.0	3.94
J06	14.34	29.24	296.0	4.06
K06	14.30	29.20	296.0	3.82
H07	14.21	29.02	296.0	3.97
J07	14.34	29.24	296.0	3.97
K07	14.30	29.20	296.0	3.88

Aluminum Plate with Film Cooling, $P_4=80$ inHg

Test Code	P_1 (psi)	P_{atm} (inHg)	T_1 (K)	P_{He} (psi)
H11	14.29	29.17	296.5	6.52
J11	14.30	29.20	296.0	6.45
K11	14.30	29.20	297.5	6.48
H12	14.29	29.17	296.5	6.48
J12	14.30	29.20	296.0	6.51
K12	14.30	29.20	297.5	6.40
H13	14.29	29.17	296.5	6.49
J13	14.30	29.20	296.0	6.47
K13	14.30	29.20	297.5	6.47
H14	14.29	29.17	296.5	6.55
J14	14.30	29.20	296.0	6.46
K14	14.30	29.20	297.5	6.44
H15	14.29	29.17	296.5	6.52
J15	14.30	29.20	296.0	6.47
K15	14.30	29.20	297.5	6.39
H16	14.29	29.17	296.5	6.46
J16	14.30	29.20	296.0	6.42
K16	14.30	29.20	297.5	6.43

Aluminum Plate with Film Cooling, $P_4 = 120$ inHg

Test Code	P_1 (psi)	P_{atm} (inHg)	T_1 (K)	P_{He} (psi)
H21	14.12	28.84	296.0	3.82
J21	14.14	28.87	296.5	3.80
K21	14.15	28.89	296.0	3.92
H22	14.12	28.84	296.0	3.79
J22	14.14	28.87	296.5	3.74
K22	14.15	28.89	296.0	3.90
H23	14.12	28.84	296.0	3.84
J23	14.14	28.87	296.5	3.78
K23	14.15	28.89	296.0	3.91
H24	14.12	28.84	296.0	3.91
J24	14.14	28.87	296.5	3.78
K24	14.15	28.89	296.0	3.71
H25	14.12	28.84	296.0	3.67
J25	14.14	28.87	296.5	3.72
K25	14.15	28.89	296.0	3.79
H26	14.12	28.84	296.0	3.75
J26	14.14	28.87	296.5	3.85
K26	14.15	28.89	296.0	3.77

Aluminum Plate with Film Cooling, $P_4 = 120$ inHg

Test Code	P_1 (psi)	P_{atm} (inHg)	T_1 (K)	P_{He} (psi)
H31	14.34	29.27	293.5	5.88
J31	14.33	29.25	294.0	5.85
K31	14.37	29.33	293.5	5.78
H32	14.34	29.27	293.5	5.86
J32	14.33	29.25	294.0	5.78
K32	14.37	29.33	293.5	5.93
H33	14.34	29.27	293.5	5.94
J33	14.33	29.25	294.0	5.92
K33	14.37	29.33	293.5	5.88
H34	14.34	29.27	293.5	5.85
J34	14.33	29.25	294.0	5.78
K34	14.37	29.33	293.5	5.78
H35	14.34	29.27	293.5	5.83
J35	14.33	29.25	294.0	5.83
K35	14.37	29.33	293.5	5.91
H36	14.34	29.27	293.5	5.94
J36	14.33	29.25	294.0	5.81
K36	14.37	29.33	293.5	5.78

Corian Plate with Film Cooling, $P_4 = 120$ inHg

Test Code	P_1 (psi)	P_{atm} (inHg)	T_1 (K)	P_{He} (psi)
A02	14.02	28.65	295.0	3.56
B02	14.02	28.65	295.0	3.52
C02	14.02	28.65	295.0	3.57
A03	14.02	28.65	295.0	3.50
B03	14.02	28.65	295.0	3.56
C03	14.02	28.65	295.0	3.60
A04	14.02	28.65	295.0	3.64
B04	14.02	28.65	295.0	3.50
C04	14.02	28.65	295.0	3.51
A05	14.02	28.65	295.0	3.59
B05	14.02	28.65	295.0	3.60
C05	14.02	28.65	295.0	3.58
A06	14.02	28.65	295.0	3.48
B06	14.02	28.65	295.0	3.52
C06	14.02	28.65	295.0	3.55
A07	14.02	28.65	295.0	3.58
B07	14.02	28.65	295.0	3.66
C07	14.02	28.65	295.0	3.58

Corian Plate with Film Cooling, $P_4 = 120$ inHg

Test Code	P_1 (psi)	P_{atm} (inHg)	T_1 (K)	P_{He} (psi)
A11	14.26	29.06	295.0	5.93
B11	14.26	29.06	295.0	5.88
C11	14.26	29.06	295.0	5.92
A12	14.26	29.06	295.0	6.02
B12	14.26	29.06	295.0	5.93
C12	14.26	29.06	295.0	5.90
A13	14.26	29.06	295.0	5.90
B13	14.26	29.06	295.0	5.92
C13	14.26	29.06	295.0	5.90
A14	14.26	29.06	295.0	5.93
B14	14.26	29.06	295.0	6.01
C14	14.26	29.06	295.0	5.89
A15	14.26	29.06	295.0	5.94
B15	14.26	29.06	295.0	6.02
C15	14.26	29.06	295.0	5.90
A16	14.26	29.06	295.0	5.92
B16	14.26	29.06	295.0	5.88
C16	14.26	29.06	295.0	5.95

Aluminum Plate with no Film Cooling[a], $P_4 = 80$ inHg

Test Code	P_1 (psi)	P_{atm} (inHg)	T_1 (K)	P_{He} (psi)
T02	14.18	28.95	298.0	3.52
U02	14.18	28.95	298.0	3.60
V02	14.18	28.95	298.0	3.63
T11	14.18	28.95	298.0	6.22
U11	14.18	28.95	298.0	6.13
V11	14.18	28.95	298.0	6.15

[a] Film cooling injection holes sealed with epoxy.

Aluminum Plate with no Film Cooling[a], $P_4 = 120$ inHg

Test Code	P_1 (psi)	P_{atm} (inHg)	T_1 (K)	P_{He} (psi)
T21	14.18	28.95	298.0	3.49
U21	14.18	28.95	298.0	3.54
V21	14.18	28.95	298.0	3.48
T31	14.18	28.95	298.0	5.62
U31	14.18	28.95	298.0	5.72
V31	14.18	28.95	298.0	5.66

[a] Film cooling injection holes sealed with epoxy.

Corian Plate with no Film Cooling, $P_4 = 120$ inHg

Test Code	P_1 (psi)	P_{atm} (inHg)	T_1 (K)	P_{He} (psi)
Q01	14.34	29.25	297.0	3.64
Q02	14.34	29.25	297.0	3.60
Q03	14.34	29.25	297.0	3.60
Q04	14.34	29.25	297.0	3.61
R01	14.35	29.28	297.0	5.78
R02	14.35	29.28	297.0	5.72
R03	14.35	29.28	297.0	5.77
R04	14.35	29.28	297.0	5.83

Appendix E: Film Cooling Parameters and Flow Conditions

The data presented in this appendix was calculated using the computer programs SHOCK.FOR and AVERAGE.FOR according to the procedure described in Section 5.3. The programs were executed in the AFIT VAX/VMS mainframe.

Aluminum Plate with Film Cooling, $P_4=80$ inHg

Test Code	M_s	$M_{s,theo}$	P_2 (psi)	P_∞ (psi)	M_2	T_2 (K)	ρ_2 Kg/m³	a_1 (m/s)	γ_1	DR	VR	B	I
H03	1.245	1.296	24.96	25.12	0.334	347.1	1.32	401.5	1.45	1.54	0.23	0.35	0.08
J03	1.226	1.294	25.14	25.47	0.311	343.2	1.34	402.3	1.45	1.53	0.18	0.53	0.19
K03	1.238	1.296	25.24	25.37	0.325	346.9	1.34	401.2	1.45	1.52	0.22	0.33	0.07
H04	1.249	1.297	25.07	25.81	0.338	347.9	1.33	400.3	1.45	1.54	0.48	0.74	0.35
J04	1.232	1.295	25.47	26.09	0.318	344.2	1.36	400.4	1.45	1.53	0.47	0.71	0.33
K04	1.242	1.295	25.22	26.00	0.329	347.8	1.33	402.8	1.45	1.55	0.50	0.78	0.39
H05	1.241	1.297	25.19	26.54	0.328	346.1	1.34	400.3	1.45	1.55	0.66	1.02	0.68
J05	1.230	1.294	25.43	26.70	0.316	344.2	1.34	403.6	1.45	1.56	0.66	1.03	0.68
K05	1.236	1.295	25.41	26.89	0.323	346.6	1.35	401.8	1.45	1.55	0.70	1.08	0.76
H06	1.235	1.296	25.37	27.54	0.321	345.0	1.35	402.3	1.45	1.57	0.84	1.32	1.11
J06	1.230	1.294	25.67	27.58	0.315	344.1	1.36	403.8	1.45	1.57	0.80	1.26	1.01
K06	1.240	1.296	25.20	27.16	0.328	347.3	1.34	400.5	1.45	1.55	0.79	1.23	0.98
H07	1.242	1.296	25.42	28.16	0.329	346.4	1.34	402.8	1.45	1.59	0.91	1.45	1.33
J07	1.226	1.294	25.79	28.65	0.311	343.3	1.37	402.2	1.45	1.57	0.98	1.54	1.52
K07	1.245	1.295	25.37	28.48	0.334	348.5	1.34	401.6	1.45	1.58	0.96	1.52	1.46

E.2

Aluminum Plate with Film Cooling, $P_4 = 80$ inHg

Test Code	M_s	$M_{s,theo}$	P_2 (psi)	P_{oc} (psi)	M_2	T_2 (K)	ρ_2 Kg/m³	a_1 (m/s)	γ_1	DR	VR	B	I
H11	1.224	1.273	24.57	24.89	0.303	346.5	1.03	456.7	1.49	1.93	0.31	0.60	0.19
J11	1.230	1.274	24.72	25.11	0.309	347.3	1.05	454.8	1.49	1.93	0.34	0.66	0.22
K11	1.235	1.273	24.14	24.71	0.315	349.9	1.01	456.4	1.49	1.95	0.41	0.79	0.32
H12	1.227	1.273	24.34	25.33	0.306	347.1	1.03	455.7	1.49	1.95	0.54	1.06	0.58
J12	1.235	1.273	24.54	25.73	0.315	348.7	1.03	456.3	1.49	1.97	0.57	1.13	0.65
K12	1.250	1.274	24.26	25.61	0.332	353.2	1.01	454.4	1.49	1.97	0.58	1.15	0.67
H13	1.226	1.273	24.38	26.25	0.305	346.9	1.03	455.9	1.49	1.97	0.74	1.45	1.07
J13	1.228	1.274	24.81	26.39	0.307	347.0	1.05	455.3	1.49	1.96	0.67	1.32	0.89
K13	1.245	1.274	24.43	26.21	0.326	352.3	1.02	456.2	1.49	1.98	0.67	1.34	0.90
H14	1.222	1.273	24.40	26.92	0.300	346.1	1.03	457.4	1.49	1.99	0.86	1.71	1.48
J14	1.239	1.274	24.65	27.24	0.319	349.3	1.04	455.0	1.49	1.99	0.82	1.63	1.34
K14	1.237	1.274	24.39	26.99	0.318	350.5	1.02	455.4	1.49	1.98	0.83	1.65	1.37
H15	1.224	1.273	24.55	27.91	0.303	346.5	1.03	456.7	1.49	2.00	0.98	1.95	1.91
J15	1.228	1.274	24.70	29.16	0.307	347.0	1.04	455.3	1.49	2.02	1.10	2.21	2.42
K15	1.231	1.274	24.56	28.14	0.311	349.0	1.04	454.2	1.49	1.99	0.99	1.96	1.94
H16	1.219	1.274	24.56	29.16	0.297	345.2	1.04	455.2	1.49	2.00	1.16	2.32	2.68
J16	1.232	1.274	24.75	30.28	0.311	347.7	1.05	454.0	1.49	2.03	1.19	2.42	2.89
K16	1.248	1.274	24.55	29.17	0.330	352.8	1.02	455.2	1.49	2.04	1.04	2.11	2.19

E.3

Aluminum Plate with Film Cooling, $P_4=120$ inHg

Test Code	M_s	$M_{s,theo}$	P_2 (psi)	P_∞ (psi)	M_2	T_2 (K)	ρ_2 Kg/m³	a_1 (m/s)	γ_1	DR	VR	B	I
H21	1.323	1.377	28.70	28.96	0.418	363.1	1.46	400.6	1.45	1.60	0.21	0.34	0.07
J21	1.314	1.377	28.87	28.96	0.409	361.3	1.47	400.2	1.45	1.59	0.13	0.20	0.03
K21	1.317	1.375	28.73	28.90	0.412	362.0	1.45	402.4	1.45	1.61	0.17	0.27	0.05
H22	1.325	1.377	28.93	29.54	0.420	363.4	1.47	400.1	1.45	1.61	0.32	0.51	0.16
J22	1.328	1.377	29.01	29.78	0.423	363.9	1.48	399.2	1.45	1.61	0.36	0.57	0.20
K22	1.318	1.375	28.77	29.61	0.413	362.2	1.45	402.0	1.45	1.62	0.38	0.61	0.23
H23	1.322	1.376	28.83	30.38	0.417	362.9	1.46	400.9	1.45	1.63	0.51	0.83	0.42
J23	1.325	1.377	29.00	30.44	0.421	363.5	1.47	399.9	1.45	1.62	0.49	0.79	0.38
K23	1.318	1.375	28.78	30.32	0.412	362.1	1.45	402.2	1.45	1.63	0.51	0.83	0.43
H24	1.328	1.376	28.81	31.11	0.423	364.2	1.45	402.2	1.45	1.65	0.60	1.00	0.60
J24	1.325	1.377	29.02	31.39	0.421	363.5	1.48	399.9	1.45	1.63	0.62	1.01	0.62
K24	1.320	1.377	28.93	31.25	0.415	28.93	1.48	398.6	1.45	1.62	0.62	1.01	0.62
H25	1.322	1.378	29.00	32.30	0.418	362.6	1.49	397.9	1.45	1.63	0.73	1.19	0.87
J25	1.329	1.377	29.10	32.34	0.425	364.1	1.48	398.8	1.45	1.64	0.71	1.16	0.82
K25	1.325	1.377	28.79	32.16	0.420	363.4	1.46	400.1	1.45	1.65	0.73	1.20	0.88
H26	1.317	1.377	28.99	32.98	0.413	361.8	1.45	399.3	1.45	1.64	0.81	1.32	1.07
J26	1.321	1.376	29.05	32.97	0.416	362.8	1.47	401.1	1.45	1.66	0.79	1.31	1.03
K26	1.326	1.377	28.86	33.11	0.421	363.6	1.47	399.7	1.45	1.66	0.81	1.35	1.09

E.4

Aluminum Plate with Film Cooling, P_4=120 inHg

Test Code	M_s	$M_{s,theo}$	P_2 (psi)	P_{oc} (psi)	M_2	T_2 (K)	ρ_2 Kg/m³	a_1 (m/s)	γ_1	DR	VR	B	I
H31	1.316	1.352	28.15	28.72	0.404	361.9	1.21	438.6	1.48	1.92	0.30	0.57	0.17
J31	1.307	1.352	28.08	28.59	0.395	360.0	1.22	438.0	1.48	1.90	0.29	0.54	0.16
K31	1.312	1.353	28.29	28.77	0.400	360.9	1.23	436.4	1.48	1.90	0.27	0.52	0.14
H32	1.307	1.352	28.36	29.30	0.395	359.9	1.23	438.2	1.48	1.91	0.39	0.74	0.28
J32	1.312	1.353	28.21	29.37	0.400	360.9	1.23	436.4	1.48	1.91	0.42	0.81	0.34
K32	1.313	1.351	28.18	29.36	0.400	361.3	1.21	439.8	1.48	1.94	0.42	0.82	0.35
H33	1.312	1.351	28.21	29.90	0.400	361.1	1.21	440.0	1.48	1.95	0.50	0.98	0.50
J33	1.313	1.352	28.42	30.12	0.401	361.4	1.22	439.6	1.48	1.95	0.50	0.98	0.49
K33	1.316	1.352	28.23	29.95	0.404	361.9	1.21	438.6	1.48	1.94	0.50	0.98	0.49
H34	1.318	1.352	28.28	31.03	0.406	362.3	1.22	438.0	1.48	1.96	0.63	1.23	0.77
J34	1.312	1.353	28.44	31.08	0.400	360.9	1.24	436.4	1.48	1.93	0.63	1.21	0.76
K34	1.312	1.353	28.49	31.01	0.400	360.9	1.24	436.4	1.48	1.93	0.61	1.18	0.73
H35	1.319	1.352	28.23	31.80	0.408	362.6	1.22	437.5	1.48	1.97	0.71	1.39	0.99
J35	1.319	1.353	28.29	31.85	0.408	362.6	1.22	437.5	1.48	1.97	0.71	1.39	0.98
K35	1.314	1.351	28.38	31.98	0.402	361.5	1.22	439.3	1.48	1.98	0.72	1.42	1.02
H36	1.312	1.351	28.22	32.76	0.400	361.1	1.21	440.1	1.48	2.00	0.80	1.61	1.29
J36	1.321	1.353	28.15	32.80	0.409	362.8	1.21	437.1	1.48	1.99	0.80	1.59	1.26
K36	1.323	1.353	28.10	32.82	0.411	363.2	1.21	436.4	1.48	1.98	0.80	1.59	1.27

E.5

Corian Plate with Film Cooling, $P_4 = 120$ inHg

Test Code	M_s	$M_{s,tbco}$	P_2 (psi)	P_{oc} (psi)	M_2	T_2 (K)	ρ_2 Kg/m³	a_1 (m/s)	γ_1	DR	VR	B	I
A02	1.329	1.381	29.09	29.15	0.425	362.7	1.51	395.8	1.45	1.58	0.10	0.16	0.02
B02	1.331	1.381	28.96	29.15	0.428	363.1	1.50	395.1	1.44	1.57	0.18	0.28	0.05
C02	1.329	1.381	28.80	28.98	0.425	362.6	1.49	396.0	1.45	1.58	0.18	0.28	0.05
A03	1.333	1.381	29.18	30.07	0.429	363.3	1.51	394.7	1.44	1.58	0.38	0.60	0.23
B03	1.329	1.381	28.71	29.67	0.425	362.7	1.49	395.8	1.45	1.59	0.40	0.63	0.25
C03	1.327	1.380	28.80	29.94	0.423	362.3	1.49	396.5	1.45	1.60	0.44	0.70	0.30
A04	1.334	1.380	28.80	30.30	0.431	363.9	1.48	397.2	1.45	1.61	0.49	0.79	0.38
B04	1.333	1.381	28.71	30.22	0.429	363.3	1.49	394.7	1.44	1.59	0.49	0.79	0.39
C04	1.342	1.381	28.74	30.23	0.439	365.3	1.48	394.9	1.44	1.60	0.48	0.77	0.37
A05	1.327	1.380	28.81	31.04	0.424	362.4	1.49	396.3	1.45	1.61	0.60	0.97	0.58
B05	1.327	1.380	29.01	31.23	0.423	362.3	1.50	396.5	1.45	1.61	0.60	0.96	0.58
C05	1.318	1.380	29.42	31.44	0.414	360.5	1.53	396.1	1.45	1.60	0.58	0.93	0.54
A06	1.324	1.381	28.78	31.96	0.420	361.5	1.50	394.4	1.44	1.61	0.72	1.16	0.83
B06	1.331	1.381	28.92	32.04	0.428	363.1	1.50	395.1	1.44	1.62	0.70	1.13	0.79
C06	1.330	1.381	28.78	31.97	0.426	362.8	1.49	395.6	1.44	1.62	0.71	1.15	0.81
A07	1.328	1.380	28.85	32.71	0.424	362.5	1.49	396.1	1.45	1.63	0.78	1.27	0.98
B07	1.333	1.380	28.69	32.58	0.429	363.7	1.47	397.5	1.45	1.65	0.77	1.27	0.97
C07	1.328	1.380	28.95	32.82	0.424	362.5	1.50	396.1	1.45	1.63	0.78	1.27	0.98

E.6

Corian Plate with Film Cooling, $P_4=120$ inHg

Test Code	M_s	$M_{s,theo}$	P_2 (psi)	P_{oc} (psi)	M_2	T_2 (K)	ρ_2 Kg/m³	a_1 (m/s)	γ_1	DR	VR	B	I
B11	1.310	1.353	28.44	28.66	0.398	362.9	1.21	440.6	1.48	1.91	0.19	0.36	0.07
C11	1.297	1.352	28.56	28.71	0.384	360.1	1.22	441.6	1.48	1.90	0.16	0.31	0.05
A12	1.280	1.351	28.68	29.45	0.365	356.5	1.23	443.9	1.48	1.91	0.38	0.72	0.27
B12	1.296	1.352	28.27	29.33	0.383	359.9	1.21	441.8	1.48	1.92	0.42	0.81	0.34
C12	1.309	1.352	28.48	29.40	0.396	362.6	1.21	441.1	1.48	1.93	0.38	0.73	0.28
A13	1.298	1.352	28.69	30.30	0.385	360.3	1.23	441.1	1.48	1.93	0.51	0.98	0.50
B13	1.297	1.352	28.36	30.11	0.384	360.1	1.22	441.6	1.48	1.93	0.54	1.04	0.56
C13	1.298	1.352	28.64	30.31	0.385	360.3	1.23	441.1	1.48	1.93	0.52	1.00	0.52
A14	1.296	1.352	28.42	30.93	0.383	359.9	1.22	441.8	1.48	1.95	0.64	1.24	0.79
B14	1.291	1.351	28.30	30.89	0.377	358.9	1.21	443.7	1.48	1.96	0.66	1.29	0.84
C14	1.299	1.352	28.53	31.17	0.386	360.4	1.23	440.9	1.48	1.95	0.65	1.26	0.81
A15	1.306	1.352	28.89	32.19	0.393	362.1	1.23	442.0	1.48	1.97	0.70	1.38	0.96
B15	1.280	1.351	28.51	31.91	0.365	356.5	1.22	443.9	1.48	1.96	0.77	1.51	1.16
C15	1.288	1.352	28.84	32.13	0.374	358.0	1.25	441.1	1.48	1.95	0.74	1.44	1.06
A16	1.286	1.352	28.94	32.87	0.373	357.8	1.25	441.6	1.48	1.96	0.80	1.57	1.26
B16	1.300	1.353	28.65	32.66	0.387	360.6	1.23	440.6	1.48	1.97	0.78	1.54	1.21
C16	1.295	1.352	28.65	32.67	0.382	359.7	1.23	442.3	1.48	1.98	0.79	1.57	1.24

E.7

Aluminum Plate with no Film Cooling[a]

Test Code	M_s	$M_{s,theo}$	P_2 (psi)	M_2	T_2 (K)	ρ_2 Kg/m^3	a_1 (m/s)	γ_1
T02	1.262	1.300	24.34	0.353	352.3	1.31	396.4	1.44
U02	1.275	1.299	24.46	0.368	355.2	1.29	397.8	1.45
V02	1.256	1.299	24.58	0.346	351.3	1.31	398.3	1.45
T11	1.267	1.277	23.31	0.351	357.7	0.97	451.9	1.48
U11	1.273	1.278	23.38	0.358	359.0	0.98	449.7	1.48
V11	1.293	1.277	23.44	0.379	363.3	0.97	450.2	1.48
T21	1.349	1.379	28.88	1.349	370.3	1.48	395.9	1.44
U21	1.366	1.379	28.51	0.463	374.1	1.44	396.7	1.44
V21	1.349	1.379	29.35	0.447	370.4	1.50	395.7	1.44
T31	1.329	1.356	27.43	0.418	370.4	1.17	437.8	1.48
U31	1.345	1.356	27.30	0.433	374.0	1.14	440.0	1.48
V31	1.349	1.356	27.78	0.438	374.8	1.17	438.7	1.48

[a] Film cooling injection holes sealed with epoxy.

E.8

Corian Plate with no Film Cooling

Test Code	M_s	$M_{s,theo}$	P_2 (psi)	M_2	T_2 (K)	ρ_2 Kg/m^3	a_1 (m/s)	γ_1
Q01	1.335	1.376	28.39	0.431	366.3	1.45	397.1	1.45
Q02	1.327	1.376	28.50	0.423	364.7	1.47	396.4	1.44
Q03	1.327	1.376	28.40	0.423	364.7	1.47	396.4	1.44
Q04	1.326	1.376	28.49	0.423	364.6	1.47	396.6	1.44
R01	1.315	1.353	27.46	0.403	366.1	1.18	439.1	1.48
R02	1.319	1.354	27.49	0.407	366.9	1.18	437.8	1.48
R03	1.326	1.353	27.44	0.415	368.6	1.17	438.9	1.48
R04	1.322	1.353	27.29	0.410	367.8	1.16	440.2	1.48

Appendix F: Heat Transfer Parameters

Thermodynamic properties, heat transfer parameters, and gage heat fluxes were calculated according to the procedure described in Section 5.4. Thermodynamic properties and heat transfer parameters were just calculated for the no film cooling case. The same variables could not be calculated for the film cooling case because there was no way to determine either the adiabatic wall temperature or the heat transfer coefficient. Gage heat flux is available for the film cooling and no film cooling case in both plates. Repetition tests were then averaged to reduce measurement uncertainties, obtaining a representative result neccesary to analyze and optimize film cooling.

Section 1: Thermodynamic Properties

Aluminum Plate, No Film Cooling, $T_w = T_1$

Test Code	Pr	r_c	c_p J/KgK	T^* K	ρ_2^a Kg/m³	μ^a Pa-sec x10⁵	k^a W/Km² x10²	T_{aw} K
T02	0.686	0.882	1187.8	333.8	1.377	2.07	2.821	360.9
U02	0.686	0.882	1193.1	336.1	1.366	2.09	2.835	364.7
V02	0.686	0.882	1195.1	332.9	1.382	2.07	2.812	359.5
T11	0.682	0.880	1413.2	337.3	1.032	2.15	2.750	367.2
U11	0.682	0.880	1403.8	338.3	1.042	2.15	2.761	368.8
V11	0.682	0.880	1405.8	341.8	1.032	2.17	2.783	374.4
T21	0.686	0.882	1185.8	348.5	1.568	2.14	2.927	384.7
U21	0.686	0.882	1189.1	351.8	1.528	2.16	2.948	389.8
V21	0.686	0.882	1185.1	348.6	1.595	2.14	2.928	384.8
T31	0.683	0.880	1353.4	347.8	1.247	2.19	2.848	384.0
U31	0.682	0.880	1362.9	350.7	1.220	2.20	2.863	388.7
V31	0.683	0.880	1357.2	351.4	1.246	2.20	2.871	389.8

[a] Property evaluated at T^*

F.2

Corian Plate, No Film Cooling, $T_w = T_1$

Test Code	Pr	r_c	c_p J/KgK	T^* K	ρ_2^a Kg/m³	μ^a Pa-sec x10⁵	k^a W/Km² x10²	T_{aw} K
Q01	0.686	0.882	1193.0	345.0	1.544	2.13	2.899	379.7
Q02	0.686	0.882	1190.4	343.6	1.561	2.12	2.890	377.5
Q03	0.686	0.882	1190.4	343.6	1.555	2.12	2.890	377.5
Q04	0.686	0.882	1191.1	343.6	1.560	2.12	2.889	377.3
R01	0.682	0.880	1362.1	344.0	1.252	2.17	2.819	378.6
R02	0.683	0.880	1356.4	344.7	1.258	2.17	2.826	379.6
R03	0.682	0.880	1361.1	346.1	1.245	2.18	2.833	381.9
RO4	0.682	0.880	1366.8	345.4	1.233	2.18	2.826	380.8

a Property evaluated at T^*

F.3

Section 2: Heat Transfer Parameters

Aluminum Plate with No Film Cooling

Gage Position X/D	Re_x x10^{-5}	St_{th} x10^3	$h_{o,th}$ W/Km^2	$q_{o,th}$ kW/m^2	q_o kW/m^2	h_o W/Km^2	St_o x10^3
TEST T02							
3.9	5.535	3.496	870.4	54.78	58.02	921.9	3.703
5.9	5.735	3.471	864.3	54.39	59.39	943.6	3.790
7.8	5.936	3.448	858.3	54.02	54.36	863.7	3.469
9.8	6.136	3.425	852.6	53.66	51.45	817.5	3.284
15.6	6.739	3.361	836.8	52.67	55.29	878.5	3.529
20.5	7.240	3.313	824.9	51.92	54.14	860.2	3.455
30.3	8.242	3.229	803.8	50.59	49.80	791.3	3.178
TEST U02							
3.9	5.729	3.472	904.1	60.29	60.17	902.3	3.466
5.9	5.936	3.448	897.7	59.86	62.45	936.5	3.597
7.8	6.144	3.424	891.6	59.45	58.43	876.2	3.365
9.8	6.351	3.402	885.7	59.06	51.72	775.6	2.979
15.6	6.975	3.338	869.2	57.96	59.55	893.0	3.430
20.5	7.493	3.291	856.8	57.14	56.51	847.4	3.255
30.3	8.531	3.207	834.9	55.68	51.15	767.1	2.946
TEST V02							
3.9	5.466	3.505	866.4	53.30	57.80	939.6	3.802
5.9	5.664	3.480	860.3	52.92	61.27	996.1	4.030
7.8	5.862	3.457	854.4	52.55	57.06	927.6	3.753
9.8	6.060	3.434	848.7	52.21	51.84	842.8	3.410
15.6	6.655	3.370	833.0	51.24	60.72	987.1	3.994
20.5	7.150	3.322	821.1	50.51	57.72	938.3	3.796
30.3	8.140	3.237	800.1	49.22	50.26	817.1	3.306

F.4

Aluminum Plate with No Film Cooling

Gage Position X/D	Re_x x10^{-5}	St_{th} x10^3	$h_{o,th}$ W/Km^2	$q_{o,th}$ kW/m^2	q_o kW/m^2	h_o W/Km^2	St_o x10^3
TEST T11							
3.9	4.569	3.641	923.6	63.88	58.89	851.5	3.357
5.9	4.734	3.616	917.1	63.43	59.71	863.4	3.404
7.8	4.900	3.591	910.8	62.99	54.80	792.4	3.124
9.8	5.065	3.567	904.8	62.57	52.89	764.7	3.015
15.6	5.563	3.501	888.0	61.41	58.67	848.3	3.345
20.5	5.976	3.451	875.3	60.54	55.21	798.3	3.147
30.3	6.804	3.363	852.9	58.99	51.75	748.3	2.950
TEST U11							
3.9	4.682	3.623	936.6	66.27	59.30	838.0	3.242
5.9	4.851	3.598	929.9	65.80	62.08	877.3	3.394
7.8	5.021	3.573	923.6	65.35	57.06	806.4	3.120
9.8	5.190	3.549	917.5	64.92	52.65	744.0	2.879
15.6	5.700	3.484	900.4	63.72	60.62	856.7	3.314
20.5	6.124	3.434	887.6	62.81	57.49	812.4	3.143
30.3	6.972	3.346	864.9	61.20	50.79	717.8	2.777
TEST V11							
3.9	4.900	3.591	980.3	74.91	62.90	823.1	3.015
5.9	5.077	3.565	973.4	74.38	64.15	839.5	3.075
7.8	5.255	3.541	966.7	73.87	58.50	765.6	2.804
9.8	5.432	3.517	960.3	73.38	57.37	750.8	2.750
15.6	5.965	3.452	942.5	72.02	62.67	820.1	3.004
20.5	6.409	3.403	929.1	71.00	60.89	796.8	2.919
30.3	7.296	3.316	905.3	69.18	55.14	721.6	2.643

F.5

Aluminum Plate with No Film Cooling

Gage Position X/D	Re_x $\times 10^{-5}$	St_{th} $\times 10^3$	$h_{o,th}$ W/Km^2	$q_{o,th}$ kW/m^2	q_o kW/m^2	h_o W/Km^2	St_o $\times 10^3$
TEST T21							
3.9	7.895	3.256	1191.8	103.3	102.1	1177.8	3.218
5.9	8.181	3.233	1183.3	102.6	104.5	1205.7	3.294
7.8	8.468	3.211	1175.2	101.9	98.09	1131.6	3.092
9.8	8.753	3.190	1167.4	101.2	93.33	1076.7	2.942
15.6	9.612	3.131	1145.8	99.32	105.9	1221.9	3.339
20.5	10.33	3.086	1129.4	97.90	103.8	1197.9	3.273
30.3	11.76	3.007	1100.5	95.40	90.02	1038.5	2.838
TEST U21							
3.9	7.992	3.249	1215.6	111.6	102.4	1115.7	2.982
5.9	8.281	3.226	1207.0	110.8	105.3	1147.2	3.066
7.8	8.571	3.203	1198.7	110.0	100.6	1096.1	2.929
9.8	8.860	3.182	1190.8	109.3	92.16	1004.0	2.683
15.6	9.730	3.123	1168.7	107.3	106.8	1163.2	3.109
20.5	10.45	3.079	1152.1	105.8	102.6	1117.8	2.987
30.3	11.90	3.000	1122.6	103.0	92.05	1002.8	2.680
TEST V21							
3.9	8.036	3.245	1208.2	104.9	105.9	1219.8	3.276
5.9	8.327	3.222	1199.6	104.2	108.6	1250.3	3.358
7.8	8.619	3.200	1191.4	103.4	103.6	1192.7	3.203
9.8	8.909	3.179	1183.5	102.8	97.69	1125.1	3.022
15.6	9.784	3.120	1161.5	100.9	110.5	1272.2	3.417
20.5	10.51	3.075	1145.0	99.41	110.0	1266.9	3.403
30.3	11.97	2.996	1115.7	96.87	92.87	1069.6	2.873

F.6

Aluminum Plate with No Film Cooling

Gage Position X/D	Re_x x10^{-5}	St_{th} x10^3	$h_{o,th}$ W/Km^2	$q_{o,th}$ kW/m^2	q_o kW/m^2	h_o W/Km^2	St_o x10^3
			TEST T31				
3.9	6.380	3.404	1173.5	100.9	100.8	1172.5	3.401
5.9	6.611	3.380	1165.2	100.2	105.2	1224.0	3.551
7.8	6.843	3.357	1157.2	99.49	98.20	1142.2	3.314
9.8	7.074	3.335	1149.5	98.83	89.91	1045.8	3.034
15.6	7.768	3.273	1128.2	97.00	103.6	1204.6	3.494
20.5	8.346	3.226	1112.1	95.61	101.6	1182.1	3.429
30.3	9.501	3.144	1083.7	93.17	86.90	1010.8	2.932
			TEST U31				
3.9	6.478	3.394	1205.0	109.3	100.1	1103.9	3.109
5.9	6.712	3.370	1196.5	108.6	101.7	1121.5	3.159
7.8	6.948	3.347	1188.3	107.8	96.54	1064.4	2.998
9.8	7.182	3.325	1180.4	107.1	93.58	1031.8	2.906
15.6	7.887	3.263	1158.5	105.1	104.2	1149.0	3.236
20.5	8.473	3.217	1142.0	103.6	101.7	1121.6	3.159
30.3	9.647	3.134	1112.8	100.9	90.00	992.1	2.795
			TEST V31				
3.9	6.663	3.375	1228.3	112.8	106.8	1163.7	3.198
5.9	6.904	3.351	1219.6	112.0	108.2	1178.6	3.239
7.8	7.146	3.328	1211.2	111.2	100.7	1096.4	3.013
9.8	7.387	3.306	1203.2	110.4	95.80	1043.6	2.868
15.6	8.112	3.245	1180.9	108.4	106.3	1158.3	3.183
20.5	8.716	3.199	1164.0	106.9	105.3	1147.2	3.152
30.3	9.923	3.117	1134.2	104.1	92.83	1011.2	2.779

F.7

Corian Plate with No Film Cooling

TEST Q01							
Gage Position X/D	Re_x $\times 10^{-5}$	St_{th} $\times 10^3$	$h_{o,th}$ W/Km^2	$q_{o,th}$ kW/m^2	q_o kW/m^2	h_o W/Km^2	St_o $\times 10^3$
2.5	7.699	3.273	1146.3	94.75	91.58	1107.9	3.164
4.0	8.113	3.239	1134.3	93.76	92.22	1115.7	3.186
6.0	8.665	3.197	1119.5	92.54	90.80	1098.5	3.137
10.0	9.769	3.121	1093.0	90.34	81.12	981.4	2.802
15.0	11.15	3.039	1064.5	87.99	102.0	1233.6	3.522
TEST Q02							
2.5	7.640	3.278	1132.9	91.16	92.74	1152.5	3.335
4.0	8.051	3.244	1121.0	90.21	90.30	1122.2	3.247
6.0	8.599	3.201	1106.4	89.03	89.33	1110.1	3.212
10.0	9.694	3.126	1080.2	86.92	82.20	1021.5	2.956
15.0	11.06	3.044	1052.0	84.65	102.2	1269.7	3.674
TEST Q03							
2.5	7.613	3.280	1129.7	90.90	91.23	1133.7	3.292
4.0	8.023	3.246	1117.9	89.96	89.14	1107.8	3.217
6.0	8.568	3.204	1103.3	88.78	87.59	1088.5	3.161
10.0	9.660	3.128	1077.1	86.68	78.14	971.1	2.820
15.0	11.02	3.046	1049.0	84.42	96.63	1200.8	3.487
TEST Q04							
2.5	7.625	3.279	1131.6	90.90	93.59	1165.1	3.376
4.0	8.035	3.245	1119.8	89.96	93.82	1167.9	3.385
6.0	8.582	3.203	1105.2	88.78	93.04	1158.2	3.356
10.0	9.675	3.127	1079.0	86.68	77.69	967.1	2.803
15.0	11.04	3.045	1050.8	84.41	98.97	1232.0	3.570

F.8

Corian Plate with No Film Cooling

Gage Position X/D	Re_x x10^{-5}	St_{th} x10^3	$h_{o,th}$ W/Km^2	$q_{o,th}$ kW/m^2	q_o kW/m^2	h_o W/Km^2	St_o x10^3
TEST R01							
2.5	6.320	3.411	1142.6	93.19	93.74	1149.3	3.431
4.0	6.660	3.376	1130.7	92.22	93.10	1141.4	3.408
6.0	7.113	3.331	1115.9	91.02	92.68	1136.3	3.392
10.0	8.019	3.252	1089.4	88.86	82.86	1015.9	3.033
15.0	9.152	3.168	1061.0	86.54	106.0	1299.2	3.879
TEST R02							
2.5	6.327	3.410	1143.6	93.28	93.26	1143.4	3.410
4.0	6.667	3.375	1131.7	92.30	93.52	1146.6	3.419
6.0	7.121	3.331	1116.9	91.10	91.62	1123.3	3.350
10.0	8.028	3.252	1090.4	88.94	78.35	960.6	2.865
15.0	9.162	3.167	1062.0	86.62	98.71	1210.2	3.609
TEST R03							
2.5	6.457	3.396	1166.5	99.02	94.05	1108.0	3.226
4.0	6.804	3.361	1154.4	97.99	94.24	1110.2	3.233
6.0	7.267	3.317	1139.3	96.70	92.83	1093.6	3.184
10.0	8.193	3.239	1112.3	94.41	78.75	927.7	2.701
15.0	9.350	3.154	1083.3	91.95	101.79	1199.2	3.492
TEST R04							
2.5	6.349	3.408	1154.8	96.80	91.36	1089.9	3.217
4.0	6.690	3.373	1142.8	95.79	90.57	1080.5	3.189
6.0	7.146	3.329	1127.9	94.54	89.80	1071.3	3.162
10.0	8.056	3.250	1101.1	92.30	81.77	975.5	2.879
15.0	9.194	3.165	1072.4	89.89	102.0	1216.4	3.590

F.9

Section 3: Gage Heat Flux in kW/m²

Aliminum Plate with Film Cooling

Test Code	Gage Position (X/D)						
	3.9	5.9	7.8	9.8	15.6	20.5	30.3
H03	52.90	56.92	54.00	49.49	56.55	52.37	51.05
J03	52.28	53.84	52.30	49.33	59.55	55.95	48.92
K03	58.99	59.74	58.06	54.43	61.72	56.98	54.92
H04	42.16	45.19	44.68	44.61	52.04	53.84	46.77
J04	40.82	44.25	43.91	41.90	50.10	50.15	48.10
K04	44.23	48.42	48.53	43.42	54.29	53.57	46.33
H05	41.76	42.80	41.69	39.14	43.71	45.37	42.64
J05	40.14	43.63	42.89	40.10	47.45	48.43	45.69
K05	43.04	46.44	45.15	42.02	50.12	51.70	48.15
H06	50.87	49.10	45.04	44.04	48.20	50.72	42.52
J06	46.51	50.82	45.97	41.53	46.60	47.15	44.50
K06	48.38	51.59	47.03	39.92	45.64	47.22	41.72
H07	56.11	57.50	48.39	44.30	49.70	50.58	43.16
J07	50.75	54.48	48.85	44.01	48.21	49.45	43.90
K07	54.80	60.55	54.88	42.96	48.44	47.06	44.65

Aluminum Plate with Film Cooling

Test Code	Gage Position (X/D)						
	3.9	5.9	7.8	9.8	15.6	20.5	30.3
H11	44.09	48.46	48.68	45.01	51.19	49.12	48.53
J11	51.49	55.71	50.29	50.70	57.37	57.61	52.92
K11	48.25	51.12	50.07	49.53	60.43	53.18	53.43
H12	43.74	47.67	50.11	46.36	56.34	55.60	51.76
J12	45.89	47.33	46.25	46.24	53.25	53.38	47.60
K12	47.37	52.79	49.74	45.42	52.54	52.10	49.28
H13	49.67	53.08	47.11	42.38	48.90	47.85	42.27
J13	48.20	50.90	46.43	44.35	51.57	51.47	46.99
K13	47.56	49.06	48.06	46.83	54.06	53.79	49.55
H14	53.68	56.31	49.70	43.70	44.05	47.19	44.15
J14	55.42	58.98	54.14	46.65	49.82	47.65	46.90
K14	53.35	59.32	53.45	46.42	50.42	52.62	47.41
H15	61.69	64.14	54.95	47.46	53.73	47.69	46.49
J15	---	---	---	---	---	---	---
K15	65.36	66.19	58.21	48.67	50.54	47.17	45.21
H16	66.36	64.40	53.67	49.27	49.16	47.36	45.51
J16	---	---	---	---	---	---	---
K16	71.14	72.34	61.87	51.41	53.23	51.86	43.55

F.11

Aluminum Plate with Film Cooling

Test Code	Gage Position (X/D)						
	3.9	5.9	7.8	9.8	15.6	20.5	30.3
H21	85.44	89.20	87.56	84.06	99.34	96.29	87.75
J21	83.45	88.85	84.53	82.76	97.03	93.84	85.65
K21	82.56	82.63	82.67	84.36	98.65	96.28	83.30
H22	69.75	74.39	73.89	76.30	89.82	89.25	82.61
J22	72.44	83.57	80.89	74.49	91.00	90.74	83.22
K22	72.61	77.19	78.29	72.30	88.48	84.53	80.87
H23	67.76	71.99	69.01	72.36	84.71	89.10	78.86
J23	66.89	71.25	74.40	71.38	88.15	87.32	81.06
K23	66.91	76.52	74.38	70.44	85.71	88.43	78.06
H24	68.76	75.47	72.93	65.68	79.42	82.13	78.16
J24	72.78	76.06	72.86	69.64	81.46	83.63	76.08
K24	72.79	78.01	72.80	69.06	82.14	83.14	76.13
H25	74.01	82.07	73.64	68.37	79.67	80.86	72.73
J25	77.98	81.27	75.13	65.64	76.21	79.81	73.54
K25	74.22	82.79	77.58	65.94	76.44	80.41	73.54
H26	81.09	86.46	81.21	70.58	---	82.27	72.59
J26	82.42	89.31	82.00	70.15	---	79.87	74.76
K26	83.48	87.27	77.08	73.30	---	78.26	76.79

F.12

Aluminum Plate with Film Cooling

Test Code	Gage Position (X/D)						
	3.9	5.9	7.8	9.8	15.6	20.5	30.3
H31	74.88	82.40	82.65	77.39	92.87	95.17	83.08
J31	75.48	80.12	81.07	77.85	92.74	93.31	84.88
K31	70.43	75.24	77.10	72.21	87.45	85.57	80.07
H32	68.98	74.86	74.01	73.16	87.32	87.40	82.11
J32	68.21	76.08	72.49	72.60	87.36	88.84	79.09
K32	65.34	74.77	76.18	68.80	88.61	85.93	79.15
H33	71.95	74.39	73.22	71.17	84.93	86.89	78.05
J33	69.01	77.22	74.84	67.13	83.23	83.62	79.29
K33	66.98	73.90	71.47	67.95	83.36	85.26	75.90
H34	74.06	82.79	75.42	67.17	82.25	81.32	76.56
J34	71.20	79.88	74.68	69.05	82.34	84.02	76.80
K34	73.41	81.06	77.14	68.52	81.22	83.24	78.58
H35	85.97	87.48	76.38	74.26	81.44	82.38	71.13
J35	83.60	88.09	84.85	74.56	84.96	87.53	75.63
K35	85.00	91.00	79.00	70.73	79.25	81.05	74.65
H36	93.02	97.72	81.51	73.52	81.17	79.68	7b.65
J36	93.31	98.06	86.93	74.03	80.04	78.23	75.55
K36	93.86	95.75	82.13	75.18	84.03	85.82	73.56

F.13

Corian Plate with Film Cooling

Test Code	Gage Position (X/D)					
	2.5	4.0	6.0	10.0	15.0	22.0
A02	94.17	106.52	92.99	85.46	104.61	97.16
B02	87.18	97.54	88.45	88.07	106.07	105.05
C02	87.13	99.95	91.42	84.14	105.47	102.91
A03	44.37	58.83	62.33	68.96	89.10	91.75
B03	41.33	56.19	60.26	67.29	88.72	88.54
C03	38.62	56.52	56.67	61.64	81.13	83.22
A04	34.81	50.72	47.50	56.80	76.66	81.38
B04	40.15	49.97	54.96	66.70	82.02	89.75
C04	40.10	51.09	55.00	64.54	81.10	88.26
A05	45.03	55.78	51.83	61.61	76.50	83.26
B05	50.12	59.49	59.26	69.49	86.69	95.22
C05	45.16	54.09	55.80	59.39	75.37	81.88
A06	57.70	68.92	59.51	54.63	71.47	81.76
B06	53.75	68.78	57.84	57.11	74.03	80.92
C06	53.07	67.21	54.87	54.46	70.79	80.44
A07	67.34	74.65	61.40	53.61	68.66	78.21
B07	65.81	74.22	67.80	64.01	79.74	86.55
C07	67.63	71.94	71.27	68.12	84.39	91.70

F.14

Corian Plate with Film Cooling

Test Code	Gage Position (X/D)					
	2.5	4.0	6.0	10.0	15.0	22.0
A11	---	---	---	---	---	---
B11	65.07	83.08	80.51	81.09	101.70	96.60
C11	72.19	86.89	85.15	85.16	101.00	98.73
A12	38.18	57.09	60.53	69.97	91.39	93.07
B12	42.56	50.22	62.13	73.86	93.57	95.93
C12	39.38	54.81	58.47	65.85	80.88	82.14
A13	40.32	55.38	49.09	55.38	74.04	80.04
B13	47.61	56.28	59.33	68.44	84.93	89.18
C13	43.89	57.52	51.36	55.20	72.37	79.43
A14	55.20	63.77	57.87	59.98	76.38	82.28
B14	57.12	69.36	56.26	56.44	72.89	79.13
C14	58.10	65.52	59.80	66.60	80.78	88.46
A15	66.40	70.12	65.57	68.33	83.57	88.72
B15	70.15	72.71	67.70	66.61	80.07	82.46
C15	67.66	75.64	63.91	60.07	73.57	79.79
A16	75.57	80.33	68.22	63.01	77.02	80.55
B16	76.68	82.94	73.11	67.19	83.84	88.87
C16	72.37	79.82	70.95	68.23	81.60	86.92

F.15

Average Gage Heat Flux Results in kW/m^2

Aluminum Plate

Test Code	Gage Position, X/D						
	3.9	5.9	7.8	9.8	15.6	20.5	30.3
HJK03	54.72	56.83	54.79	51.08	59.27	55.10	51.63
HJK04	42.40	45.95	45.71	43.31	52.14	52.52	47.07
HJK05	41.65	44.29	43.24	40.42	47.09	48.50	45.49
HJK06	48.59	50.50	46.01	41.83	45.24	48.36	42.91
HJK07	53.89	57.51	50.71	43.76	48.78	49.03	43.90
HJK11	47.94	51.76	49.68	48.41	56.33	53.30	51.63
HJK12	45.67	49.26	48.70	46.01	54.04	53.69	49.55
HJK13	48.48	51.01	47.20	44.52	51.51	51.04	46.27
HJK14	54.15	58.20	52.43	45.59	48.10	49.15	46.15
HJK15	63.53	65.17	56.58	48.07	52.14	47.43	45.85
HJK16	69.17	69.56	57.76	50.72	51.90	48.68	44.21
HJK21	83.82	86.89	84.92	83.73	98.34	95.47	85.57
HJK22	71.60	78.38	77.69	74.36	89.77	88.17	82.23
HJK23	67.19	73.25	72.59	71.39	86.19	88.28	79.33
HJK24	71.44	76.51	72.86	68.13	81.01	82.97	76.79
HJK25	75.40	82.04	75.45	66.65	77.44	80.36	73.27
HJK26	82.33	87.68	80.10	71.34	---	80.13	74.71

Aluminum Plate

Test	Gage Position, X/D						
Code	3.9	5.9	7.8	9.8	15.6	20.5	30.3
HJK31	73.60	79.25	80.27	75.82	91.02	91.35	82.68
HJK32	67.51	75.24	74.23	71.52	87.76	87.39	80.12
HJK33	69.31	73.57	73.18	68.75	83.84	85.26	77.75
HJK34	72.89	81.24	75.75	68.25	81.94	82.86	77.31
HJK35	84.86	88.86	80.08	73.18	81.88	83.65	73.80
HJK36	93.40	97.18	83.52	74.24	81.75	81.24	73.25
TUV02	58.66	61.04	56.62	51.67	58.52	56.12	50.40
TUV11	60.36	61.98	56.79	54.30	60.65	57.86	52.56
TUV21	103.5	106.1	100.8	94.4	107.7	105.5	91.65
TUV31	102.6	105.1	98.5	93.1	104.7	102.9	89.9

F.17

Corian Plate

Test	Gage Position, X/D						
Code	2.5	4.0	6.0	10.0	15.0	22.0	30.0
ABC02	89.49	101.3	90.95	85.89	105.4	101.7	---
ABC03	41.44	57.18	59.75	65.96	86.32	87.84	---
ABC04	38.35	50.59	52.49	62.68	79.93	86.46	---
ABC05	46.77	56.45	55.63	63.50	79.52	86.79	---
ABC06	54.84	67.97	57.41	55.40	72.10	81.04	---
ABC07	66.93	73.60	66.82	61.91	77.60	85.49	---
ABC11	68.62	84.99	82.83	83.13	101.4	97.67	---
ABC12	40.04	54.04	60.38	69.89	88.61	90.38	---
ABC13	43.94	56.39	53.26	59.67	77.11	82.88	---
ABC14	56.81	66.22	57.98	60.99	76.68	83.29	---
ABC15	68.07	72.82	65.73	65.00	79.07	83.66	---
ABC16	74.87	81.03	70.76	66.14	80.82	85.45	---
Q1234	92.29	91.37	90.19	79.79	99.94	---	---
R1234	93.10	92.86	91.73	80.43	102.1	---	---

F.18

Vita

Marco R. Valencia was born on 7 October 1966 in Guayaquil, Ecuador. He graduated from Vicente Rocafuerte High School in 1984, and entered Escuela Superior Politécnica del Litoral in Guayaquil in May 1984. He married María García on 26 December 1987. He graduated with a Bachelor of Science degree in Mechanical Engineering in December 1988. As a Distinguished Graduate, he was selectioned by the Ecuadorian Air Force for a Master of Science Degree at Air Force Institute of Technology, USA in 1990. He entered the School of Engineering, AFIT, in May 1991.

REPORT DOCUMENTATION PAGE

Form Approved
OMB No. 0704-0188

1. AGENCY USE ONLY (leave blank)	2. REPORT DATE	3. REPORT TYPE AND DATES COVERED
	28 May 1993	Final

4. TITLE AND SUBTITLE
Experimental Investigation of the Effects of Blowing Ratio Parameter on the Heat Transfer to a Film-Cooled Flat Plate

5. FUNDING NUMBERS

6. AUTHOR(S)

Marco R. Valencia, B.S.

7. PERFORMING ORGANIZATION NAME(S) AND ADDRESS(ES)

AFIT/ENY

Wright-Patterson AFB OH 45431

8. PERFORMING ORGANIZATION REPORT NUMBER

AFIT/GAE/ENY/93J-01

9. SPONSORING/MONITORING AGENCY NAME(S) AND ADDRESS(ES)

Aero Propulsion and Power Directorate
WL/POTC
Wright-Patterson AFB OH 45431

10. SPONSORING/MONITORING AGENCY REPORT NUMBER

11. SUPPLEMENTARY NOTES

12a. DISTRIBUTION/AVAILABILITY STATEMENT

Approved for public release; distribution unlimited

12b. DISTRIBUTION CODE

13. ABSTRACT (Maximum 200 words)

The effects of blowing ratio on film cooling effectiveness were investigated. Two round-nosed test plates w used. One made of aluminum and the second of corian (low thermal conductivity). Injection at 35 degree the downstream direction was studied. Helium was mixed with air to produce a density ratio (coolan mainstream) of 1.6 and 2.0, while the blowing ratio varied from 0.3 to 2.2. Surface temperature was measu by thin film gages located up to a nondimensional downstream distance X/D of 30. Two injection regir weak and strong, were found. In the weak regime, film cooling reduced gage heat flux at all thin film g locations, however, film cooling was more effective for $X/D < 10$. In the strong regime, the effectivenes film cooling for $X/D < 10$ was greatly reduced. Maximum film cooling effectiveness occured between the w and strong regime at a blowing ratio of 1.0. Changing the density ratio from 1.6 to 2.0 varied the measu gage heat flux less than 5 percent. Gage heat flux was correlated by the velocity ratio scaling param $(X/D)VR^{-4/3}$ in both injection regimes. Gage heat flux with no film cooling, assuming a turbulence level o percent, deviated less than 8 percent from theoretical results using the corian plate, and less than 10 per using the aluminum plate.

14. SUBJECT TERMS
Film Cooling, Heat Transfer, Shock Tube, Turbulent Flow, Density Ratio, Blowing Ratio, Flat Plate, Gas Turbine.

15. NUMBER OF PAGE
181

16. PRICE CODE

17. SECURITY CLASSIFICATION OF REPORT	18. SECURITY CLASSIFICATION OF THIS PAGE	19. SECURITY CLASSIFICATION OF ABSTRACT	20. LIMITATION OF AB$
UNCLASSIFIED	UNCLASSIFIED	UNCLASSIFIED	UL

NSN 7540-01-280-5500

Standard Form 298 (Rev
Prescribed by ANSI Std 239-18
298-102